AD-A089 943 STATE UNIV OF NEW YORK AT BUFFALO DEPT OF BIOLOGY F/G 11/2
STRUCTURE-PROPERTY-ENVIRONMENTAL RELATIONS IN GLASS AND GLASS-C--ETC(U)
MAR 80 L L HENCH AFOSR-77-3210
UNCLASSIFIED AFOSR-TR-80-0775 NL

1 OF 2
AD A089943

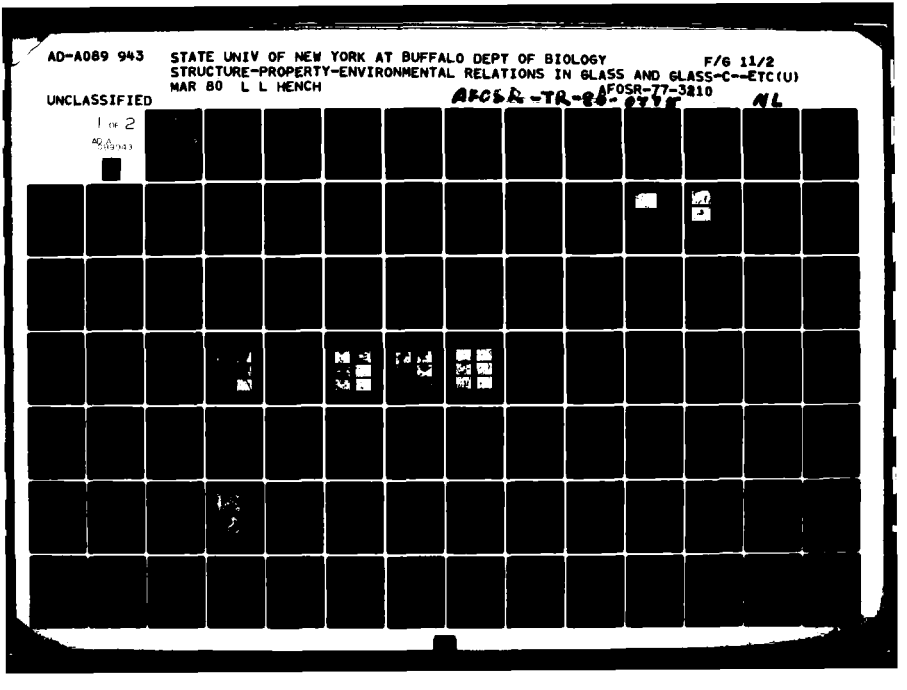

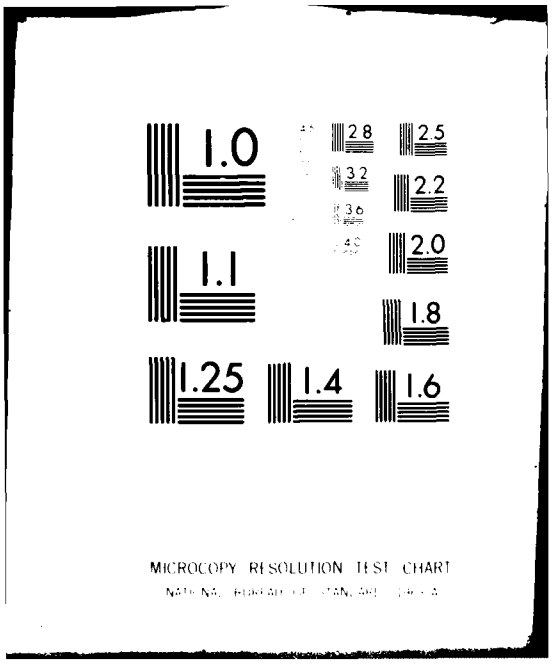
1.0
2.8
2.5
3.2
2.2
3.6
2.0
1.1
1.8
1.25
1.4
1.6
MICROCOPY RESOLUTION TEST CHART

LEVEL II

2

STRUCTURE-PROPERTY-ENVIRONMENTAL RELATIONS IN GLASS AND GLASS-CERAMICS

Final

THIRD ANNUAL AND SUMMARY REPORT

to

AIR FORCE OFFICE OF SCIENTIFIC RESEARCH
Bolling Air Force Base, D.C. 20332

GRANT NO. 77-3210

Period Covered:
March 1, 1977 - February 28, 1980

Submitted by

L. L. Hench
Professor and Head
Ceramics Division
Department of Materials Science and Engineering
University of Florida
Gainesville, Florida 32611

March, 1980

Unclassified

SECURITY CLASSIFICATION OF THIS PAGE (When Data Entered)

(19) REPORT DOCUMENTATION PAGE	READ INSTRUCTIONS BEFORE COMPLETING FORM
1. REPORT NUMBER (18) AFOSR-TR-80-0875	2. GOVT ACCESSION NO. AD-A089 943	3. RECIPIENT'S CATALOG NUMBER
4. TITLE (and Subtitle) (6) STRUCTURE-PROPERTY-ENVIRONMENTAL RELATIONS IN GLASS AND GLASS-CERAMICS	5. TYPE OF REPORT & PERIOD COVERED Final Report Mar. 1, 1977-Feb. 29, 1980
	6. PERFORMING ORG. REPORT NUMBER
7. AUTHOR(s) (10) L. L. HENCH	8. CONTRACT OR GRANT NUMBER(s) (15) AFOSR-77-3210
9. PERFORMING ORGANIZATION NAME AND ADDRESS University of Florida Department of Materials Science & Engineering Gainesville, FL 32611	10. PROGRAM ELEMENT, PROJECT, TASK AREA & WORK UNIT NUMBERS 61102F (16) 2303/A3
11. CONTROLLING OFFICE NAME AND ADDRESS Air Force Office of Scientific Research /NC (11) Bolling Air Force Base, DC 20332	12. REPORT DATE Mar 1980
	13. NUMBER OF PAGES (12) 155
14. MONITORING AGENCY NAME & ADDRESS (if different from Controlling Office)	15. SECURITY CLASS. (of this report) Unclassified
	15a. DECLASSIFICATION DOWNGRADING SCHEDULE

16. DISTRIBUTION STATEMENT (of this Report)

Approved for public release; distribution unlimited

(9) Final rept. 1 Mar 77-29 Feb 80

17. DISTRIBUTION STATEMENT (of the abstract entered in Block 20, if different from Report)

18. SUPPLEMENTARY NOTES

19. KEY WORDS (Continue on reverse side if necessary and identify by block number)

glass, glass-ceramics, ceramed, surface characterization, corrosion parameters lithia-disilicate, stoichiometric, scanning electron microscopy, infrared reflection spectroscopy, Auger electron spectroscopy, electron microprobe analysis, surface area-to-solution volume, environmental sensitivity, microstructural depth compositional profile, corrosion path, isochronal, solubility, interfacial (cont.)

20. ABSTRACT (Continue on reverse side if necessary and identify by block number)

The overall objectives of this study of glass, glass-ceramics, Si_3N_4 and SiC is aimed at developing predictive relationship for the lifetime of materials under various combinations of chemical, mechanical, and thermal environments. Several analytical surface techniques are now being routinely applied to the characterization of glass and glass surfaces. A clearer understanding of corrosion mechanisms and kinetics emerges when a combination of surface and solution analyses is employed. Glass corrosion mechanisms and kinetics, plus analytical techniques and testing methods used for measuring glass corrosion have been reviewed. (continued)

DD FORM 1 JAN 73 1473

Unclassified

SECURITY CLASSIFICATION OF THIS PAGE (When Data Entered)

KEY WORDS--Continued

analysis, grain boundary, selective leaching, ion exchange, kinetics, corrosion mechanism, durability, silicon nitride, surface flaws, mixed alkali effect, solution pH, atomic adsorption, atom emission solution analysis, glass powders, concentration cells, surface films passivating nucleation, crystallization, alkali ions, silica, lifetime predictions, depth of analysis, types of glass surfaces, bulk glass, homogenize, precipitation, leached layer, silica-rich layer, aluminosilicate films, total dissolution, network dissolution, phase boundary attack, electric field, local temperature, micro cracks, electron beam simulated desorption, electron signal decay, liquid nitrogen temperature, resident time, thermal conductivity, second resident time, oxidation, oxide layer, nucleation kinetics, growth kinetics, ZrO_2, silicon carbide, microprocessing of ceramics, CVD SiC, alumina, single crystal sapphire, oriented surface layer.

ABSTRACT--Continued

Application to both simple binary and complex multicomponent glass systems are illustrated.

The corrosion behavior of stoichiometric $Li_2O \cdot 2SiO_2$ (33L) glass and glass-ceramics in acidic, neutral and basic solutions has been studied using infrared reflection spectroscopy, scanning electron microscopy and solution analyses. Glass-ceramics containing a volume fraction of crystallization ranging from 0-90% were investigated. Selective Li^+ leaching and glass network dissolution are major mechanisms of corrosion in 33L glass and glass-ceramics. In addition, attack of the glass at the glass crystal phase boundary contributes significantly to surface deterioration of the glass ceramics. The relative importance of network dissolution, a Li^+ leaching and phase boundary attack is dependent on the extent of crystallization and solution pH.

In the corrosion study of a non-stoichiometric system, a Li_2O-Al_2O_3-CaO-SiO_2 glass was heat treated to provide various stages of crystallization. The glassy phase was much richer in alkaline and alkaline earth species than the crystalline phase. The corrosion behavior of the resulting glass-ceramics were studied using infrared reflection spectroscopy (IRRS), scanning electron microscopy, and solution analyses. The mechanisms controlling corrosion vary depending on the degree of crystallization (V_v). The higher V_v glass-ceramics exhibited poorer resistance to aqueous attack than did the low V_v glass-ceramics even though the crystalline phase itself was more durable.

Migration of sodium in thin films of soda-silica glass deposited on a stainless steel substrate has been studied. The amounts of charge trapping and local heating were a strong function of beam parameters for thin films. The rearrangement of sodium due to charge trapping was calculated and compared to experimental data. The calculated and experimental data agree well and indicate that fields of 10^5 V/cm exist during analysis. The depth distribution of sodium indicates that either electrons or ion bombardment can cause sodium migration during analysis. The cross-section for electron induced desorption was measured to be 3×10^{-20} cm for sodium in this glass, thus it is only important at very high current densities.

It is proposed that progress in improving the properties of technical ceramics will require improved understanding of ceramic processing, especially the surfaces, interfaces and agglomeration of powders, and the interaction of surfaces with the environment. New surface analysis instruments such as infrared reflection spectroscopy (IRRS) and Auger electron spectroscopy are used to describe surface compositional changes of SiC, Si_3N_4, and Al_2O_3. Preferred crystallographic pathways of surface attack are observed for both SiC and Si_3N_4 single and polycrystalline samples. Formation of an oxynitride surface phase on Si_3N_4 powders significantly alters the surface charge distribution and decrease the isoelectric point of the powders. Variations in processing of dense Al_2O_3 result in a deep surface layer of preferred orientation detection by IRRS methods.

TABLE OF CONTENTS

SECTION I

INTRODUCTION

Significant progress has been made towards developing characterization techniques for the evaluation of the environmental sensitivity of glass, glass-ceramics, Si, Si_3N_4, and SiC. This report is a compilation of five papers that have been submitted for publication based primarily on our second and third year efforts. A brief review of each of these papers is presented in the following paragraphs. A summary of results achieved during the three-year period is included in Section VII of this report.

Solution analyses and weight losses traditionally have been used for studying glass corrosion. These techniques provide very little if any information concerning the nature of the reaction layer remaining on the glass surface after corrosion. Several analytical surface techniques are now being applied routinely to the characterization of glass and glass surfaces. A clearer understanding of corrosion mechanisms and kinetics emerges when a combination of surface and solution analyses is employed. This first paper provides a review of glass corrosion mechanisms and kinetics, analytical techniques used for measuring glass corrosion and testing methods. Application to both simple binary and complex multicomponent glass systems is illustrated.

The corrosion behavior of stoichiometric $Li_2O \cdot 2SiO_2$ (33L) glass and glass-ceramics in acidic, neutral and basic solutions has been studied using infrared reflection spectroscopy, scanning electron microscopy and

solution analyses. Glass-ceramics containing a volume fraction of crystallization ranging from 0-90% were investigated. The composition of the glassy phase is the same as the crystalline phase. Selective Li^+ leaching from the glassy phase and glass network dissolution are the major mechanisms of corrosion in 33L glass and glass-ceramics. In addition, phase boundary attack contributes significantly to surface deterioration of the glass-ceramics. The relative importance of network dissolution, Li^+ leaching and phase boundary attack is dependent on both the extent of crystallization and solution pH. In general, the materials containing high volume fractions of crystals (90%) corroded via a network dissolution mechanism in all media, materials containing no crystals (0%) corroded by ion exchange in low pH media and network dissolution in high pH media and materials containing 20-60% crystals corroded both mechanisms in all media.

The procedure of ceraming to produce a glass-ceramic usually improves the mechanical strength of the final product, but its effects on chemical durability are not always predictable. For instance, when a non-stoichiometric glass is crystallized the composition of the glass may be significantly different from the crystalline phase producing a different major mode of corrosion than observed for stoichiometric materials.

In the present investigation, a Li_2O-Al_2O_3-CaO-SiO_2 glass was heat-treated to provide various stages of crystallization. The glassy phase was much richer in alkaline and alkaline earth species than the crystalline phase. The corrosion behavior of the resulting glass-ceramics were studied using infrared reflection spectroscopy (IRRS), scanning electron

microscopy (SEM), and solution analyses. The mechanisms controlling the extent of corrosion vary depending on the degree of crystallization (V_v). The higher V_v glass-ceramics exhibited poorer resistance to aqueous attack than did the low V_v glass-ceramics, even though the crystalline phase itself was more durable.

Migration of sodium in thin films of soda-silica glass deposited on a stainless steel substrate has been studied. The amounts of charge trapping and local heating were a strong function of beam parameters for thin films. For example, the time required for the sodium Auger signal to decay to 50% of its initial value increased as the beam energy was increased or as the current density was decreased. The rearrangement of sodium due to charge trapping was calculated and compared to experimental data. The calculated and experimental data agree well and indicate that fields of $\sim 10^5$ V/cm exist during analysis. The depth distribution of sodium indicates that either electrons or ion bombardment can cause sodium migration during analysis. The cross-section for electron induced desorption was measured to be 3×10^{-20} cm^2 for sodium in this glass, therefore it is only important at very high current densities.

It is proposed that progess in improving the properties of technical ceramics will require improved understanding of ceramic processing, especially the surfaces, interfaces and agglomeration of powders, and the interaction of surfaces with the environment. New surface analysis instruments such as infrared reflection spectroscopy (IRRS) and Auger electron spectroscopy are used to describe surface compositional changes of SiC, Si_3N_4, and Al_2O_3. Preferred crystallographic pathways of surface

attack are observed for both SiC and Si_3N_4 single and polycrystalline samples. Formation of an oxynitride surface phase on Si_3N_4 powders significantly alters the surface charge distribution and decreases the isoelectric point of the powders. Variations in processing of dense Al_2O_3 result in a deep surface layer of preferred orientation which can be detected non-destructively with IRRS methods.

SECTION II

CORROSION OF GLASS SURFACES

By

D. E. Clark and E. Lue Yen-Bower

Introduction

The phenomenon of glass corrosion has been studied for well over fifty years and has resulted in the publication of several hundred articles, numerous reviews,[1-9] at least one book,[10] and two extensive bibliographies.[11,12] Deriving broad generalizations from the literature concerning glass corrosion is often difficult due to the lack of uniformity in testing procedures as well as the failure of many investigators to recognize the importance of critical corrosion parameters. It is now well known that in addition to controlling the temperature and duration of exposure, parameters such as glass surface area-to-solution volume ratio SA/V,[13] powders versus bulk specimens, surface roughness,[14] solution chemistry,[15] and type of test (i.e., static versus dynamic),[10] are important in the characterization of glass corrosion.

Until recently, the conventional techniques for evaluation glass durability were 1) titration, in which the volume of acid required to neutralize the corrosion solution was measured, and 2) change in specimen weight, in which the mass of glass dissolved during corrosion was determined. Poorly characterized glass powders often were used to accelerate the rate of corrosion and produce a measurable change in solution chemistry or weight loss within a reasonable exposure time. Neither titration nor weight loss shed much light on the corrosion mechanisms, the species being leached from the glass, or the nature of the leached layer remaining on the glass surface. Furthermore, these methods of analyses were particularly ineffective for monitoring corrosion of durable glasses in which only small changes in solution chemistry and weight control occurred.

Glass and glass-ceramics are assuming increasing importance in high technology industries including the medical,[16] dental,[17] chemical,[18]

communications, aerospace, and nuclear[19] fields. Since many of the properties of glass are determined by their surfaces, it is essential that we learn how to predict the surface chemistry of these materials in order to optimize their performance.

The deficiencies in most of the early studies were due to the lack of adequate methods for monitoring quantitatively the reactions that occurred on the glass surfaces as a result of corrosion. In the last 10-15 years, instrumental techniques have become available for characterizing both glass surfaces and the solutions in which the glass have been immersed.[10,20] In addition to the concentrations of species in solution, the concentration of species at the glass surface and at various depths within the surface can be measured, providing a basis for establishing a mass balance between the glass and solution after corrosion. When a combination of several techniques is used, a more complete understanding of the glass corrosion processes can be achieved.

In the present study we illustrate the use of five techniques (infrared reflection spectroscopy (IRRS), electron microprobe analysis (EMP), Auger electron microscopy coupled with Ar ion milling (AES-IM), scanning electron microscopy with energy dispersive x-ray analysis (SEM-EDXA) and solution analyses), for glass surface and corrosion solution characterization.

Corrosion Testing Methods

As shown in Fig. 1, numerous tests have been devised for the purpose of evaluating glass corrosion. Most of these test methods are designed primarily for convenient analysis of the corrosion solution although two of the tests (Fig. 1d and f) provide for both corrosion solution and specimen analyses.

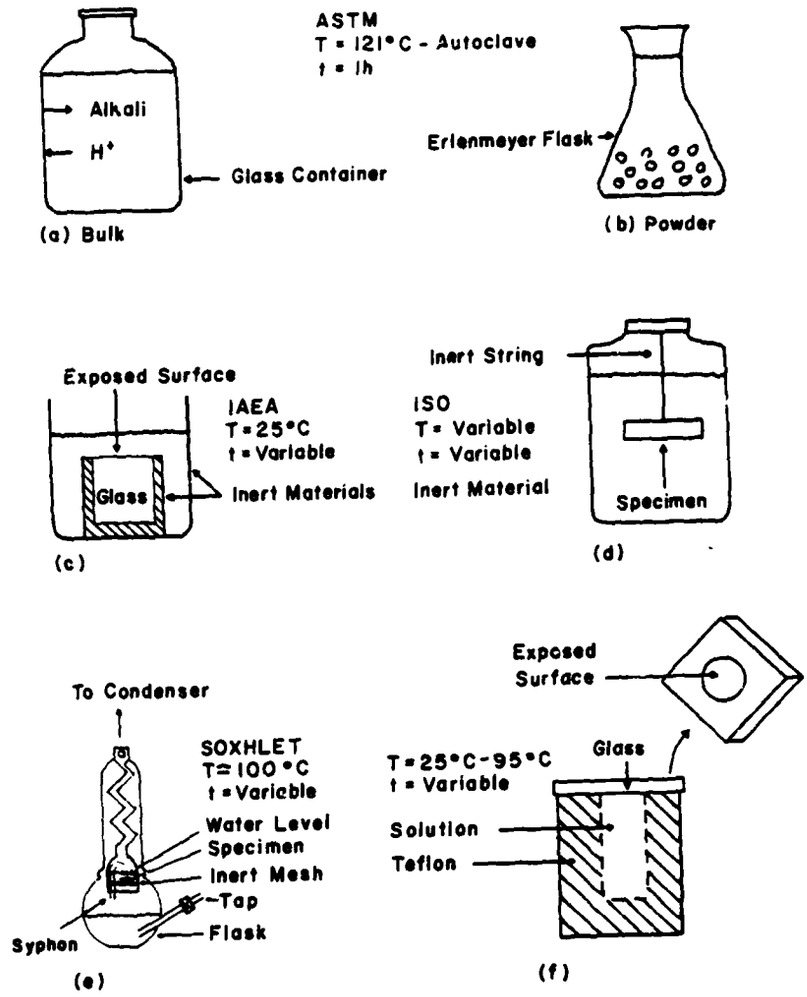

Fig. 1. Tests for measuring glass corrosion.

In the ASTM[21] bulk glass corrosion test (Fig. 1a) the container is filled to 90% overflow capacity with demineralized water or standardized H_2SO_4 and placed in an autoclave at 121°C for 1 h. The SA/V may vary depending on the size of the container but is generally ∿12 cm^{-1}. The same exposure temperature and time are used for the ASTM[21] powder corrosion test (Fig. 1b). Ten grams of glass powder are placed in ∿30 ml of demineralized water contained in a glass (previously leached) flask and the entire assembly is placed in the autoclave. Although great care is exercised in preparation of the glass powders, a constant SA/V is difficult to maintain due to decreases in the glass particle diameter with exposure time. The results of both ASTM tests are reported in volume of acid consumed in the test or required to neutralize the corrosion solution.

Two tests have been developed to measure the leach rate of nuclear waste glass materials. In the IAEA[22] method (Fig. 1c), the waste glass is cast into a container of inert material such as stainless steel. The container with solidified glass is placed into a bath of demineralized water maintained at 25° ± 5°C. Only the upper surface of the glass is exposed to the solution producing an effective SA/V = 0.1 cm^{-1}. The other glass surfaces are isolated from the solution as illustrated in Fig. 1c. The ISO[23] test requires that a representative sample of glass, either cast or core drilled from actual waste solidification products, be suspended into a specified quantity of solution providing an SA/V = 0.1 cm^{-1} (Fig. 1d). All surfaces of the specimen should be mechanically or fire polished and the exposure temperature is maintained at 23°C. In both the IAEA and ISO tests the corrosion solutions are drawn off at specified intervals and analyzed for γ, α and β activity, from which leach rates may be calculated. The glass samples are placed into fresh solutions

after each exposure interval. If simulated waste glasses are used, the solutions may be analyzed using standard solution techniques. The data are often expressed in units of g/cm^2-d for each specie of interest (i.e., grams of Cs per square centimeter of exposed glass per day of exposure). These units are satisfactory for expressing the rate of leaching if congruent dissolution is the dominant mechanisms of corrosion. However, if ion exchange which is root time dependent, is rate controlling, gm/cm^2-d can be misleading because of the magnitude of this expression will depend on the time interval used for its evaluation.

The Soxhlet technique (Fig. 1e) features a constant flow of refluxed water at approximately 100°C over a block or powdered glass specimen. The SA/V is difficult to define in this test because the specimen is not always immersed in the same solution. The solution surrounding the specimen is constantly siphoned off (into the large flask) so that products of corrosion remain in contact with the glass for short periods of time. Solution is drawn from the flask at various intervals and analyzed using standard techniques. Corrosion is measured by determining the weight loss of the glass or by elemental analysis of the solution. A problem with this method is that portions of the apparatus are constructed of glass, the leaching properties of which may influence the chemistry of the corrosion solution.

A corrosion test with which we have a great deal of experience in this laboratory is shown in Fig. 1f. The cavity in the center of a Teflon cube is filled with solution (1 ml) and a flat glass specimen (1.5 x 1.5 x 0.5 cm) is mounted to provide a SA/V = 0.77 cm^{-1}. Prior to assembly, the glass specimen is polished to a 600 grit surface finish using SiC paper. The

corrosion cell-glass assembly is placed into a constant temperature bath or autoclave for various times and temperatures. After exposure the corroded glass surfaces are analyzed by IRRS and the solutions are analyzed using an atomic absorption spectrophotometer (AA) and a pH meter. Selected glass specimens are evaluated further with SEM-EDXA, AES-IM and the EMP.

Mechanisms and Kinetics of Glass Corrosion

Glasses corrode via ion exchange or network dissolution, or a combination of both mechanisms, and the reactions may be written as follows where the subscripts (g) and (soln) refer to the glass and solution phases, respectively:

$$SiONa(g) + H_2O \rightarrow SiOH(g) + Na^+ + OH^- \quad \text{(ion exchange)} \qquad (1)$$

$$[-O-\underset{\underset{O}{|}}{\overset{\overset{O}{|}}{Si}}-O-\underset{\underset{O\ (g)}{|}}{\overset{\overset{O}{|}}{Si}}-OH] + 4OH^- \rightarrow [-O-\underset{\underset{O\ (g)}{|}}{\overset{\overset{O}{|}}{Si}}-OH] + [OH-\underset{\underset{OH\ (soln)}{|}}{\overset{\overset{OH}{|}}{Si}}-OH] \quad \text{(network dissolution)} \qquad (2)$$

Schmidt[24] and Sanders et al.[25] present a solution parameter based on the ratio of concentration of species in solution to the ratio of concentration of the same species in the glass. This solution parameter, α, may be expressed by

$$\alpha = \frac{Y\ (Soln)}{X\ (Soln)} \cdot \frac{X\ (Glass)}{Y\ (Glass)} \qquad (3)$$

where for a binary glass: X = moles of alkali oxide

Y = moles of SiO_2

The dominant mechanism of corrosion often can be determined from the value of α obtained at the time that the experiment was concluded. When $\alpha \rightarrow 1$, the ratio of SiO_2 alkali oxide in solution is the same as in the glass, and the

glass is dissolving by network dissolution (equation (2)). As $\alpha \rightarrow 0$, the primary mechanism of corrosion is occurring via the ion exchange reaction shown in equation (1). The ion exchange mechanism results in the development of a hydrated SiO_2-rich film on the glass surface.

There is usually an interval of time when both mechanisms are operative, resulting in the development and dissolution sequence of the film as shown in Fig. 2. Consider an alkali binary silicate glass corroded using the test shown in Fig. 1f. Initially, the solution pH of the air-saturated demineralized water is $\sim$5.5. In the early stages of corrosion, ion exchange occurs between the alkali ions from the glass and the H^+ (or H_3O^+) from solution, leading to an increase in solution OH^- concentration as shown in equation (1), and therefore an increase in pH. A SiO_2-rich film develops during this period and its thickness increases with time (Fig. 2b). When the solution pH reaches $\sim$9, the rate of attack by OH^- on the glass network increases significantly as illustrated by equation (2).[26,27] The SiO_2-rich film continues to grow until the rate of network attack is equal to the rate of ion exchange indicated by the maximum (point (c) in Fig. 2). In an unreplenished solution with a large SA/V, the pH will rapidly rise above 9 and the film may be completely dissolved (point d). The solution parameter, α, in equation (3) will equal 1 at point d and will remain at this value until complete dissolution of the glass occurs. We have observed total dissolution of a 33 mol % Na_2O - 67 mol % SiO_2 (33N) glass exposed to a static solution. Obviously the film that forms on 33N glass is not protective. Some glasses containing CaO and Al_2O_3 can form protective or stabilized SiO_2-rich films that are fairly resistant to both ion exchange and network dissolution. For these glasses, the time required to reach point c in Fig. 2 may be many centuries, and point d may never be attained.

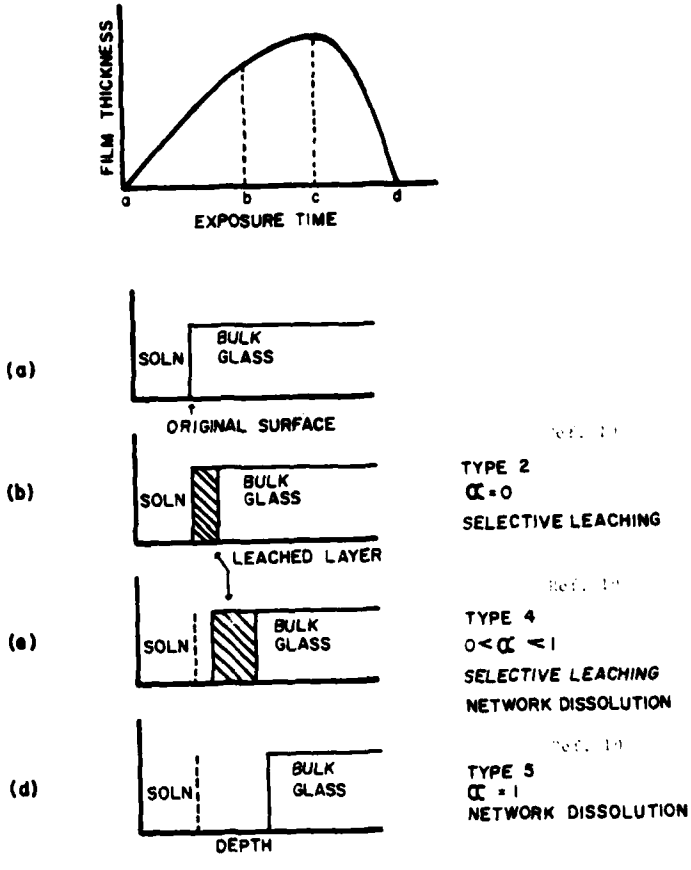

Fig. 2. Schematic of corrosion film development and destruction on a binary alkali-silicate glass.

The equation governing the rate of release of various species into the corrosion solution is given by Das and Douglas[28] as:

$$Q = at^{1/2} + bt \tag{4}$$

where Q = quantity of alkali extracted in time, t.

t = exposure time

a, b = reaction rate constants for the ion exchange and network dissolution reactions, respectively, and are temperature dependent.

In the time regime where α, as defined by equation (3), is near zero, equation (4) may be reduced to:

$$Q = at^{1/2} \tag{5}$$

and when $\alpha \rightarrow 1$, equation (4) may be written as

$$Q = bt \tag{6}$$

Boksay et al.[29] considered the ion exchange process with respect to a moving boundary caused by network dissolution. The rate equation based on a moving boundary is more complex than equation (3). However, when network dissolution is negligible, their equation reduces to the familiar form shown in equation (5). Doremus[30] extended the theory of Boksay et al. to include a concentration-dependent interdiffusion coefficient between H^+ (or H_3O^+) and alkali ions.

Reactions not defined by equations (1) and (2), such as precipitation, hydration, and complex surface film formation, may also occur during corrosion. Surface analyses of these glasses involving these reactions are usually more difficult to understand than those involving only ion exchange and network

dissolution, and the corrosion rates for the former do not always obey equations (4)-(6).

Corrosion Characterization Techniques

A. Infrared Reflection Spectroscopy - Sequential Polishing

Infrared reflection spectroscopy has been used by numerous investigators for characterizing glass surfaces.[31-33] Recently the technique has been applied to the study of glass corrosion.[34-36] Some advantages of IRRS are that it is inexpensive, nondestructive, rapid, and provides structural information on the glass surface.

Figure 3a shows the infrared reflection spectra of a 33 mol % Na_2O - 67 mol % SiO_2 (33N) both before and after corrosion. Prior to corrosion there are two major peaks in the spectral region between 1400 cm^{-1} and 600 cm^{-1}. The peak at 1050 cm^{-1} is due to the silicon-bridging oxygen stretching vibrations in an alkali environment,[34] and the peak at 950 cm^{-1} is produced from silicon-nonbridging oxygen vibrations.[34] After corrosion, the 1050 cm^{-1} peak has increased in intensity (%R) and its maximum has shifted to a higher wavenumber (i.e., higher frequency) while the 950 cm^{-1} peak has decreased in intensity and wavenumber (i.e., frequency). The spectrum for the corroded glass approaches the spectrum for vitreous silica, indicating that the surface of this specimen is SiO_2-rich (i.e., has a higher concentration of Si-bridging oxygens than the bulk glass).

The infrared reflection spectra for a PNL* soda-borosilicate simulated simulated nuclear waste glass (76-68) is shown in Fig. 3b. The spectrum of the uncorroded glass is typical for a variety of multicomponent glasses. Reflection bands occur at approximately the same positions in the spectrum

---

*PNL-Battelle Pacific Northwest Laboratories

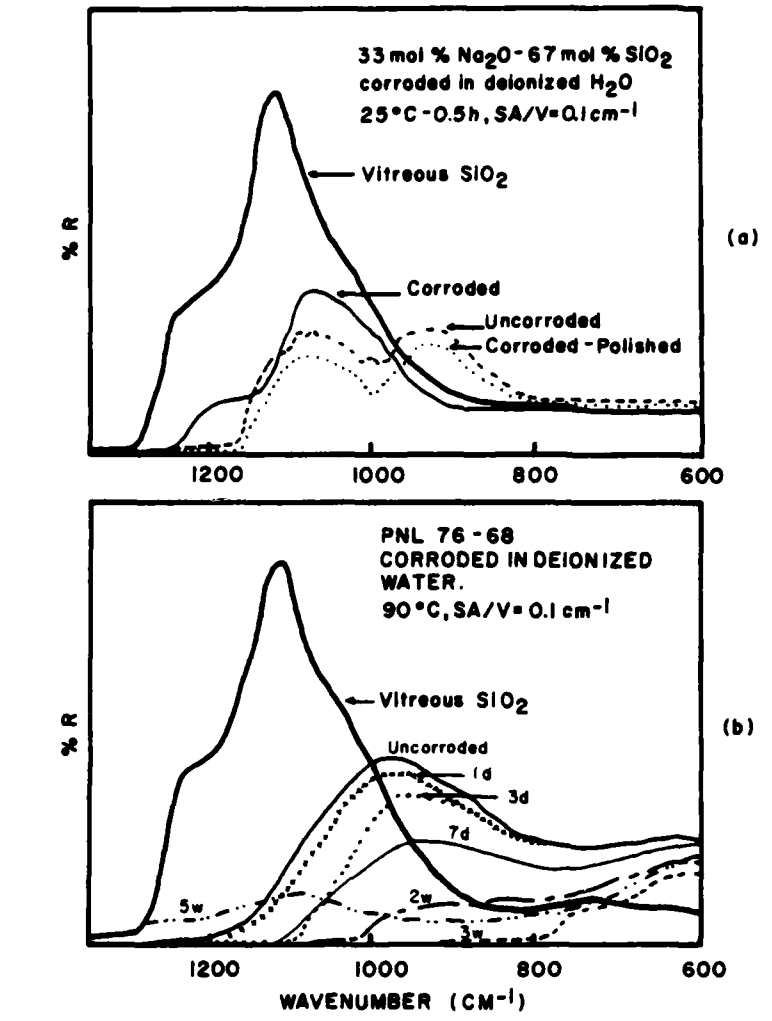

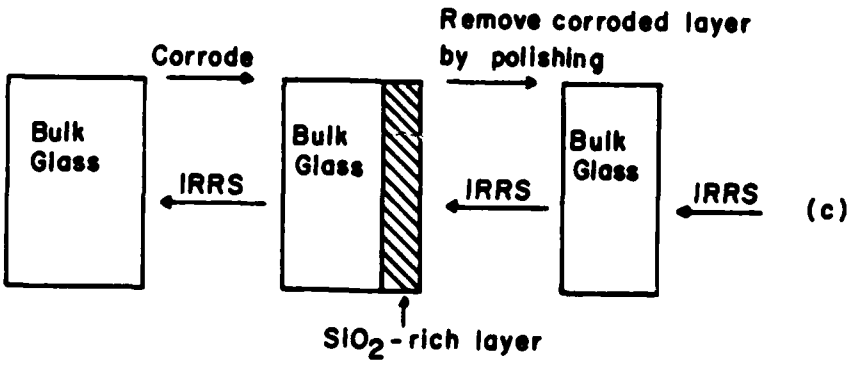

Fig. 3. Infrared reflection spectra of a) 33N glass before corrosion, after corrosion, and after removing the corrosion film by polishing, b) PNL 76-68 simulated nuclear waste glass before and after corrosion, and c) schematic of sequential polishing-IRRS technique.

as for the binary glasses. However, the saddle region at 1000 cm^{-1} in the spectrum of the binary glass is not observed in the uncorroded waste glass spectrum. During corrosion, the reflected intensity of the waste glass decreases markedly suggesting either severe surface roughening due to network dissolution, or the formation of a surface film not specified by equations (1) and (2).

The thickness of the surface films can be measured using the procedure shown in Fig. 3c. The corroded specimen is weighed, polished with 600 grit SiC, and the corroded surface is checked at subsequent stages with the IRRS. The weight of material removed can be converted to thickness and when the spectrum of the polished specimen is the same as the spectrum of the uncorroded specimen (Fig. 3a), the film thickness may be calculated from:

$$t = \frac{\Delta wt}{(\rho)(SA)} \ (\mu m) \qquad (7)$$

where wt = total weight removed during polishing

ρ = density of the glass

SA = surface area of glass that is removed during polishing.

The thickness of the SiO_2-rich film on 33N glass after 0.5 h at 25°C and SA/V = 0.1 cm^{-1} was 3.6 μm. This procedure yielded a film thickness of 22.4 μm for a zinc borosilicate simulated nuclear waste glass (PNL composition 72-68) corroded in 0.1 M HCl for 10 h at 100°C. However, when a specimen of this same glass was exposed to 100°C water for 10 h its infrared reflection spectrum was identical to the spectrum for the uncorroded glass, suggesting a near zero film thickness. Neglecting network dissolution, these data suggest that the waste glass is less durable in acid than in water and considerably more durable in water than 33N.

The accuracy of the sequential polishing method is probably no better than 1.0 μm and it is most useful for evaluating thick films. Pitting and other surface irregularities may also affect the calculated film thickness.

B. Scanning Electron Microscopy - Energy Dispersive X-ray Analysis

The SEM is valuable for monitoring the morphological surface changes that accompany glass corrosion. Surface morphology must be understood before any of the data from other techniques such as IRRS, AES, EMP and solution analysis can be reliably interpreted.

Extensive ion exchange produces a thick and usually highly stressed SiO_2-rich film. Upon dehydration of the films, these stresses can lead to cracking on some glasses as shown in Fig. 4a. Even more durable simulated nuclear waste glasses exhibit surface cracking after exposure although it is usually less pronounced than on simple binary alkali silicates (Fig. 4b). The exact time at which cracking occurs depends on the composition of the glass as well as the exposure conditions. Surface cracks have been observed with optical microscopy on a variety of binary and ternary alkali and alkali-alkaline earth silicate glasses after they have been removed from the corrosion solution and permitted to air dry for several hours. However, durable glasses with thin leached layers may require exposure to the vacuum of the SEM, AES, or EMP before cracks develop.

When a binary alkali silicate glass is exposed for a sufficiently long time to a static solution, network dissolution becomes important (due to a high pH), either partially or completely dissolving the SiO_2-rich film. If complete dissolution of the film occurs, a surface that is compositionally, but not necessarily morphologically equivalent to the uncorroded glass, is

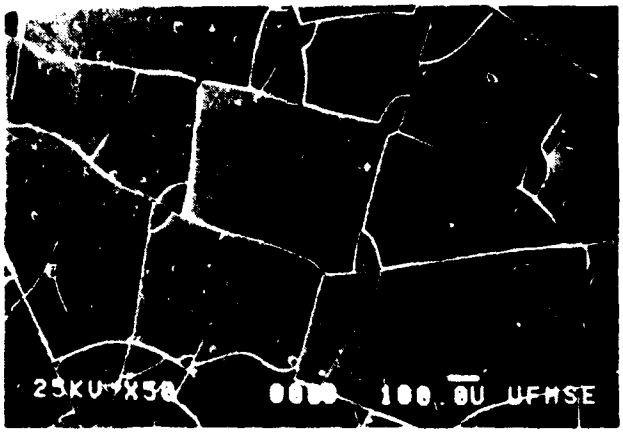

33 mol % Li_2O - 67 mol % SiO_2
95°C - 119 h, H_2O
SA/V = 0.77 cm^{-1}

(a)

PNL Glass composition(76-68)
90°C - 5 weeks, H_2O
SA/V = 0.1 cm^{-1}

(b)

Fig. 4. Scanning electron micrographs after corrosion for a) 33 mol % Li_2O - 67 mol % SiO_2, 95°C - 119 h in demineralized H_2O, SA/V = 0.1 cm^{-1}, c) 33 mol % Na_2O - 67 mol % SiO_2, 39°C - 223 h, demineralized H_2O, SA/V = 0.77 cm^{-1}, d) commercial glass, 100°C - 100% relative humidity - 20 days, and 3) EDXA spectra for the glass shown in (d).

(c) 33 mol % Na_2O - 67 mol % SiO_2
39°C - 2.23 h, H_2O
SA/V = 0.77 cm^{-1}

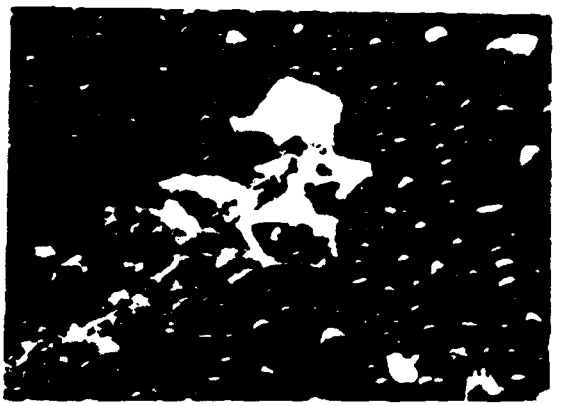

(d) Commercial Glass
100°C - 100 % Relative Humidity
20 Days

(e) EDXA Spectra

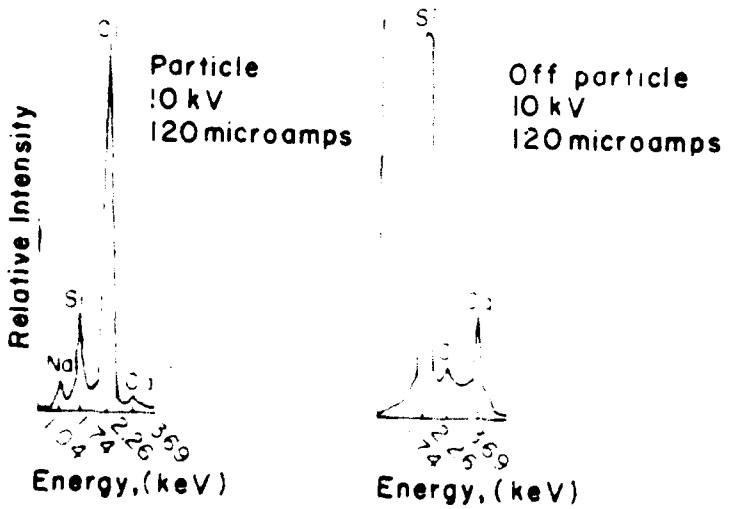

Fig. 4. Continued

obtained. A distinguishing feature of glass surfaces altered by network dissolution is severe roughening as illustrated in Fig. 4c (pitting in this case).

Window panes typically are exposed to high humidity conditions. This type of exposure (referred to as weathering) can lead to discrete precipitate formation on the glass surface as shown in Fig. 4d. The consitituents of the precipitates, determined using an energy dispersive x-ray analyzer attached to the SEM, were found to be Na, Ca, and Cl (Fig. 4e). These precipitates are not tightly bound to the glass surface and are easily removed by rinsing with water.

C. Electron Microprobe Analysis

When glasses are corroded via the ion exchange mechanism, electron microprobe analysis may be used to determine the effects of composition, temperature, SA/V, and additives such as CaO and Al_2O_3 on the leach rates. The problems associated with analyzing glasses with the EMP, as well as other electron beam analyses such as AES, are well recognized.[37-40] A time-dependent signal response is usually obtained from glasses. That is, the analyses obtained are dependent upon the length of time the electron beam impinges upon the glass surface. There are several potential explanations for this behavior: 1) electric field effects, 2) electron beam stimulated desorption of various species, and 3) thermal effects. Whatever the cause, the problem can be minimized by techniques such as cooling the specimen to liquid nitrogen temperature, defocusing the beam to decrease the current density, and translating the specimen under the beam.

The method used for the EMP data presented in this study was to defocus the electron beam and translate the glass under the beam. Figure 5 shows the

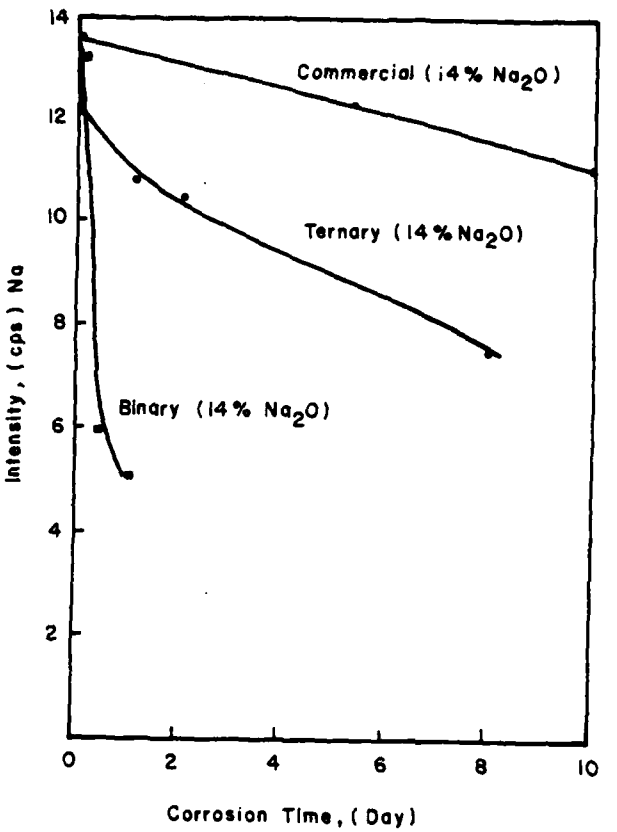

Fig. 5. EMP analysis of three glasses containing equivalent mol % of Na_2O after various exposure times to deionized water. The corrosion test used for this experiment is shown in Fig. 1f.

results for three glasses using this method. X-ray intensity of Na is plotted as a function of corrosion time. The slopes of the lines are related to the rate of Na release from the glass. Initially, all three glasses contained equivalent concentrations of Na_2O. However, Na is leached from the binary glass much faster than from the ternary and commercial glasses. The ternary glass contains 10 mol % CaO and the commercial glass contains 10 mol % CaO plus a small % of Al_2O_3. Hence, the presence of CaO and Al_2O_3 in glass significantly improves its leach resistance.

D. Auger Electron Spectroscopy - Ar Ion Milling

AES is one of the best techniques available for analyzing glass surfaces. Its small sampling depth, ~5-50 Å depending on the element,[10] makes it useful for characterizing very durable glasses in which the surfaces have been leached to only a few hundred angstroms. Such thin leached layers are usually not detectable with IRRS, SEM-EDXA and EMP because of their larger sampling depths (~5000 Å).

The Auger spectra in Fig. 6 were measured at liquid nitrogen temperature in order to minimize the alkali mobility problems and obtain data that were independent of electron beam impingement time. Figure 6a shows the AES spectrum of a durable commercial soda-lime-silicate glass prior to exposure. The peak height (dN/dE) is related to the concentration of the element responsible for that peak. After corrosion (Fig. 6b), the Na peak has nearly disappeared, indicating that this element has been leached from the glass surface. The depth of leaching was determined by sputtering the surface with a 2KeV Ar ion beam for specified times and analyzing with AES after each sputtering time. Figure 6c shows the composition (mol %) as a function of

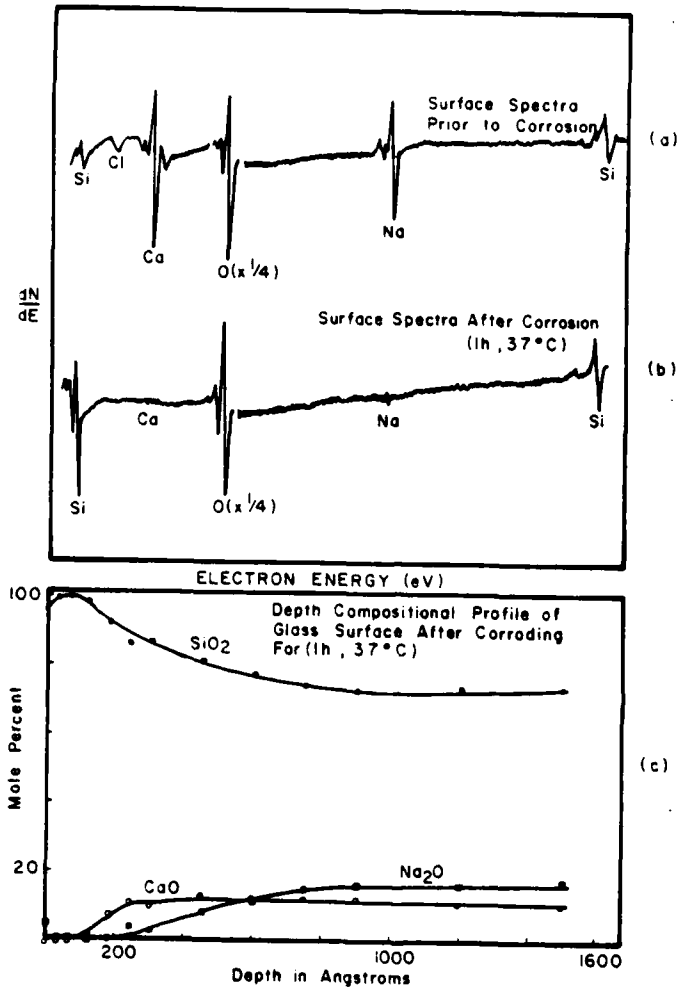

Fig. 6. a) Auger surface spectrum of a commercial soda-lime-silica glass before corrosion. Courtesy of Carlo Pantano.[41]

b) After corrosion.[41]

c) Depth compositional profile obtained by AES-IM of the soda-lime-silica glass after corrosion.[41]

d) Auger surface spectrum of PNL 76-68 glass after corrosion.

e) Depth compositional profile obtained by AES-IM of the PNL 76-68 glass after corrosion. Rate of I.M. is between 30-100 Angstroms per minute. Data is normalized to the oxygen peak.

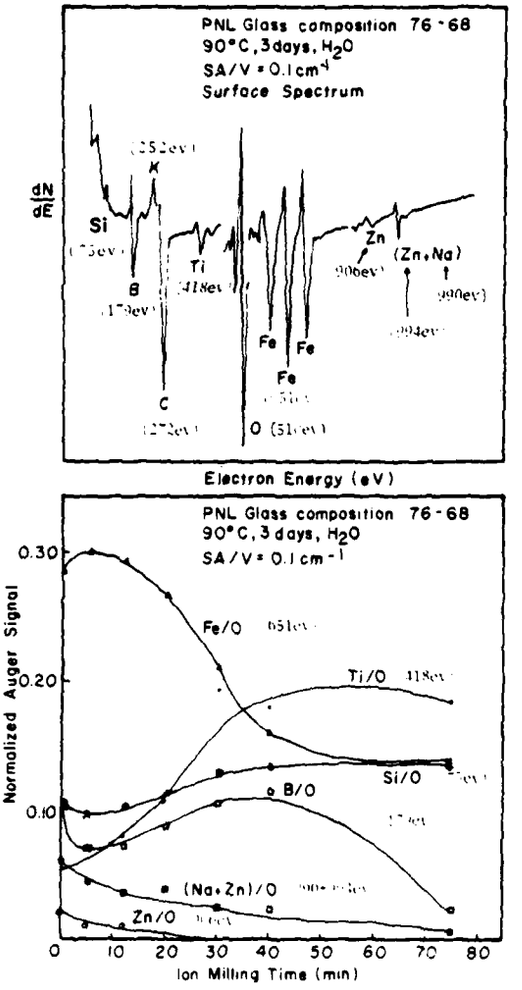

Fig. 6. Continued

depth within the glass surface. This depth compositional profile, which was constructed from many spectra such as those in Fig. 6b, indicates that Na has been leached to a depth of ~600 Å (0.06 μm) after 1 h at 37°C in water. The SiO_2 concentration is higher in the Na-depleted region, demonstrating the presence of the SiO_2-rich film discussed earlier. Exchange of Na^+ from the glass with H^+ (or H_3O^+) from the solution is responsible for the formation of the SiO_2-rich film.

The Auger spectra and depth compositional profiles are more complex for simulated nuclear waste glasses which contain 20 to 30 species. A spectrum of a PNL simulated waste glass is shown in Fig. 6d for a specimen corroded 3 days at 90°C using the test cell in Fig. 1d. The depth compositional profile (Fig. 6e) for this specimen indicates a buildup of Fe on the glass surface. The thickness of the Fe layer increased with exposure time up to 5 weeks (duration of experiment). These data suggest that the behavior observed in the infrared reflection spectrum of Fig. 3b may be due to the presence of this Fe layer on the glass surface.

One deficiency of AES in glass corrosion studies (also EMP and IRRS) is that the extent of network dissolution cannot be evaluated. The Auger spectrum of a corroded glass in which the SiO_2-rich film has been dissolved would be identical to the spectrum of the uncorroded glass. However, when AES-IM used in conjunction with solution analyses, both the extent of ion exchange (from AES-IM) and network dissolution (from solution analyses) can be determined.

E. Solution Analyses

Atomic absorption spectrophotometry (AA), atomic emission spectrophotometry (AE), pH, and colorimetry are used routinely to analyze corrosion

solution. With AA and AE, the concentration of individual elements in solution can be measured and converted to a useful corrosion index such as that defined by equations (4)-(6). The sensitivities of these methods are different for each element and are theoretically less than 1 ppm. In practice, the most reliable data can be obtained if the concentrations are greater than 1 ppm. Nevertheless, AA and AE provide far better accuracy than standard titration methods in which the individual concentrations of elements are not determined.

Monitoring the solution pH as a function of exposure time is essential because the dominant mechanisms of corrosion are dependent on this parameter as discussed above. The pH is usually measured using a calibrated pH meter with suitable probe.

Table I presents solution data obtained from a 33 mol % Na_2O - 67 mol % SiO_2 glass (33N) corroded under several different conditions of temperature and SA/V. An increase in either temperature or SA/V produces an increase in specie concentration in solution for a specified exposure time. However, the mechanisms responsible for these increases are different. At a constant SA/V, increasing the tempertures causes an increase in rate at which species are removed from glass (i.e., increase in reaction rate constant). An increase in SA/V at constant temperature merely provides a larger surface area of glass from which to obtain these species. The actual rate of specie release per unit area is not dependent on SA/V as long as the mechanism of corrosion does not change.

The values of α are listed in Table I. It can be seen that at very short times and low exposure temperatures α is small, indicating that ion exchange is the major mechanism of corrosion. Shortly after the pH increases above

TABLE I - Solution Data for a 33 Mol % Na_2O - 67 Mol % SiO_2 Glass

Temp °C	Time (h)	SA/V (cm^{-1})	pH	Na^+ (ppm)	SiO_2 (ppm)	α
25	0.5	0.1	8.68	10	2	0.08
25	0.5	1.0	10.06	110	124	0.43
90	0.5	0.1	11.24	1600	4286	1.00

$\sim$9, $\alpha \rightarrow 1$ due to network dissolution. The time at which α reaches 1 corresponds to point d in Fig. 2. When α is 1, as is the case for the specimen corroded for 0.5 h at 90°C with SA/V = 0.1 cm^{-1}, the film thickness is equal to zero. The SEMs representative of ion exchange and network dissolution are shown in Figs. 4a and c, respectively.

Solution data for a PNL 76-68 glass are presented in Table II. It can be seen that this glass is significantly more durable than the binary soda-silicate glass exposed to the same temperature and SA/V. Glass constituents other than those in Table II might also be present in the corrosion solution in concentrations below the detection limits of our AA spectrophotometer. Although a significant buildup of Fe on the glass surface was observed with AES (Fig. 63), no iron was detected in the corrosion solution. Alpha values are not usually calculated for these multicomponent glasses due to the complexity of the surface reactions.

Solution data are not always adequate for characterizing glass corrosion. For instance, solution data alone can be misleading when solution limits are exceeded and precipitation from solution onto the specimen surface occurs. A more reliable interpretation results if solution data are supplemented with surface analysis data.

Summary

The first priority in any glass corrosion experiment is the selection of a suitable test procedure. The test procedure should ensure that all critical parameters are controlled properly for the duration of the experiment. Additionally, the test should be designed so that sufficient information can be derived from both solution and sample. The static corrosion test

TABLE II - Solution Data for a Soda Borosilicate Simulated Nuclear Waste Glass. PNL Composition 76-68.

Temp °C	Time	SA/V (cm^{-1})	pH	ppm*					
				B_2O_3**	SiO_2†	Na_2O	MoO_3	Cs_2O	CaO
90	1 day	0.1	5.87	7.08	4.50	2.29	0.15	0.21	0.31
			6.15	7.08	5.00	2.29	0.30	0.21	0.31
90	1 week	0.1	6.28	21.89	18.25	7.28	0.75	0.64	0.35
			6.25	28.98	21.50	7.41	0.75	0.64	0.35
90	5 weeks	0.1	4.35	48.30	62.50	35.04	0.75	2.33	1.12
			4.14	52.81	82.50	32.35	0.60	2.65	1.12

Table illustrates data from duplicate test specimens

*Sr and Fe were searched for but not found in any of the corrosion solutions.

**Determined with colorimetry (Carmine method).

†Determined with colorimetry (Heterpoly Blue method).

shown in Fig. 1f and the modified ISO test illustrated in Fig. 1d have been extensively used in our laboratory and both have provided satisfactory results.

No single analytical method is capable of completely characterizing glass corrosion processes. For instance, solution analysis provides little information on the development and growth of the SiO_2-rich surface film, or on precipitation reactions due to supersaturation. It can, however, be used to distinguish between ion exchange and network dissolution. SEM can be used to characterize the morphological surface changes that result from glass corrosion including precipitate formation, dehydration of the SiO_2-rich layer, and pitting. The development of thick SiO_2-rich film can be determined with IRRS. When the sequential polishing technique is coupled with IRRS the growth and dissolution of thick SiO_2-rich films can often be monitored.

Very durable glasses may develop a thin SiO_2-rich layer over long exposure times. AES-IM is required to characterize these films. It is recommended that all specimens to be evaluated with AES-IM first be examined with SEM in order to reveal surface morphology that might influence the surface spectrum and ion milling characteristics of the glass.

Ideally, the study of glass corrosion should include a combination of techniques and at the very least one surface analysis and one solution analysis should be performed for each exposure condition.

Acknowledgments

This work was funded partially by the AFOSR under Grant No. 77-3210. Simulated nuclear waste samples and partial funding were also provided by Battelle Pacific Northwest Laboratories.

References

1. Bacon, F. R., "Chemical Durability of Silicate Glass", Glass Ind. 49[8] 438-439, 442-446; [9] 494-499; [10] 554-559 (1960).

2. Doremus, R. H., Glass Science, New York: John Wiley & Sons, 1973, Chapter 3, "Chemical and Surface Properties", pp. 213-252.

3. Das, C. R., "A Review of the Chemical Resistance of Glass", Indian Ceram. Soc., 24 [1] 12-23 (1965).

4. Eitel, W., Silicate Science, Vol. 8 in series. New York: Academic Press (1976): Chapter V, "Chemical Durability of Glass", pp. 237-277; update of Vol. 2, pp. 487-519 (1965).

5. Ernsberger, F. M., "Properties of Glass Surfaces", pp. 529-572 in Annual Review of Materials Science, ed., by R. A. Huggins, Annual Reviews, Inc., Palo Alto, Calif., Vol. 2 (1972).

6. Hench, L. L., and D. E. Clark, "Physical Chemistry of Glass Surfaces", J. Noncryst. Sol., 28, 83-105 (1978).

7. Holland, L., The Properties of Glass Surfaces, London: Chapman Hall, Chapter 3, "Surface Chemistry and Corrosion of Glass", 122-192 (1964).

8. Morey, G. W., The Properties of Glass, New York: Reinbold (1938); 2nd edition (1954), Chapter IV, "The Chemical Durability of Glass", pp. 101-131.

9. Weyl, W. A., and E. C. Marboe, The Constitution of Glasses: A Dynamic Interpretation, Vol. II, pt2, Chapter XXIII, "Surface Chemistry of Glasses", pp. 1010-1278, New York: Wiley (1967).

10. Clark, D. E., C. G. Pantano, Jr., and L. L. Hench, Corrosion of Glass, Books for Industry, New York, 77 pp. (1979).

11. Beattie, I. R., "Corrosion of Glass Surfaces: Bibliography", J. Soc. Glass Technol., 36, 37-45 NR (1952).

12. Gottardi, V., ed., The Chemical Durability of Glass - A Bibliographic Review of the Literature, International Commission on Glass, Institut du Verre, Paris, I., 76 pp. (1965); II., 109 pp. (1973).

13. Ethridge, E. C., D. E. Clark, and L. L. Hench, "Effects of Glass Surface-Area to Solution-Volume Ratio on Glass Corrosion", Phys. Chem. Glasses, 20 [2] 35-40 (1979).

14. Sanders, D. M., and L. L. Hench, "Surface Roughness and Glass Corrosion", Bull. Am. Ceram. Soc., 52 [9] 666-669 (1973).

15. Dilmore, M. F., D. E. Clark, and L. L. Hench, "Corrosion Behavior of Lithia Disilicate Glass in Aqueous Solutions of Aluminum Compounds", Am. Ceram. Soc. Bull., 58 [11] 1111-1114 (1979).

16. Hench, L. L., "Bio Ceramics", Science of Ceramics, 9, 193-211 (1977).

17. Barrett, J. M., D. E. Clark and L. L. Hench, "Glass Ceramic Dental Restorations", Patent Pending.

18. Clark, D. E., and E. C. Ethridge, "Corrosion of Enamels", accepted by the J. Am. Ceram. Soc.

19. Mendel, J., "High Level Waste Glass", Nuclear Technology, 32, 82-87 (1977).

20. Clark, D. E., E. Lue Yen-Bower, and L. L. Hench, "Corrosion Behavior of Zinc-Borosilicate Simulated Nuclear Waste Glass", International Symposium Proceedings on Ceramics in Nuclear Waste Management, Cincinnati, Ohio, May 1979.

21. American Society for Testing and Materials, "Standard Method of Test for Resistance of Glass Containers to Chemical Attack", ASTM Designation C225-73, ASTM Standards, Pt. 13, 184-189 (1973).

22. International Atomic Energy Agency (IAEA) ed. by Hespe, E. D., "Leach Testing of Immobilized Radioactive Waste Solids", A Proposal for a Standard Method, Atomic Energy Review 9, 195-207 (1971).

23. International Standards Organization (ISO), "Long-Term Testing of Radioactive Waste Solidification Products", draft.

24. Schmidt, Yu. A., Structure of Glass, Vol. 1, translated from Russian by E. B. Uvarov, Consultants Bureau, N.Y., 1958.

25. Sanders, D. M., and L. L. Hench, "Mechanisms of Glass Corrosion", J. Amer. Ceram. Soc., 56 [7] 373-77 (1973).

26. El-Shamy, T. M., J. Lewins and R. W. Douglas, "Dependence on pH of Decomposition of Glasses by Aqueous Solutions", Glass Technol., 13 [3] 81-87 (1972).

27. Douglas, R. W., and T. M. El-Shamy, "Reactions of Glasses with Aqueous Solutions", J. Amer. Ceram. Soc., 50 [1] 1-8 (1967).

28. Das, C. R., and R. W. Douglas, "Studies on the Reaction Between Water and Glass. Part 3", Phys. and Chem. Glasses, 8 [5] 178-184 (1967).

29. Boksay, Z., G. Bouquet, and S. Dobos, "The Kinetics of the Formation of Leached Layers on Glass Surfaces", Phys. and Chem. Glasses, 9 [2] 69-71 (1968).

30. Doremus, R. H., "Interdiffusion of Hydrogen and Alkali Ions in A Glass Surface", J. Noncryst. Sol., 19, 137-144 (1975).

31. Jellyman, P. E., and J. Procter, "Infrared Reflection Spectra of Glasses", J. Soc. Glass Technol., 39, 173-192 (1955).

32. Sweet, J. R., and W. B. White, "Study of Sodium Silicate Glasses and Liquids by Infrared Reflectance Spectroscopy", Phys. Chem. Glasses, 10 [6] 246-251 (1969).

33. Simon, I., and H. O. McMahon, "Study of Some Binary Silicate Glasses by Means of Reflection in the Infrared", J. Amer. Ceram. Soc., 36 [5] 106-164 (1953).

34. Sanders, D. M., W. B. Person, and L. L. Hench, "New Methods for Studying Glass Corrosion Kinetics", Appl. Spectrosc., 26 [5] 530-536 (1972).

35. Clark, D. E., M. F. Dilmore, E. C. Ethridge, and L. L. Hench, "Aqueous Corrosion of Soda-Silica and Soda-Lime-Silica Glass", J. Amer. Ceram. Soc., 59 [1] 62-65 (1976).

36. Pfund, A. J., "The Aging of Glass Surfaces," J. Optical Soc. of Amer., 36 [2] 95-99 (1946).

37. Pantano, C. G., Jr., D. B. Dove, and G. Y. Onoda, Jr., "AES Analysis of Sodium in a Corroded Bioglass Using a Low-Temperature Technique", Appl. Phys. Lott, 26 [11] 601-602 (1975).

38. Clark, D. E., L. L. Hench, and W. A. Acree, "Electron Microprobe Analysis of Na_2O-CaO-SiO_2 Glass", J. Amer. Ceram. Soc., 58 [11-12] 531-532 (1975).

39. Lineweaver, J. L., "Oxygen Outgassing Caused by Electron Bombardment of Glass", J. Appl. Phys., 34 [6] 1786-1791 (1963).

40. Varshneya, A. A., A. R. Cooper and M. Cable, "Changes in Composition During Electron Microprobe Analysis of K_2O-SrO-SiO_2 Glass", J. Appl. Phys., 37 [5] 2199 (1966).

41. Pantano, C. G., Jr., Compositional Analysis of Glass Surfaces and their Reaction in Aqueous Environments, A Dissertation presented to the Graduate Council of the University of Florida, Gainesville, Florida (1976).

SECTION III

AQUEOUS CORROSION OF $Li_2O \cdot 2SiO_2$ GLASS-CERAMICS

By

W. J. McCracken, D. E. Clark and L. L. Hench

Introduction

The corrosion behavior of $Li_2O \cdot 2SiO_2$ (33L) glass has been studied extensively.[1-3] During the early stage of reaction with a neutral aqueous environment, Li^+ is selectively leached from the glass surface via ion exchange with H^+ (or H_3O^+) from the solution. In a closed system in which the ratio of glass surface area to volume of solution (SA/V) is high, the pH of the solution will increase with exposure time. If the pH is permitted to go above approximately 9 a second mechanism of glass corrosion will become important.[4,5] This mechanism involves dissolution of the glass network and is due to OH^- attack on the silicon-oxygen bonds. The relative importance of the ion exchange and network dissolution reactions is dependent on numerous factors including solution pH, exposure temperature, time and (SA/V). The corrosion mechanisms and kinetics of vitreous $Li_2O \cdot 2SiO_2$ have been studied by Sanders and Hench[1] and Ethridge and Hench[3] for a wide range of environments. Additionally, the crystallization kinetics for this glass have been well characterized by Hench *et al.*[6] and Freiman and Hench.[7,8] It is well known that controlled nucleation and crystallization can significantly improve the mechanical properties of the resulting glass-ceramic over those characteristic of the glass with the same composition.[9] During crystallization, the microstructure of the glass is altered by the presence of both crystals and phase boundaries. If the glass is only partially crystallized, the microstructure may consist of isolated crystals dispersed in a vitreous matrix. Recent evidence indicates that even the vitreous phase in the glass-ceramic may have a structure that is different from that of the as-cast glass.[10] Thus, it is not unreasonable to assume that the corrosion behavior of the glass-ceramic may be quite different from that of the glass.

The objective of this study is to establish the effects of controlled crystallization on the chemical durability of the $Li_2O \cdot 2SiO_2$ glass-ceramic system. The 33L composition has been chosen for two reasons: 1) as already mentioned, the crystallization and corrosion behavior of the glass are well characterized, and 2) since this is a stoichiometric composition, the crystalline phase has the same composition as the glass phase. This permits the evaluation of corrosion independent of compositional variations that may accompany crystallization of nonstoichiometric compositions.

Experimental

The $Li_2O \cdot 2SiO_2$ (33L) glass and glass-ceramic specimens used in this study were prepared using techniques described in a previous paper.[10] Briefly, the glass was melted in an electric muffle furnace at 1350°C for 24 h. Crylinders 2.5 cm in diameter and 6.0 cm long were cast in a graphite mold and annealed at 350°C for 4 h. These glass cylinders were nucleated at 457°C for 24 h and crystallized at 550°C for various times yielding 20%, 60% and 90% volume fraction (V_v) crystallization. The percentage volume fraction crystallization was determined by using optical scanning techniques of applied stereology.[11] The cylinders were sliced with a diamond wafering saw into 0.3 cm thick disks the surfaces of which were polished through 600 grit with SiC paper prior to exposure.

Specimens of 33L glass and partially crystallized 33L glass were exposed to an environment of either demineralized water, 0.1M NaOH, or 0.1M HCl maintained at 100°C* for up to 10 h. Duplicate specimens were tested for

*Magni-Whirl(R) Constant Temperature Bath, Blue M Electric Co., Blue Island, Illinois.

each exposure condition to evaluate reproducibility. The maximum difference in the solution data between any of the duplicates was 46 ppm (265 ± 23 ppm) of SiO_2 and 11 ppm (135 ± 5.5 ppm) of Li^+. The detection limits were 1.0 ppm for SiO_2 and 0.1 ppm for Li^+. The ratio of surface area of exposed material to solution volume (SA/V) was 2.0 cm^{-1}. Infrared reflection spectra* were obtained for all specimens in the spectral region 1300-600 cm^{-1} both prior to and after aqueous exposure . SEMs** were also taken for selected samples. The corrosion solutions were analyzed by measuring pH^+, Li^+ concentration^{++}, and SiO_2 concentration^{+++}.

Results and Discussion

Scanning electron micrographs for 33L glass containing four volume fractions of crystallization (V_v = 0%, 20%, 60%, 90%) are shown in Figs. 1-4. These figures illustrate representative surfaces for each material after exposure to acidic, neutral and basic solutions. Micrographs of unreacted specimens are not shown but are similar to the micrograph of glass (V_v = 0%) exposed for 2 h to neutral solution (Fig. 1). Significant differences in the surface microstructural features as a function of percent crystallization can be seen after exposure, particularly to neutral and basic solutions. The crystalline phase is more pronounced on the specimens exposed to the neutral and basic solutions than on those exposed to the acidic solution.

---

*Model 467, Perkin-Elmer Infrared Reflection Spectrometer, Norwalk, CT.
**Model JSM-35C, JEOL Ltd., Tokyo, Japan.
$^+$Model 801A, Orion Research, Inc., Cambridge, MA.
$^{++}$Model 603, Perkin-Elmer Spectrophotometer (atomic emission), Norwalk, CT.
$^{+++}$Model DR-3803, Hach Chemical Co., Ames, IA.

The similarity between the surfaces exposed to either neutral or basic solutions is not surprising because the pH of the neutral solution increases with exposure time under static exposure conditions. The increase in solution pH is due to exchange between Li^+ ions from solution, resulting in an increase in OH^- ions in solution.[12,13] Thus, long exposure times to a static neutral solution favors network dissolution as does exposure to a basic solution even for short times.

When V_v = 0% (Fig. 1), two types of corrosion are observed over a wide range of pH values (pH = 1-13). In acidic solutions the primary mode of corrosion is ion exchange. There are two features in the micrograph in Fig. 1 that support this conclusion: 1) surface cracks, and 2) polishing scratches. The cracks are related to the ion exchange mechanism and usually appear after the specimen has been removed from solution and permitted to dry, or after the specimen has been subjected to a vacuum. The extent of ion exchange required to produce surface cracks is not known but is probably dependent on the composition of the glass. The fact that the polishing scratches do not exhibit noticeable dimensional changes during exposure to the acidic solution suggest that network dissolution is minimal in the low pH environment. In contrast, the specimens exposed to the basic solutions exhibit broadened polishing scratches and no surface cracks. Thus, the dominant mechanism of corrosion is network dissolution. The specimens exposed to the neutral solution show indications of both ion exchange and network dissolution with the latter being more apparent after long exposure times.

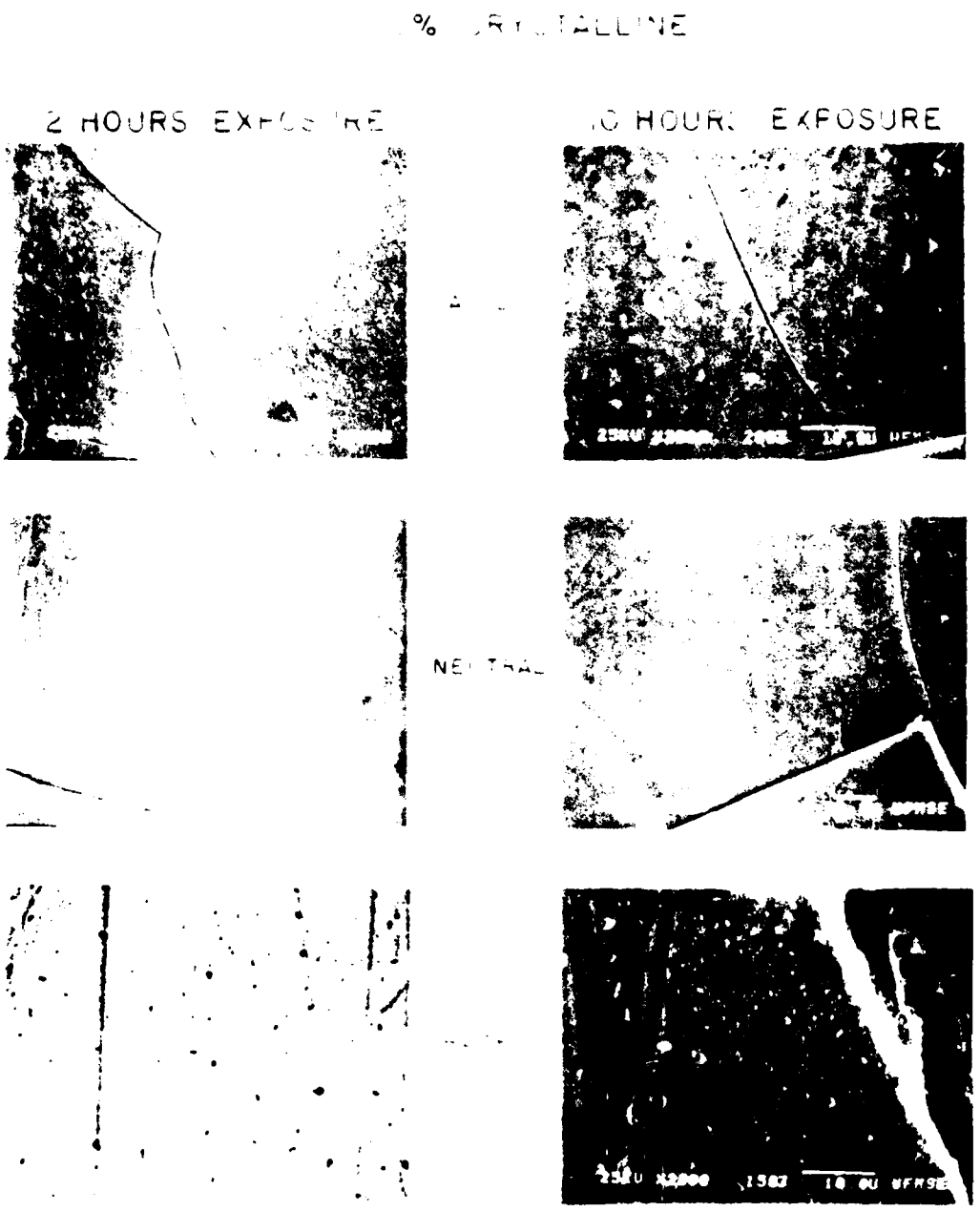

Fig. 1. Scanning electron micrographs of 33L glass after 2 h and 10 h exposure in acid, neutral, and base aqueous solution at 100°C with SA/V = 2.0 cm^{-1}.

Three types of attack are observed on the glass-ceramic containing 20 percent crystallization (Fig. 2). In acidic solutions, only ion exchange occurs as was the case with glass (V_v = 0%). However, in both neutral and basic solutions network dissolution of the glassy phase, and preferential attack of the boundary between the glassy and crystalline phases are significant. The preferential phase boundary attack may be due to stresses or compositional gradients at the interface. Similar attack has been reported by Baylor and Brown[14] for phase separated borosilicate glasses. Surface cracks in the glassy phase of the specimen exposed to the neutral solution indicates the presence of an ion exchanged layer even after 10 h of exposure. These cracks do not occur in the crystalline phase. Possibly the most important information provided by Fig. 2 is the relative durabilities of the glassy and crystalline phases. The fully exposed crystals shown in this figure demonstrate that the crystalline phase is more resistant to network dissolution than the glassy phase.

As the crystalline phase increases from V_v = 20% to V_v = 60% and V_v = 90%, the surface morphology changes from that of isolated crystals in a vitreous matrix to ones dominated by the crystalline phase (Figs. 3 and 4). This is most easily seen on the specimens exposed to the neutral and basic solutions. Network dissolution preferentially removes the glass and highlights the crystalline phase. Exposure to the acidic solution produces essentially no network dissolution but does permit ion exchange as evidenced by the surface cracks visible on the 10 h specimens in Figs. 3 and 4.

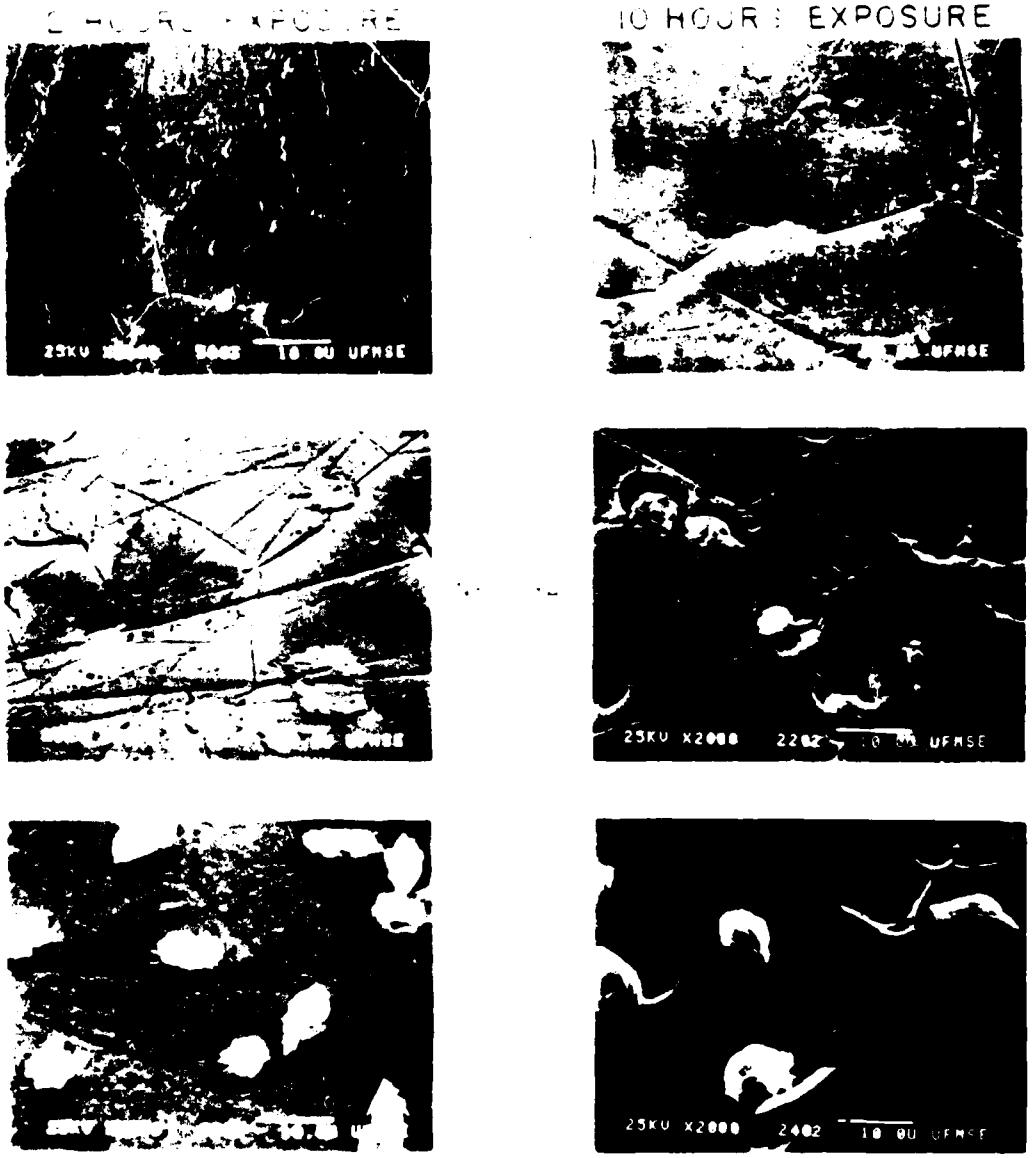

Fig. 2. Scanning electron micrographs of 33L - 60% crystalline glass-ceramic after 2 h and 10 h exposure in acid, neutral, and base aqueous solutions at 100°C with SA/V = 2.0 cm^{-1}.

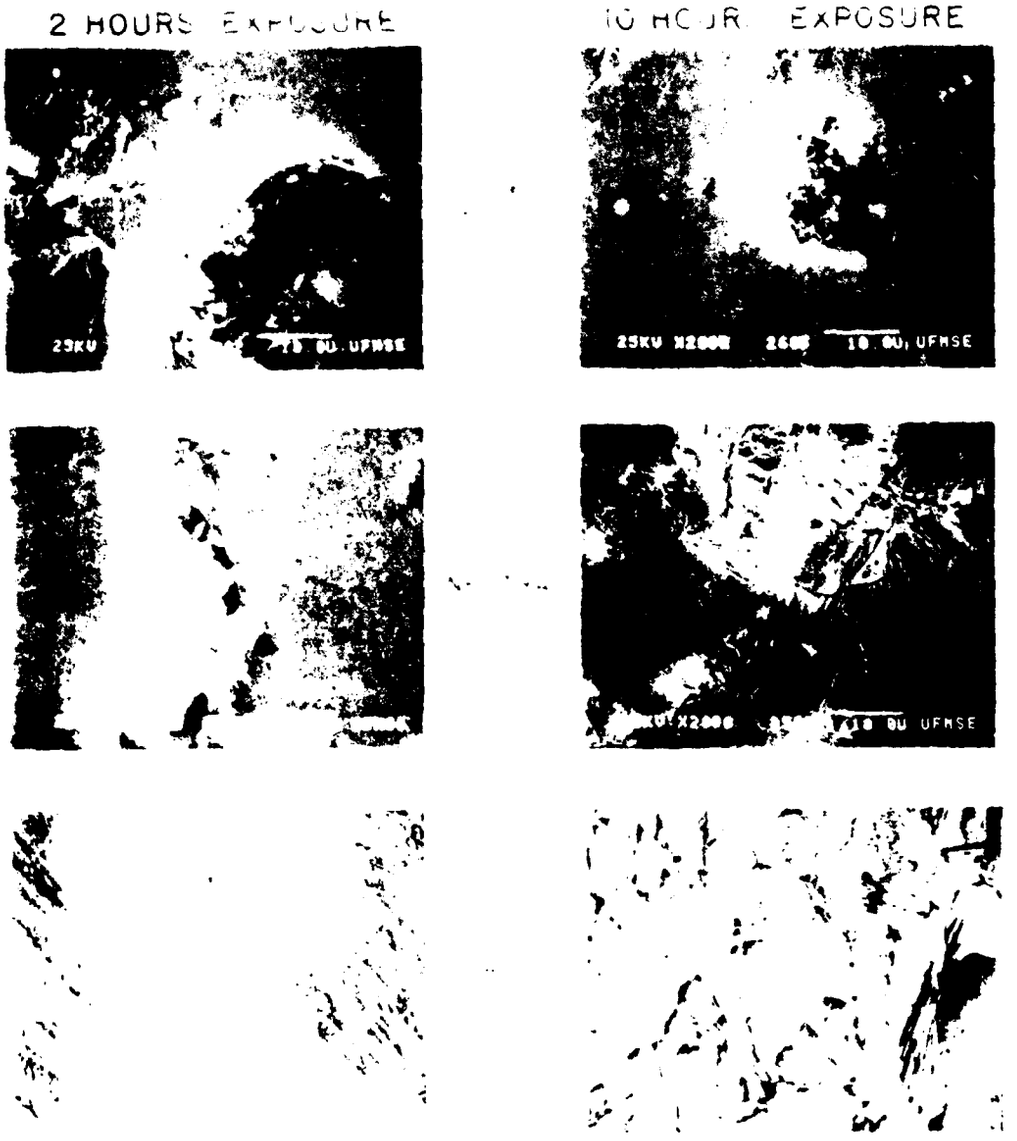

Fig. 3. Scanning electron micrographs of 33L - 60% crystalline glass-ceramic after 2 h and 10 h exposure in acid, neutral, and base aqueous solutions at 100°C with SA/V = 2.0 cm^{-1}

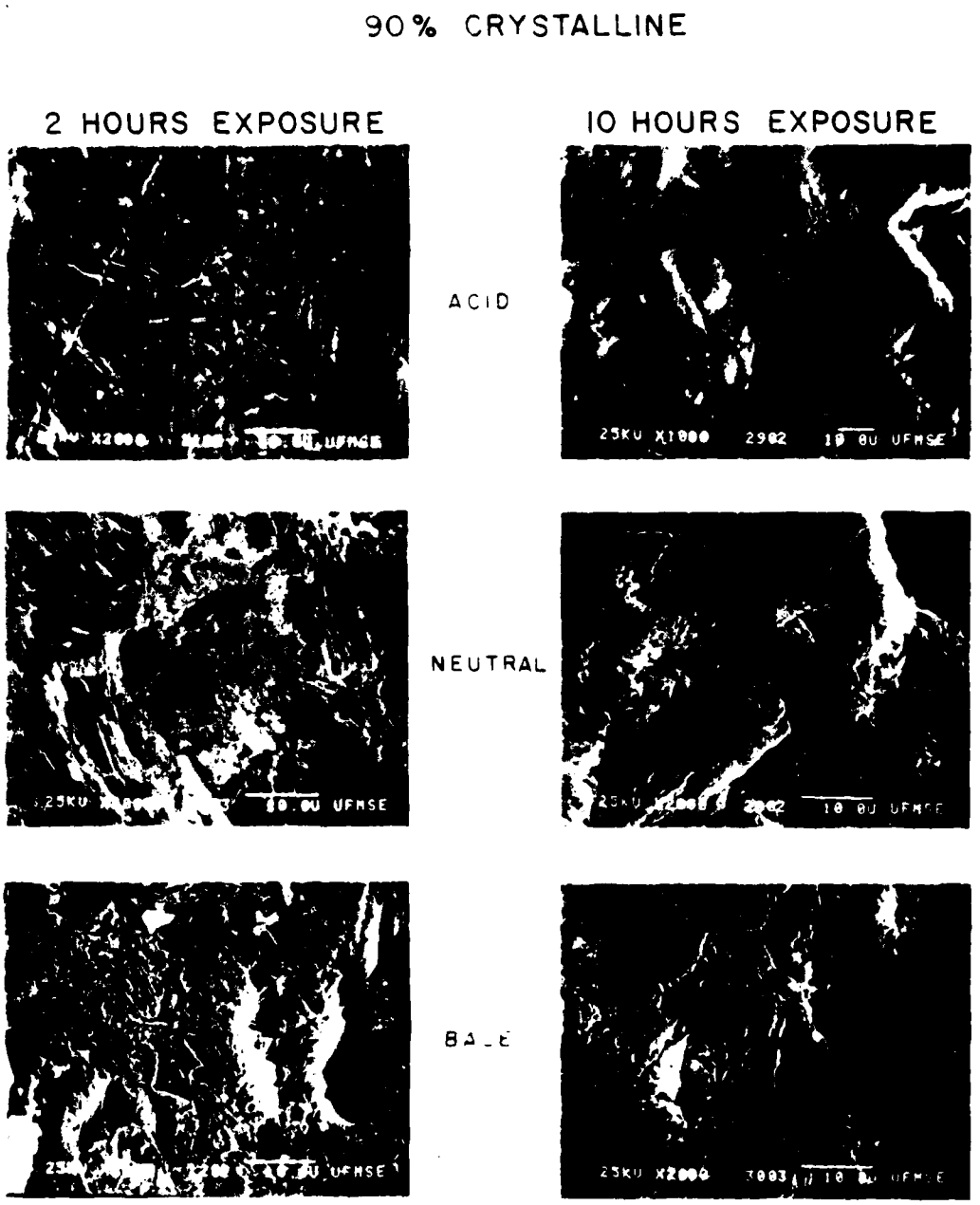

Fig. 4. Scanning electron micrographs of 33L - 90% crystalline glass-ceramics after 2 h and 10 h exposure in acid, neutral and base aqueous solutions at 100°C with $SA/V = 2.0\ cm^{-1}$.

Infrared reflection spectra shown in Fig. 5 for 33L glass exposed to a wide range of pH solutions are consistent with those reported in previous work.[2,15] In the uncorroded glass spectrum, the peak located at 1030 cm^{-1} (LS) is due to symmetrical Si-O-Si stretching vibrations in a network containing Li^+, and the peak at 930 cm^{-1} (NS) is caused by Si-nonbridging oxygen vibrations. The spectrum of vitreous silica is also included in this figure for the purpose of instrument calibration and comparison. The peak at 1100 cm^{-1} (S) for vitreous silica is due to Si-O-Si symmetrical stretching vibrations in a pure SiO_2 structure. During corrosion of 33L glass in the acidic solution, the LS peak shifts to higher wavenumbers and increases in intensity (% reflection) progressively approaching the S peak of vitreous silica as corrosion time increases. These alterations in infrared reflection spectra are caused by the leaching of Li^+ (ion exchanging with H^+ or H_3O^+) from the glass, resulting in the development of a SiO_2-rich film on the glass surface.[16] Infrared spectra show that the short time corrosion behavior of 33L glass in the static neutral solution is similar to that in the acidic solution. That is, initially there is a development of a SiO_2-rich film on the surface of the glass. However, the peak intensity decreases with long exposure times (i.e., >4 h). This is usually indicative of surface roughening due to network dissolution of the SiO_2-rich film.[12] As discussed earlier, the pH of the static neutral solution increases with exposure time, and the resulting high OH^- concentration enhances network dissolution. The general shape of the infrared spectra for 33L glass exposed to the basic solution does not change. The spectral intensity, however, continuously decreases

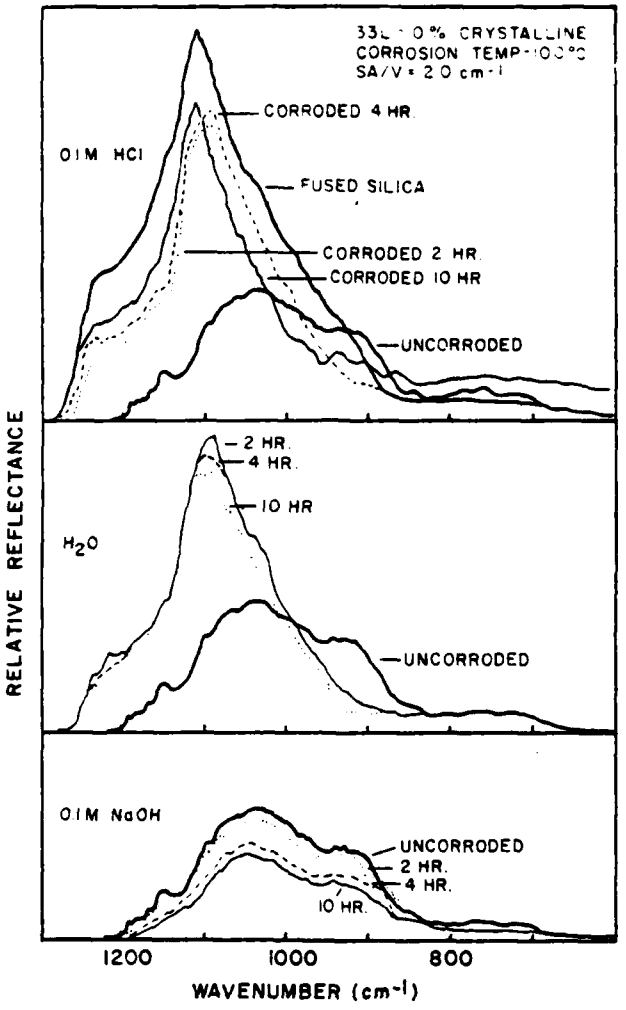

Fig. 5. Infrared reflection spectra of 33L glass before and after acid, neutral, and base aqueous solution.

with exposure time. These spectral variations indicate that no SiO_2-rich film is developed during exposure to the high pH solution. Surface roughening due to network dissolution is responsible for the decline in intensity. Network dissolution enlarges the polishing scratches and causes pitting as shown in the micrographs in Fig. 1.

Figure 6 shows the infrared reflection spectra for 33L glass with 20% crystallization exposed to the acidic, neutral and basic solutions. These spectra are basically the same as those for the glass exposed to similar environments. The major exceptions are the spectra corresponding to the 10 h exposures in neutral and basic solutions. The lower intensities observed on the 33L-20% V_v specimen for these exposures indicates increased surface roughening. The increased surface roughening is due to preferential network dissolution of the glassy phase exposing the crystals as shown in Fig. 2. These data suggest that the glassy phase of 33L - 20% V_v glass-ceramic is primarily responsible for the observed surface corrosion.

Infrared reflection spectra for 33L glass with 60% V_v and 90% V_v crystallization exposed to acidic, neutral and basic solutions are shown in Figs. 7 and 8, respectively. The similarity of the spectra for these two materials both prior to and after corrosion facilitates their joint discussion. These spectra exhibit some definite changes in surface structure and corrosion behavior compared to the 33L glass and 33L glass with 20% V_v crystallization. The broad LS peak at 1030 cm^{-1} is due with the glassy phase. The well defined peaks at 1210 cm^{-1}, 1100 cm^{-1}, and 750 cm^{-1} have been previously associated with the crystalline phase.[10] The positions of these latter three peaks for 33L-60% V_v and 33L-90% V_v

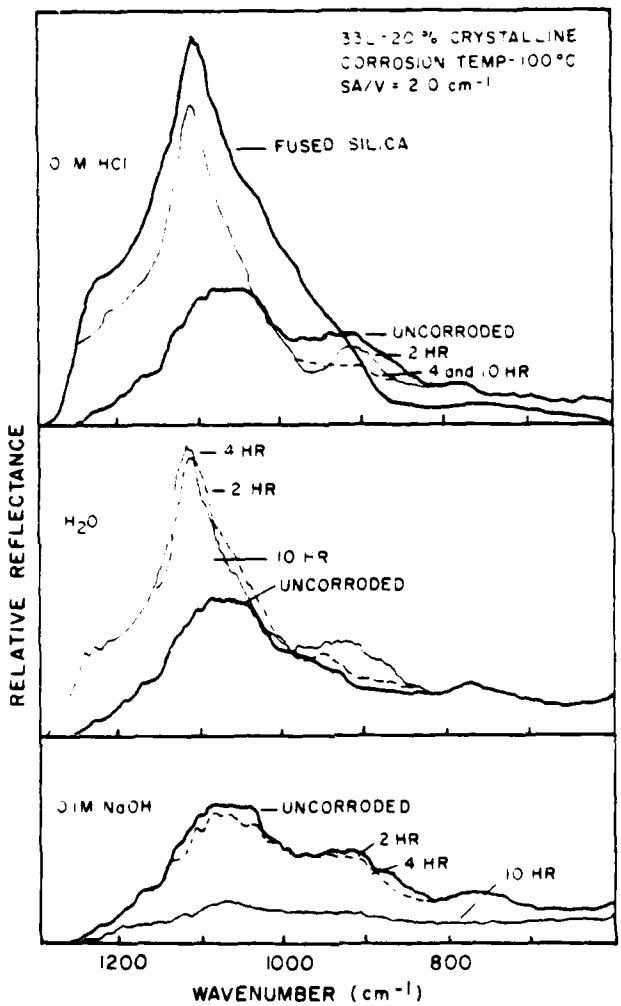

Fig. 6. Infrared reflection spectra of 33L-20% crystalline glass-ceramic before and after acid, neutral, and base aqueous corrosion.

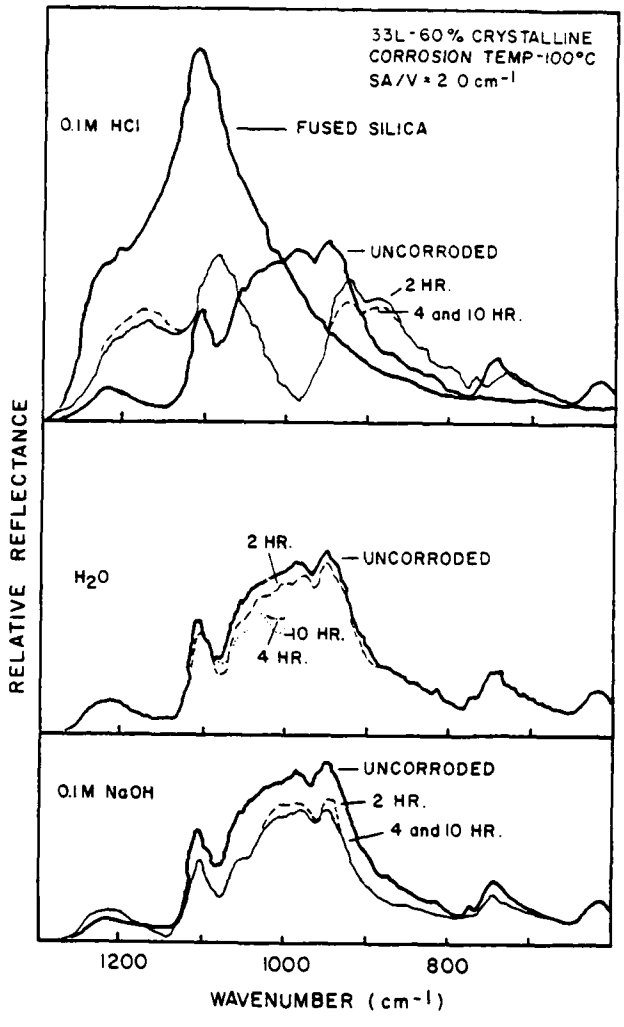

Fig. 7. Infrared reflection spectra of 33L-60% crystalline glass-ceramic before and after acid, neutral and base aqueous corrosion.

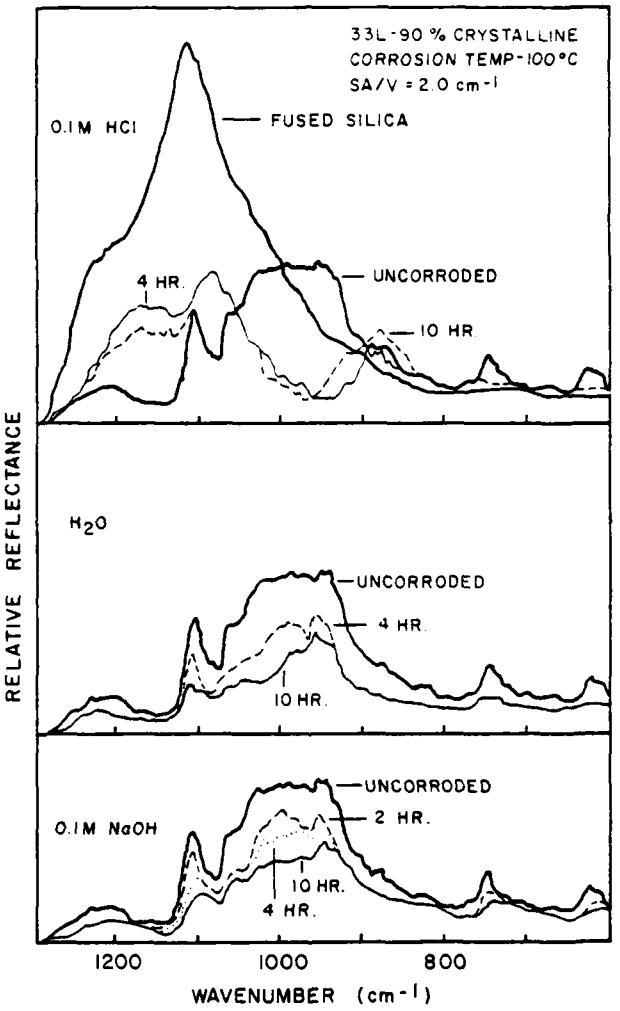

Fig. 8. Infrared reflection spectra of 33L-90% crystalline glass-ceramic before and after acid, neutral, and base aqueous corrosion.

are practically unaltered during exposure to neutral and basic solutions but their intensities generally decrease with time. However, significant peak position alterations are observed when the materials are exposed to the acidic solution. These peak position alterations are thought to be due to the exchange of Li^+ ions from both the glassy and crystalline surfaces with the H^+ (or H_3O^+) ions from the solution[17] resulting in the development of a SiO_2-rich film on both surfaces. The general decrease in spectral intensity on the surfaces exposed to the neutral and basic solutions is consistent with the preferential dissolution of the glassy phase resulting in surface roughening as shown in Figs. 3 and 4.

Solution data are presented in Fig. 9 (and tabulated in Table I) for each exposure condition and material. In general the concentrations of Li^+ and SiO_2 increased in solution as exposure time increased for all exposure times and materials. The pH of the neutral solution also increases with time for all materials. This pH increase is due to exchange of Li^+ ions from the material surface with H^+ or H_3O^+ ions from solution. Both the change in pH and Li^+ ion concentration are less for the glass-ceramics containing large percentages of crystals exposed to the neutral solution (Table I and Fig. 9C). These data suggest that the ion exchange of Li^+ is slower from the crystalline surface than from the glass surface since the glass-ceramics have a smaller area of glass exposed to the solution. The same trend in Li^+ ion concentration is observed in the materials exposed to the basic and acidic solutions (with the exception of the 10 h exposure - 90% crystal).

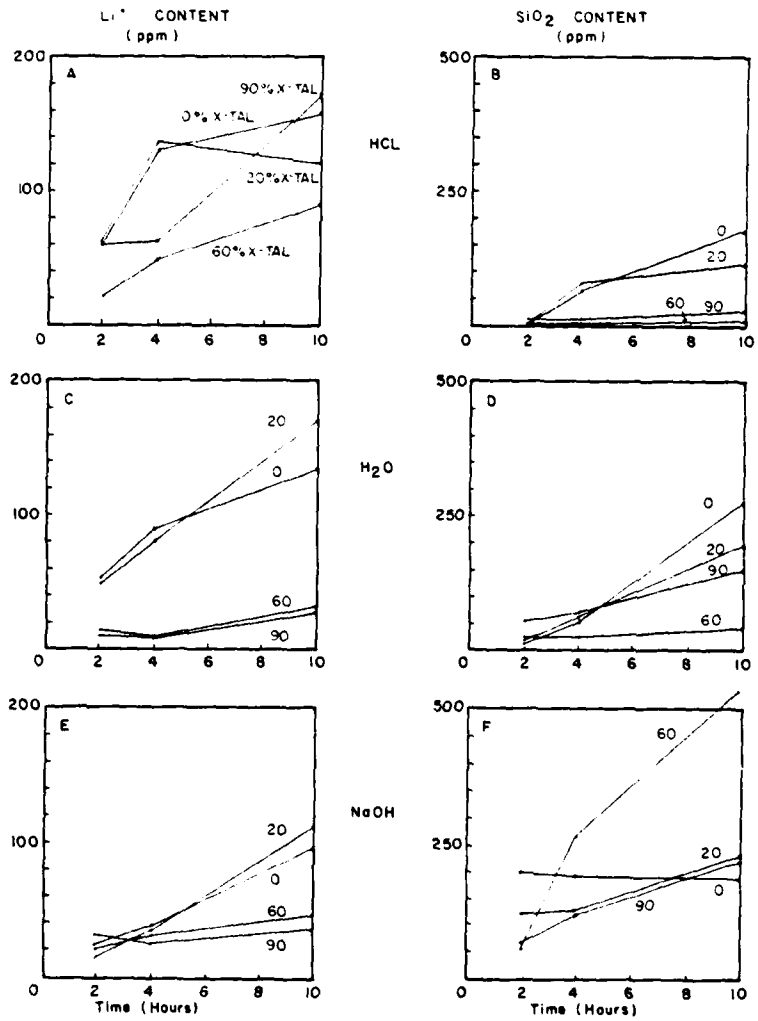

Fig. 9. Li^+ concentration and SiO_2 concentration in corrosion solution versus time for 33L glass and glass-ceramics in acid, neutral, and base aqueous solutions.

TABLE I. Solution Data for 33L Glass-Ceramic Corrosion in Acid, Neutral and Base Aqueous Environments.

		Percent Crystallization			
		Glass	20%	60%	90%
HCl					
pH	2 h	1.7	1.8	1.6	1.8
	4 h	1.8	1.8	1.7	1.9
	10 h	2.0	2.1	1.9	2.2
Li^+					
(ppm)	2 h	58	59	24	58
	4 h	125	135	50	61
	10 h	160	126	90	168
SiO_2					
(ppm)	2 h	8	5	7	13
	4 h	70	90	12	15
	10 h	180	120	15	34
H_2O					
pH	2 h	11.8	11.7	10.1	8.8
	4 h	12.0	12.0	10.5	10.4
	10 h	12.2	12.2	10.6	10.4
Li^+					
(ppm)	2 h	54	46	12	13
	4 h	90	80	11	11
	10 h	135	170	33	29
SiO_2					
(ppm)	2 h	17	21	26	55
	4 h	58	65	30	70
	10 h	272	190	45	150
NaOH					
pH	2 h	12.7	13.0	12.7	13.0
	4 h	13.0	12.7	12.7	12.7
	10 h	12.9	12.9	12.7	12.9
Li^+					
(ppm)	2 h	24	22	15	31
	4 h	40	33	36	29
	10 h	100	118	51	40
SiO_2					
(ppm)	2 h	200	118	59	65
	4 h	188	125	265	120
	10 h	185	230	525	220

Corrosion Temp. - 100°C
$SA/V = 2.0\ cm^{-1}$

Initial pH - HCl (0.1M) - 1.025
- H_2O - 6.573
- NaOH (0.1M) - 12.964

The concentrations of SiO_2 in solution is an indication of the extent of network dissolution that has occurred on the materials (Fig. 9B,D,F). As expected the samples exposed to the acidic solution exhibited the smallest change in SiO_2 concentration with time and those exposed to the basic solutions exhibited the largest change. In acidic and neutral solution the glass-ceramics with 60% crystalline phase was the most durable material; it was the least durable material in the basic solution. As discussed earlier, considerable network dissolution of the glassy phase occurs on all of the materials exposed to the basic solution or to the static neutral solution for long times (see micrographs in Figs. 1-4). The relative high concentrations of SiO_2 in the basic solution for the 60 percent crystalline specimen is thought to be related to two factors: 1) extensive preferential attack of the phase boundaries, and 2) the relative high percentage of glass in the structure (i.e., 40%). Preferential boundary attack does not occur on glass with 0 percent crystallization; only uniform network attack occurs. On the glass-ceramic containing 90 percent crystallization, preferential phase boundary attack is significant but the percent glass affected is small (i.e., 10%). However, on the glass-ceramic containing 60 percent crystallization not only is preferential phase boundary attack significant, the volume of glass affected is large.

The above discussion has demonstrated that both the mechanism of attack and extent of attack on glass-ceramics depends on the percent crystallization, environmental exposure conditions, and duration of exposure. Thus, there is a wide range of possible surface morphologies, several of which are in Fig. 10.

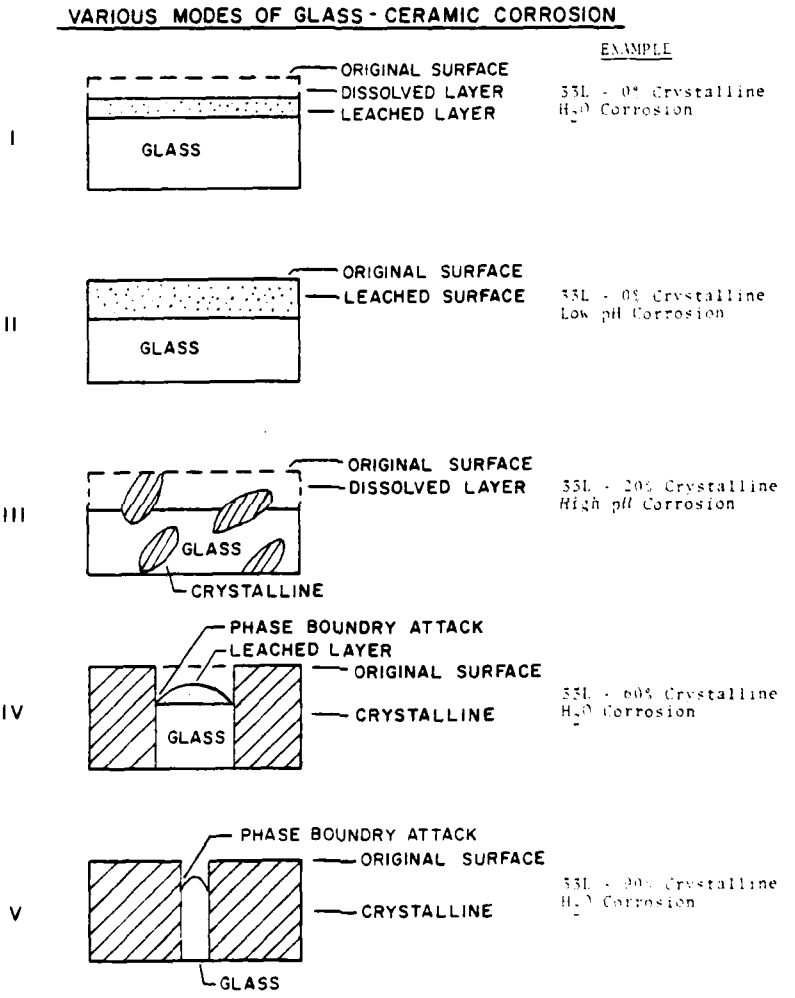

Fig. 10. Various modes of glass-ceramic corrosion for 33L glass-ceramics.

Summary

Crystallization significantly affects the corrosion behavior of $Li_2O \cdot 2SiO_2$ glass. In general, the least of surface damage is observed on all the materials when exposed to acidic solution and the most extensive surface alterations occur on all the materials exposed to the basic solutions. On glass, network dissolution occurs uniformly over the entire exposed surface. On glass-ceramics, network dissolution proceeds at different rates over the surface, with the highest rate occurring on the glassy phase. In addition to ion exchange and network dissolution, preferential attack of the boundary between the glassy and crystalline phases is important in glass-ceramic systems exposed to basic solutions, or to static neutral solutions for long times. Phase boundary attack does not appear to be significant on glass-ceramics exposed to acidic solutions. Overall the 90% crystallized glass-ceramic was the most durable material investigated.

Acknowledgments

The authors thank the Air Force Office of Scientific Research (Grant 77-3210) for partial financial support of this work.

References

1. D. M. Sanders and L. L. Hench, "Mechanisms of Glass Corrosion," J. Amer. Ceram. Soc., 57[7], 373-377 (1973).

2. D. M. Sanders, W. B. Person and L. L. Hench, "Quantitative Analysis of Glass Structure Using Infrared Reflection Spectra," Appl. Spectroscopy, 28[3], 247-255 (1974).

3. E. C. Ethridge, "Mechanisms and Kinetics of Binary Alkali-Silicate Glass Corrosion," Ph.D. Dissertation, Univ. of Fla. (1977).

4. T. M. El-Shamy, J. Lewins, and R. W. Douglas, "Dependence on the pH of the Decomposition of Glasses by Aqueous Solutions," Glass Technol., 13[3], 81-87 (1972).

5. R. W. Douglas and T. M. El-Shamy, "Reactions of Glasses with Aqueous Solutions," J. Amer. Ceram. Soc., 50[1], 1-8 (1967).

6. L. L. Hench, S. W. Freiman, and D. L. Kinser, "The Early Stages of Crystallization in $Li_2O \cdot 2SiO_2$ Glass," Phys. and Chem. of Glasses, 12[2], 58-63 (1971).

7. S. W. Freiman and L. L. Hench, "Kinetics of Crystallization in Li_2O $2SiO_2$ Glasses," J. Amer. Ceram. Soc., 51[7], 382-387 (1968).

8. S. W. Freiman and L. L. Hench, "Further Analysis of Glass Crystallization Kinetics," Ibid, 52[2], 111-112 (1969).

9. S. W. Freiman and L. L. Hench, "Effect of Crystallization on the Mechanical Properties of $Li_2O \cdot 2SiO_2$ Glass-Ceramics," Ibid., 55[2], 86-90 (1972).

10. W. J. McCracken, D. E. Clark and L. L. Hench, "Surface Characterization of Ceramed Composites and Environmental Sensitivity," in Proceedings of the Conference on Composites and Advanced Materials, Jan. 1978.

11. S. W. Freiman, "Applied Stereology," in Characterization of Ceramics, L. L. Hench and R. W. Gould, eds., Marcel Dekker, Inc., NY, 555-579 (1971).

12. D. E. Clark, C. G. Pantano, Jr., and L. L. Hench, Glass Corrosion, Books for Industry, New York, NY, (1979).

13. D. E. Clark, M. F. Dilmore, E. C. Ethridge, and L. L. Hench, "Aqueous Corrosion of Soda-Lime and Soda-Lime-Silica Glass," J. Amer. Ceram. Soc., 59[1-2], 62-65 (1976).

14. R. Baylor, Jr. and J. J. Brown, Jr., "Phase Separation of Glasses in the System $SrO-BrO_3-SiO_2$," J. Amer. Ceram. Soc., 59[3-4], 131-136 (1976).

15. D. M. Sanders and L. L. Hench, "Environmental Effects on Glass Corrosion Kinetics," Amer. Ceram. Soc. Bull., 52[9], 662-669 (1973).

16. D. E. Clark, E. C. Ethridge, M. F. Dilmore, and L. L. Hench, "Quantitative Analysis of Corroded Glass Using Infrared Frequency Shifts," Glass Tech., 18[4], 121-24 (1977).

17. J. F. Kay and R. H. Doremus, "Strength and Durability of a Glass-Ceramic Containing Spodumene Crystals," 57[11], 480-492 (1974).

SECTION IV

AQUEOUS CORROSION OF Li_2O-Al_2O_3-CaO-SiO_2 GLASS-CERAMICS

By

J. M. Barrett, D. E. Clark and L. L. Hench

Introduction

Glass-ceramics are presently used in many applications where good chemical resistance and strength are required. Examples of these may be found in the aerospace, electronics, medical, chemical, dental and household appliance industries. Additionally, the use of these materials as encapsulants for radioactive nuclear wastes generated by commercial and defense-related reactors is being considered.

Relatively little data has been reported on the corrosion properties of partially devitrified glass-ceramics. Studies by McCracken et al.[1] and Freiman and Hench[2] on stoichiometric lithia-disilicate glass-ceramics show that both the corrosion resistance and mechanical strength are improved as the extent of crystallization (ceraming) is increased. These results might be interpreted to suggest that an improvement in chemical durability always accompanies the ceraming process. Hench et al.[3] have shown that the composition of the crystalline phase is the same as the glassy phase for the stoichiometric lithia-disilicate glass-ceramics. These results suggest the absence of phase-boundary segregation in the binary lithia-disilicate system. However, this nearly ideal condition, in which no compositional variation or phase-boundary segregation occurs during crystallization, is rarely encountered in industrial glass-ceramics.

A four-component glass-ceramic (Li_2O-Al_2O_3-CaO-SiO_2) was studied in the present investigation. Unlike the binary lithia-disilicate system, the composition of the crystalline phase that develops during ceraming is

significantly different from the original glass composition. Thus, large compositional changes occur within the glassy phase of the glass-ceramic during crystallization. Since it is well known that aqueous durability is dependent on glass composition, the major objective was to evaluate the effects of the degree of crystallization on the extent of corrosion for these non-stoichiometric glass-ceramics.

Experimental Procedure

A 30.5 Li_2O-2.5 Al_2O_3-6.0 CaO-61.0 SiO_2 (mol %) glass (LACS), prepared by PPG*, was crushed and sieved to -100 mesh. Nb_2O_5 powder, and Pt as an aqueous solution of chloroplantinic acid, were added to the glass powders as nucleating agents. These mixtures were dried 3 h at 520°C and crystallized at 620°C for various times (Fig. 1). Surfaces of the discs were polished to 600 grit with dry SiC paper.

The volume fraction of crystalline phase (V_v) in the partially devitrified samples was determined using a two-dimensional systematic point count as described by Hilliard,[4] Hilliard and Cahn,[5] and DeHoff.[6] A 100-point grid was placed on scanning electron micrographs obtained for each corroded sample at a magnification of 480X. Each V_v value reported represents an average of 100 counts.

Polished samples were submerged in polyethylene bottles containing sufficient deionized water to yield a glass surface area to solution volume ratio (SA/V) of 0.77 cm^{-1}. These bottles were submerged in a water bath at 100°C for 6 h. Upon removing samples from the corrosion

*Pittsburgh Plate Glass Co., Pittsburgh, PA.

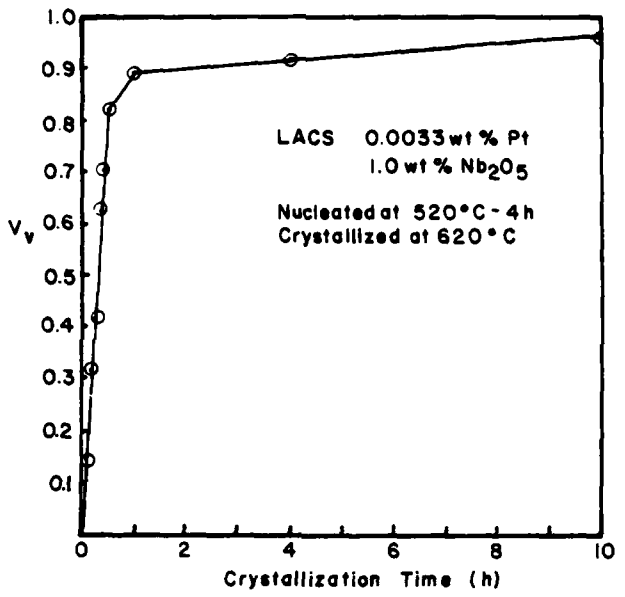

Fig. 1. V_v crystallization versus crystallization time for a Li_2O-Al_2O_3-CaO-SiO_2 glass and glass-ceramics.

cells, their surfaces were rinsed with deionized water and air dried. Samples were corroded in triplicate and solutions were analyzed for pH using a pH meter* and for cation concentrations using atomic absorption** and colorimetry***. Surfaces were evaluated using infrared reflection spectroscopy (IRRS)[+] and scanning electron microscopy (SEM)[++]. Electron microprobe analysis (EMP) was performed on both the glassy phase and crystalline phase of selected specimens.[+++]

Results and Discussion

The volume fraction of crystalline phase (V_v) resulting from the various crystallization times are shown in Fig. 1. V_v increases rapidly with time in a linear fashion up to $\sim$0.80 V_v; a rapid slowdown occurred in the rate of crystallization when $0.80 \leq V_v \leq 0.90$; a linear relationship between V_v and time was again obtained for $0.9 \leq V_v \leq 0.965$ (highest V_v achieved), but the rate of crystallization was significantly reduced in comparison to the initial rate. The kinetics of crystallization for this system differ from the sigmoidal behavior observed for the binary lithia-disilicate glass by Freiman et al.[7] X-ray diffraction analysis revealed that the crystalline phase was primarily SiO_2 in contrast to $Li_2Si_2O_5$ crystals reported[3] for the lithia-disilicate glass-ceramics. EMP analysis also indicated that the crystalline phase was higher in SiO_2 and Al_2O_3 but lower in CaO than the glassy phase.

---

*Orion Model #801A, Orion Research, Inc., Cambridge, MA.
**Perkin-Elmer Model #603, Perkin-Elmer, Norwalk, CT
***Hach Model #DR-3803, Hack Chemical Co., Ames, IA
[+]Perkin-Elmer Model #467, Perkin-Elmer, Norwalk, CT
[++]JEOL Model #JSM-35C, JEOL Ltd., Tokyo, Japan
[+++]EMP Model #MS-64, Acton Laboratories, Inc., Acton, Mass.

The rapid decrease in the crystallization rate of $V_v \geq 0.80$ is thought to be due to the depletion of SiO_2 from the glassy phase. Concurrently, the glassy phase becomes enriched with other species present in the original composition, especially Li_2O and CaO.

Figure 2 illustrates the infrared reflection spectra of LACS glass-ceramics at various stages of crystallization both before and after corrosion. IRRS has been used by other investigators[8-10] to characterize surface chemical and structural changes that accompany glass corrosion. McCracken et al.[11] have also shown that this technique is sensitive to microstructural changes that occur during crystallization of binary lithia-disilicate glass-ceramics. The infrared reflection spectrum corresponding to the annealed glass is shown in Fig. 2a. There are two maxima in this spectrum; the maximum at $\sim$1050 cm^{-1} is due to a silicon-oxygen stretch vibration;[10] the maximum at $\sim$950 cm^{-1} is due to a silicon-nonbridging oxygen stretch vibration and is associated with the alkali species.[10] Major spectral changes are observed in the glass after it is corroded at 100°C for 6 h. The maximum originally at $\sim$1050 cm^{-1} has shifted to $\sim$1100 cm^{-1}, and the $\sim$950 cm^{-1} maximum has shifted to $\sim$920 cm^{-1} while simultaneously decreasing in intensity (i.e., % reflectance). Also, there is a decrease in spectral intensity at $\sim$1000 cm^{-1} after corrosion. Other researchers have established the mechanisms responsible for these spectral changes.[8-10] The spectral alterations are attributed to an ion-exchange reaction during corrosion whereby Li^+ ions from the glass exchange with H^+ or H_3O^+ ions from solution resulting in the development of a SiO_2-rich film. If the reaction were

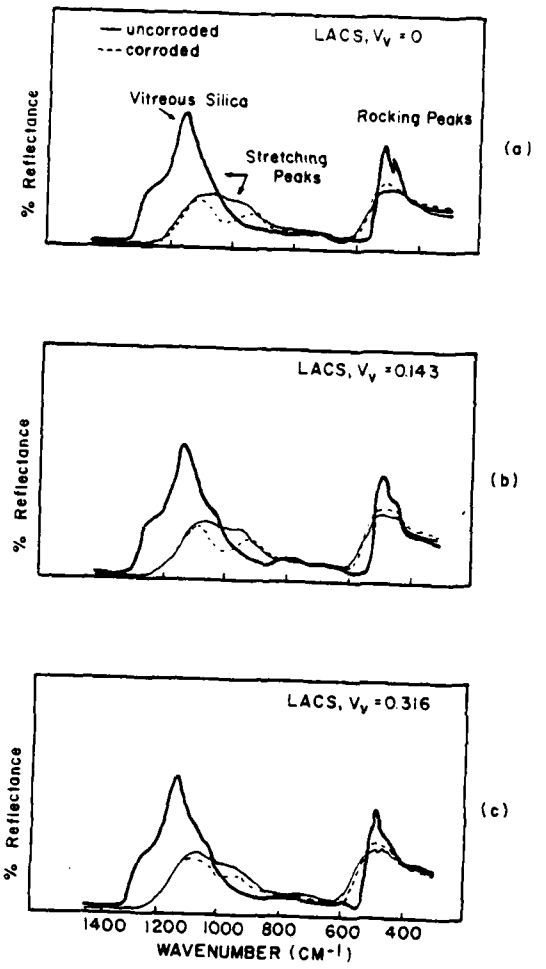

Fig. 2. IRRS of LACS glass at various stages of crystallization spectra are shown for the uncorroded glass-ceramics and for the specimens corroded at 100°C for 6 h.

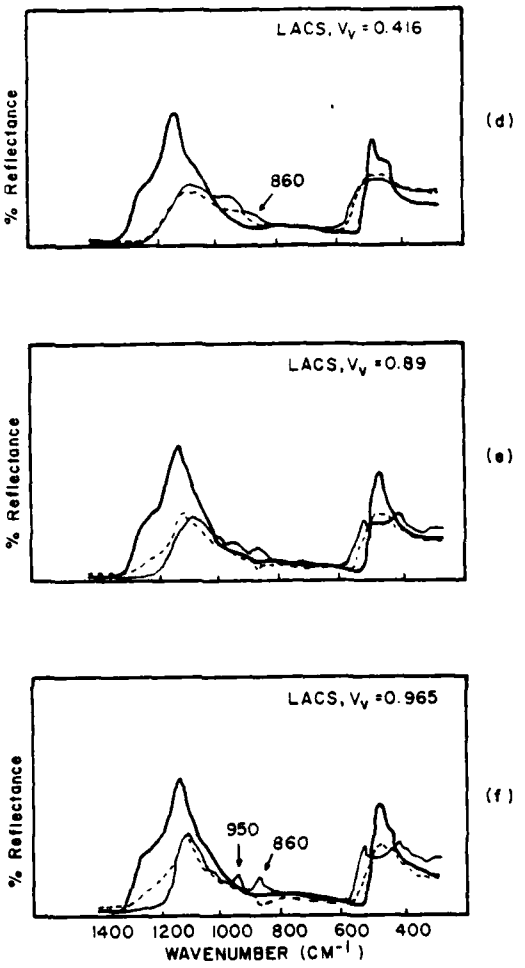

Fig. 2. Continued

permitted to continue, the spectrum of the corroded glass in Fig. 2a would become almost identical to the spectrum of vitreous silica also shown in this same figure.

The spectra corresponding to the uncorroded glass-ceramics shown in Fig. 2a-f provide information concerning the evolution of the microstructure during crystallization. As V_v increases several alterations become evident in the spectra. The maximum at $\sim$1050 cm^{-1} in the glass (Fig. 2a) gradually shifts to higher wavenumbers, becomes better defined and also increases in intensity as V_v increases. Simultaneously, the maximum at $\sim$950 cm^{-1} in the glass shifts to lower wavenumbers and decreases in intensity. A new maximum at $\sim$860 cm^{-1} appears in the spectrum corresponding to V_v = 0.316 (620°C-10 min). This maximum becomes better defined and increases in intensity as V_v increases up to 0.965 (620°C-10 h). The 860 cm^{-1} maximum has been reported by other investigations for alkali-silicate glasses containing large quantities of alkali oxides.[13] Binary glasses containing 33 mol % alkali oxide (R_2O/SiO_2 = 0.5) have on the average one non-bridging oxygen per SiO_4^{4-} tetrahedron. These non-bridging oxygens in association with the alkali species give rise to the maximum at 950 cm^{-1}. Glasses containing <33 mol % alkali oxide will also exhibit a maximum at $\sim$950 cm^{-1}, but its intensity will be less than that for a 33 mol % alkali oxide glass. Glasses containing ≥33 mol % alkali oxide will produce some SiO_4 tetrahedra with two non-bridging oxygens and as the % alkali oxide and alkaline-earth oxides increases the number of tetrahedra with two non-bridging oxygens will increase giving rise to the peak observed at $\sim$860 cm^{-1}. Thus, the

LACS + 0.01 wt % Pt
Crystallized 10 hours
Corroded 6 hours in
D.I water, 100 °C
SA/V = 0.77 cm-1

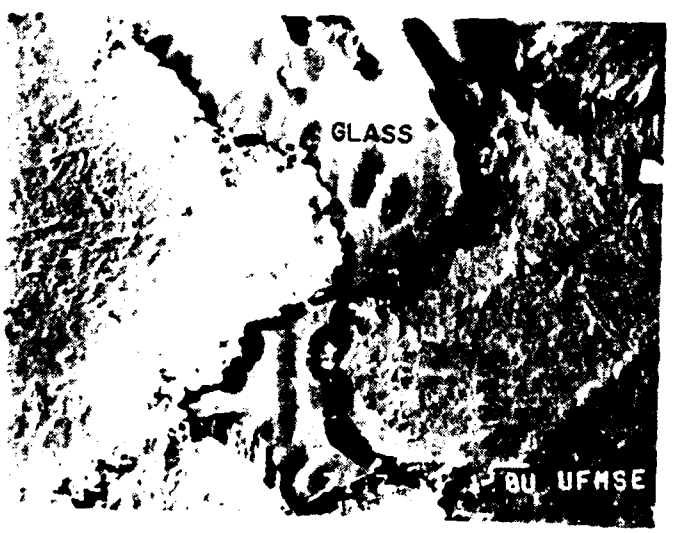

Same

Fig. 3. SEMs of LACS glass-ceramic after exposure to deionized water at 100°C for 6 h.

spectral changes observed during crystallization suggest the development of a silica-rich primary phase and a glass phase that is significantly enriched in alkali and alkaline earth oxides.

Major changes are also observed in the infrared reflection spectra between the uncorroded and corroded specimens at all values of V_v. The maximum corresponding to the silicon-oxygen stretch vibration (i.e., the 1050 cm^{-1} peak) has shifted to higher wavenumbers after corrosion (Figs. 2b-f). The magnitude of the shift (Δ wavenumbers) decreases as V_v increases. The reason for this shift has already been discussed and is due to the removal of Li^+ ions from the glass surface via ion-exchange with H^+ ions. As V_v increases, the magnitude of the shift decreases because there is less glass in the surface exposed to the corrosion solution and hence less ion-exchange. Thus, the contribution of the glassy phase to the silicon-oxygen maximum decreases as V_v increases. The maxima at 950 cm^{-1} and 860 cm^{-1} corresponding to the silicon-nonbridging oxygen vibrations have completely disappeared from corrosion and in some cases have been replaced by small valleys. These data suggest that the phase responsible for these peaks (namely the glassy phase) has been removed from the surface of the glass-ceramic. Scanning electron micrographs of corroded LACS glass-ceramics are shown in Fig. 3. These data reveal that the residual glassy phase present after crystallization has been preferentially corroded, while the crystalline phase experiences little or no decomposition as indicated by the presence of original polish scratches. In addition to the ion-exchange mechanism of corrosion indicated by IRRS, the micrographs show that significant

network dissolution has occurred to the glassy phase. The apparent increased attack observed at the phase boundary between the glass and crystals is thought to be due either to residual stresses that develop between the glass and crystals during the crystallization process or to a higher Li^+ concentration in this region resulting in a more soluble glass.

Solution data are shown in Fig. 4 for the LACS glass-ceramics after a 100°C, 6 h exposure to water. The concentrations of Li^+ and Si^{+4} and the solution pH increase as the V_v increases. The increase in pH is due to the exchange of Li^+ ions from the glass with H^+ ions from the solution, resulting in an excess of OH^- ions in solution. Although a large fraction of Li^+ in solution is probably due to ion-exchange, the increase in Si^{+4} with V_v and the micrographs shown in Fig. 3 suggest that network dissolution of the glass also contributes significantly to the high Li^+ concentration. The only known mechanism whereby Si^{+4} can be released into solution is by network dissolution. When network dissolution occurs, all species in the glass are released simultaneously. Douglas et al.[14] have shown that the rate at which OH^- destroys the network structure increases dramatically when the solution pH > 9. As indicated in Fig. 4, the pH was greater than 9 after 6 h of exposure for all values of V_v. The increase in Li^+ ions in solution with increased V_v is not due to ion-exchange from the crystalline phase, because as already noted, the IRRS peak shift which is characteristic of the ion-exchange process decreases as V_v increases. Furthermore, the micrographs show that the increase in Li^+ is not due to the network dissolution of the crystalline phase. All results indicate

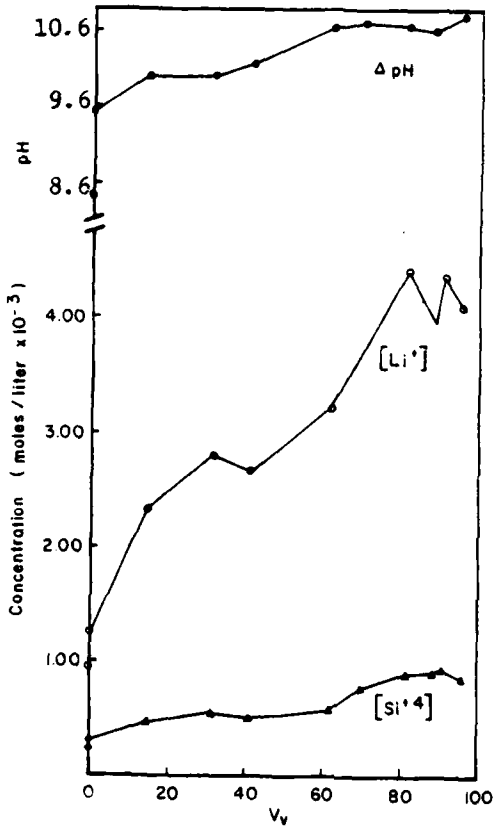

Fig. 4. Solution data for LACS glass-ceramics. Corrosion conditions: deionized water at 100°C for 6 h. Initial pH prior to corrosion was 5.6.

that the increase in Li^+ and Si^{+4} in solution with increased V_v is due to the development of a more soluble residual glassy phase.

Figure 5 is a schematic summarizing the mechanisms of glass corrosion for a partially crystallized LACS glass-ceramic. Three types of corrosion are illustrated: 1) ion-exchange of Li^+ with H^+ (or H_3O^+) resulting in the development of a SiO_2-rich surface layer on the glass; 2) network dissolution of the glassy phase; and 3) phase-boundary corrosion between the SiO_2-rich crystals and alkali-rich glass. The relative extent of each of these mechanisms varies with V_v under constant exposure conditions. At low V_v ion-exchange of the glassy phase will dominate, while at high V_v both network dissolution and phase-boundary attack are important. Under static testing conditions for long periods of time at 100°C, it is expected that ion-exchange will be only of minor importance, even at low V_v.

Summary

When a 30.5 Li_2O-2.5 Al_2O_3-6.0 CaO-61.0 SiO_2 (mol %) glass, containing Pt and Nb_2O_5 as nucleation agents, is heat-treated at 620°C, a SiO_2-rich crystalline phase forms within the parent glass. Initially, the rate of growth is rapid producing 0.89 volume fraction of crystals within 1 h. The rate of growth is significantly reduced for $V_v > 0.89$. Surrounding the crystals is an amorphous glassy phase, the composition of which becomes enriched with Li_2O and CaO as V_v increases. During exposure to an aqueous static environment, the extent of Li^+ and Si^{+4} release increases; that is, the concentration of these ions in solution

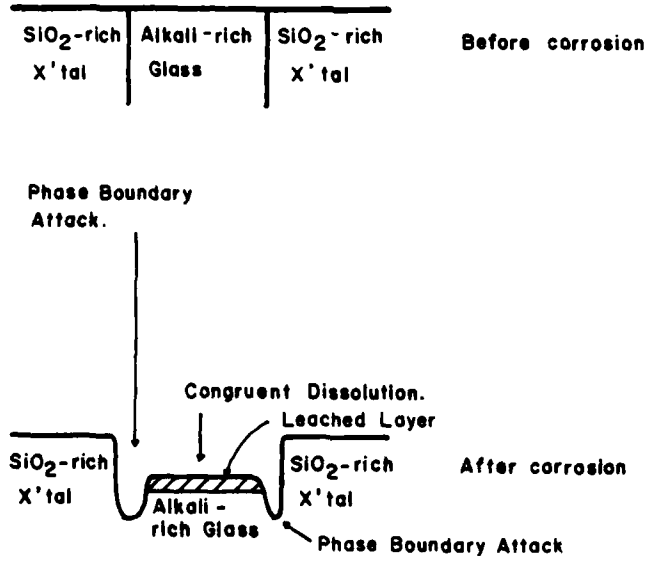

Fig. 5. Schematic of corrosion mechanisms in LACS glass-ceramics.

is greater for V_v = 0.965 than for V_v = 0, when these two glass-ceramics are corroded under identical conditions. IRRS and SEMs show that this increase is due primarily to network dissolution of the alkali-rich glassy phase. The crystalline phase is relatively unaltered either by ion-exchange or network dissolution.

Acknowledgments

The authors thank Howmedica, Inc. and the Air Force Office of Scientific Research (Grant #77-3210) for financial support of this work.

References

1. W. J. McCracken, D. E. Clark and L. L. Hench, "Aqueous Corrosion of Li_2O-$2SiO_2$ Glass-Ceramics," submitted to the J. Am. Ceram. Soc.

2. S. W. Freiman and L. L. Hench, "Effects of Crystallization on the Mechanical Properties of Li_2O-SiO_2 Glass-Ceramics, J. Am. Ceram. Soc., 55 [2], 86-90 (1972).

3. L. L. Hench, S. W. Freiman and D. L. Kinser, "The Early Stages of Crystallization in a Li_2O-$2SiO_2$," Physics and Chemistry of Glasses, 12 [2], 58-63 (1971).

4. J. E. Hilliard, "Measurement of Volume in Volume," in Quantitative Microscopy, R. T. DeHoff and F. N. Rhines, eds., McGraw Hill Book Co., New York (1968).

5. J. E. Hilliard and J. W. Cahn, "An Evaluation of Procedures in Quantitative Metallography for Volume-Fraction Analysis," Trans. Met. Soc. AIME [221], 344-52 (1961).

6. R. T. DeHoff, "Quantitative Stereology," in Characterization of Ceramics, L. L. Hench and R. W. Gould, eds., Marcel Dekker, Inc., New York (1971).

7. S. W. Freiman and L. L. Hench, "Kinetics of Crystallization in $Li_2O \cdot 2SiO_2$," J. Am. Ceram. Soc., 51 [7], 382-387 (1968).

8. D. M. Sanders and L. L. Hench, "Mechanisms of Glass Corrosion," J. Am. Ceram. Soc., 57 [7], 373-377 (1973).

9. D. E. Clark, M. F. Dilmore, E. C. Ethridge and L. L. Hench, "Aqueous Corrosion of Soda-Silica and Soda-Lime-Silica Glass," J. Am. Ceram. Soc., 59 [1-2], 62-65 (1976).

10. D. M. Sanders, W. B. Person, and L. L. Hench, "Quantitative Analysis of Glass Structure Using Infrared Reflection Spectra," Appl. Spectroscopy, 28 [3], 247-255 (1974).

11. W. J. McCracken, D. E. Clark, and L. L. Hench, "Surface Characterization of Ceramed Composites and Environmental Sensitivity," to be published in Ceramic Engineering and Science Proceedings, No. 7-8, July/Aug. (1980).

SECTION V

ELECTRON BEAM EFFECTS DURING ANALYSIS OF GLASS THIN FILM WITH AUGER ELECTRON SPECTROSCOPY

By

F. Ohuchi and P. H. Holloway

Introduction

Auger electron spectroscopy (AES) is generally considered to be a "nondestructive" surface analytical technique. However, there are many instances where the incident electron beam can alter the surface composition of the solid being analyzed. Compositional changes in glasses during electron bombardment for AES have been reported by several investigators.[1-4] Changes have been particularly severe in glasses containing alkali ions.

It has been proposed that irradiation of the glass by electron beam breaks bonds to form ion-electron pairs[5] and locally raises the temperature of the material[6,13]. Both effects cause an increase in the alkali ion mobility which increases the rate of migration. While the mobility of the alkali ion is important, the build up of electric fields and associated increase in the driving force for diffusion is also important. An electric field builds up during bombardment of the bulk glass with energetic electrons due to a diffuse negative charge layer at a depth equal to the electron range. This may become sufficiently high to cause field-assisted alkali ion diffusion away from the surface.[7,8]

Another consequence of electron bombardment is electron stimulated desorption (ESD). It is known that an electron beam can cause desorption of atoms and molecules from a surface, and alkali elements are no exception.[9] Such surface desorption would cause the alkali Auger signal to decay in a manner similar to that caused by sodium migration away from the surface.

These beam effects influence AES data and in the present study we have measured the change for thin glass films deposited on metal. With these samples we have isolated the effects of driving force, mobility, and electron stimulated desorption, and thereby studied the relative magnitude of their effects. These measurements have been coupled with theoretical modeling of sodium migration.

Experimental

Soda-silica glass films of 1000 Å and 2000 Å thickness were deposited on optically polished stainless steel. High purity SiO_2 and reagent Na_2CO_3 were simultaneously evaporated from an electron beam heated crucible and a resistively heated crucible, respectively. The vacuum was maintained at 5×10^{-5} Torr and the substrate was heated to 300°C. The deposition rate and film thickness were controlled with a quartz crystal monitor.

The Auger measurements were made in a Physical Electronics Thin Film Analyzer[+] or a Varian Auger Spectrometer[++] in a residual vacuum pressure of less than 1×10^{-8} Torr. All the samples were irradiated by an electron beam at an angle of ~ 45° to minimize unstable charging during analysis. In the former instrument (PHI), electron beams up to 3 KeV with diameter of ~ 600 um (defocused condition) were used. The samples were mounted on a carousel which could be cooled with liquid nitrogen in this instrument. The Varian instrument was capable of producing electron beams up to 10 KeV

[+] CMA 10-155, Physical Electronics Industries, Inc., Edina, MN

[++] CMA 981-2707 Varian, Vacuum Division, Palo Alto, CA

with a diameter of ~ 10 μm. A scanning capability was used to more accurately control the electron beam current density in the Varian spectrometer.

Total beam currents were measured by a Faraday cage and beam current densities were calculated based upon the scanned area.

Sputter profiling was accomplished using 2 keV argon ions with the chamber backfilled to 2×10^{-5} Torr.

Results

Figure 1 shows the Auger spectra from a 1000 Å thick glass film deposited on a stainless steel substrate. Spectra were taken using a 3 keV electron beam with a total current of 5 μA at liquid nitrogen temperature. No elements other than Si, C, O, and Na were observed. Relative peak heights for Si, O, and Na varied less than 5% at different analysis sites.

Glass thin film composition was estimated to be 15 ± 5 mole % Na_2O and 85 ± mole % SiO_2 by comparing the Auger peak heights to those from known concentration in bulk glasses.

Figure 2 shows a plot of the peak height for Na as a function of beam impingement time at a given energy (3 keV) and a current density (5×10^{-3} A/cm^2) with varying film thickness (1000 Å, 2000 Å, and bulk glass). The measurements were made at room temperature. The rates of decay were strongly dependent upon the film thickness with significantly slower decay observed for thin films as compared to bulk glass.

The decay rate of the Na signal was also dependent upon the beam energy. Figure 3 shows the time-dependence of the Na Auger signal from

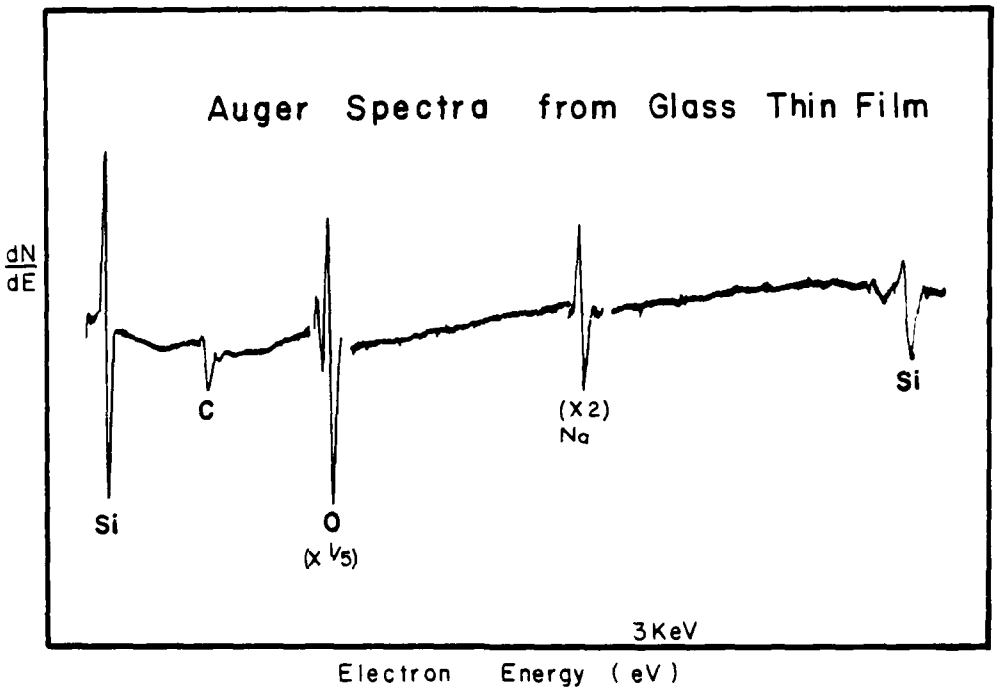

Fig. 1. Auger spectra from 1000 Å thick glass film deposited on a stainless steel substrate, taken using a 3 KeV electron beam with a total current of 5 μA at liquid nitrogen temperature.

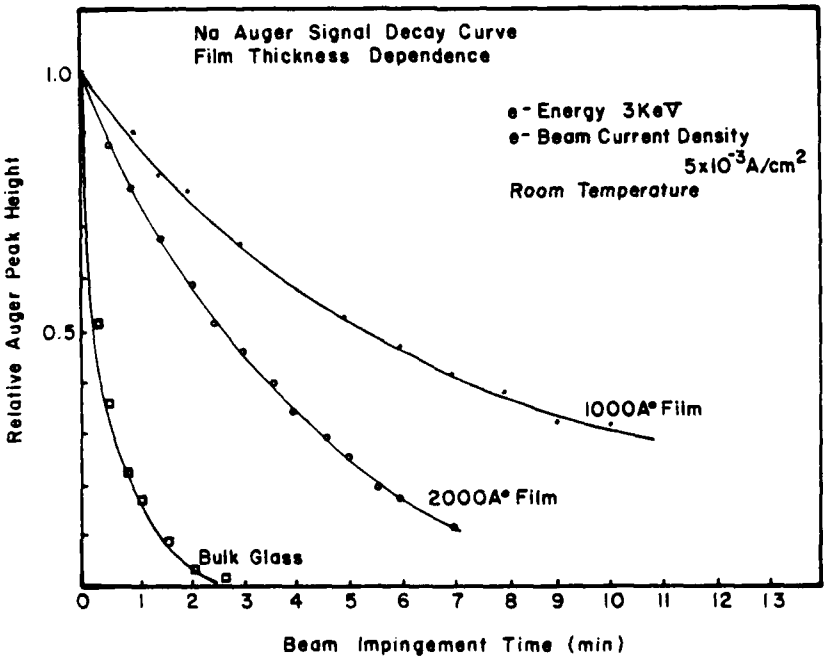

Fig. 2. Na Auger peak height as a function of beam impingement time and glass thickness for a 3 KeV electron beam with a current density of 5×10^{-3} A/cm^2 at room temperature.

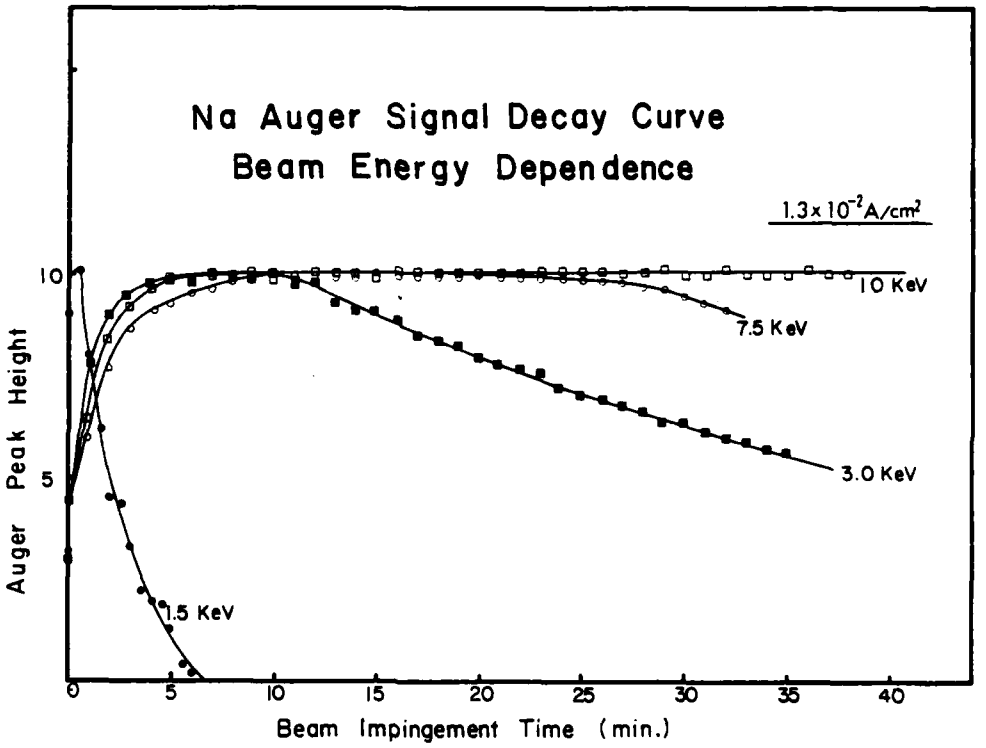

Fig. 3. Na Auger peak height as a function of beam impingement time from a 2000 Å thick film for the energy ranging from 1.5 KeV The current density is 1.4 x 10^{-3} A/cm^2 (1.3 x 10^{-2} A/cm^2 for 10 KeV energy) and the analysis was performed at room temperature.

a 2000 Å thick film at a constant current density of 1.4×10^{-3} A/cm^2 (1.3×10^{-2} A/cm^2 for 10 keV) for the energy ranging from 1.5 keV to 10 keV. All the measurements were made at room temperature. For the first few minutes, increases in the Na signal were observed. Dawson et al.[4] observed similar phenomena and attributed the effect to removal of a carbon overlayer which inelastically scattered the sodium Auger electrons. In the present case, the carbon signal was observed initially, but it decreased rapidly with electron bombardment. This is consistent with Dawson's explanation.

For 1.5 keV, the Na decay was rapid, while relatively long plateaus were observed for 3.0 keV and 7.5 keV beams. Almost no decay was observed for the 10 keV beam even though the current was higher by a factor of 10. These differences in decay rate will be attributed to changes in the electric field which is one driving force for sodium diffusion.

Figures 4a and 4b show the results obtained on the 2000 Å glass film with 3 keV and 7.5 keV electrons, respectively, when the beam current density was varied from 1.4×10^{-3} A/cm^2 to 1.25 A/cm^2. As the current density was increased, the decay rate increased drastically for either case.

The Na mobility in the glass can also be changed by varying the substrate temperature. Figure 5 shows the Na signal decay at liquid nitrogen temperature and at room temperature. Lowering the temperature results in slower decay rates.

These data show that the Na Auger signal decay depends upon the electron beam energy, current density, substrate temperature, and glass

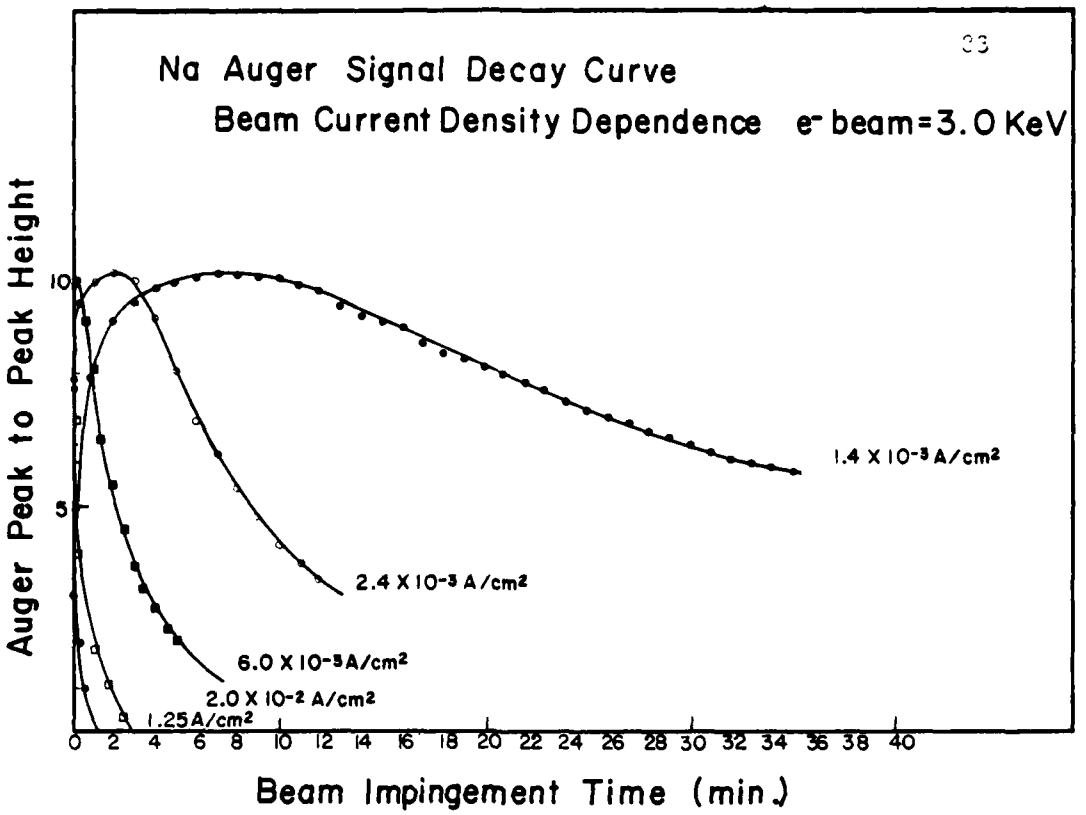

(a)

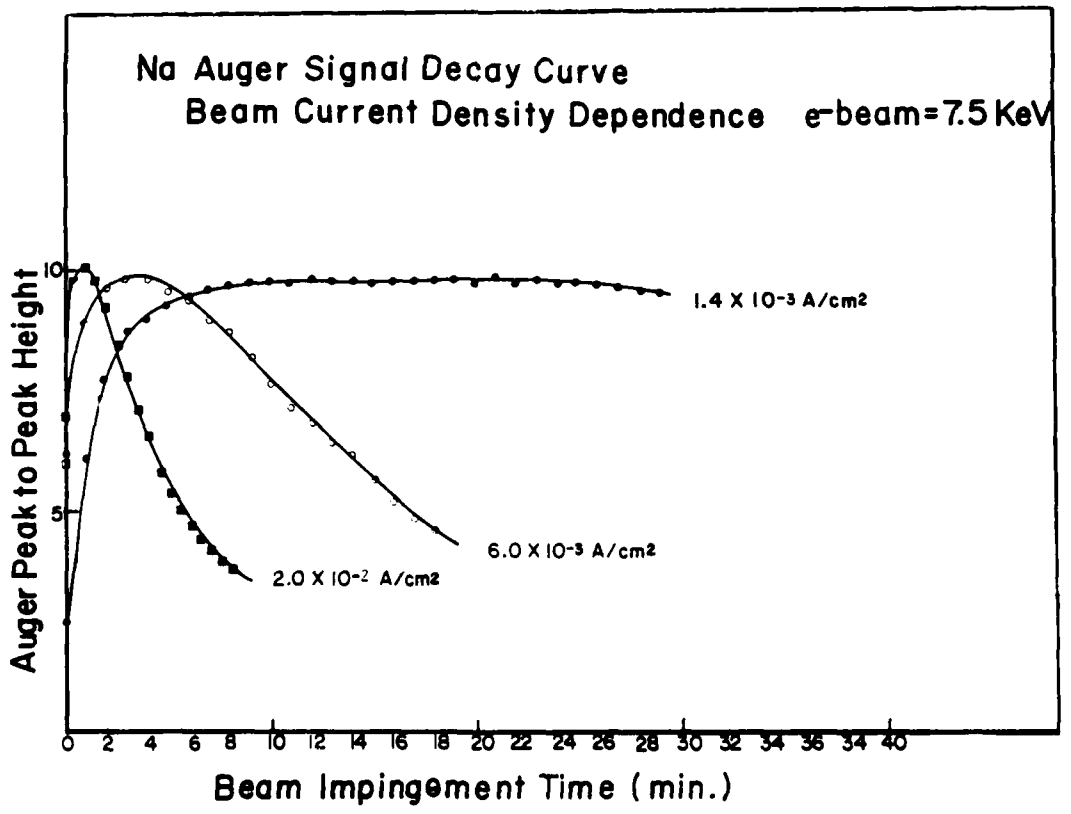

(b)

Fig. 4. Na Auger peak height as a function of beam impingement time at room temperature. (a) 3 KeV electrons with the current densities varying from 1.4×10^{-3} to 1.25 A/cm^2. (b) 7.5 KeV electrons with the current densities varying from 1.4×10^{-3} to 1.25 A/cm^2.

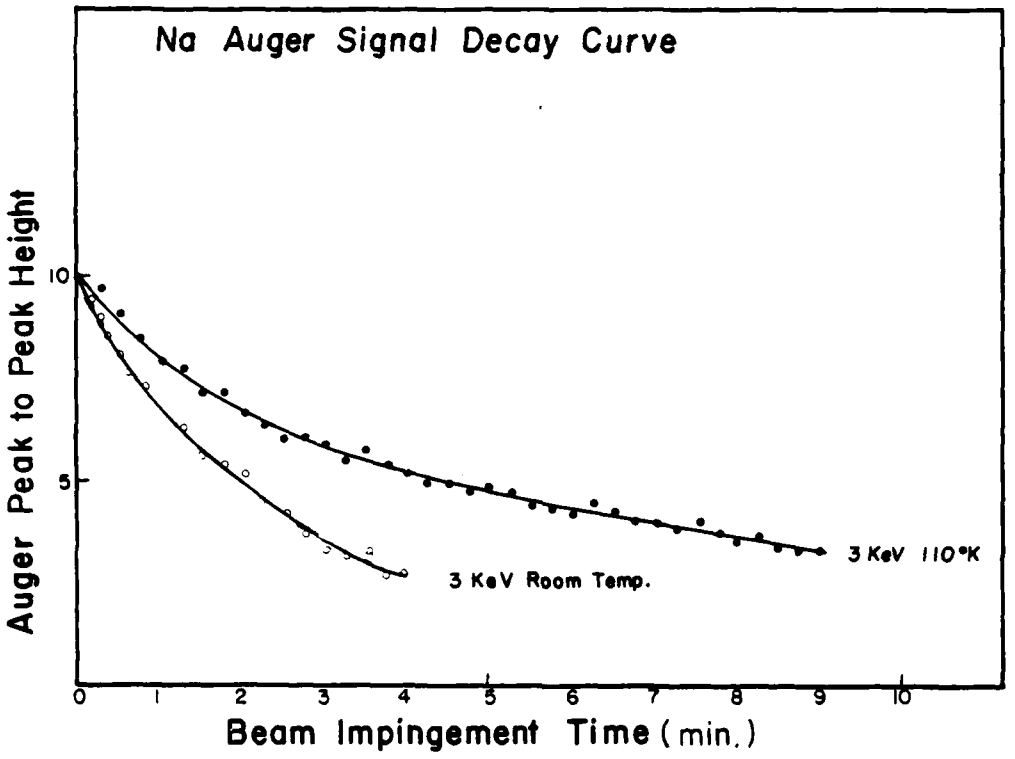

Fig. 5. Na Auger peak height as a function of beam impingement time for a 3 KeV electron beam, current density of 5×10^{-3} A/cm^2, and a 1000 Å glass film at liquid nitrogen (a) and room (b) temperatures.

thickness. However, there still remains a question as to the location of the Na after electron irradiation. The disappearance of sodium at the surface can be due either to its escape into the vacuum, to diffusion into the bulk, or to lateral surface diffusion. Figure 6 shows the decay of the Na signal upon continuous electron irradiation of the surface of a 1000 Å glass film, and the subsequent depth profile from the electron irradiated area. A 3.0 keV electron beam with a current density of 5×10^{-3} A/cm^2 was used to irradiate the surface. After the signal decayed to 25% of its maximum peak height, the Na concentration versus depth was profiled by Ar ion sputtering. A 3.0 keV, 5×10^{-3} A/cm^2 electron beam was used during sputtering, where only the Na and Fe (to detect the glass/substrate interface) signals were recorded and the beam impingement time as no more than 10 seconds at each depth profile concentration point. The depth profile from an unirradiated area of the 1000 Å film is also shown for the comparison. In either case, an accumulation of Na at the interface was observed. However, higher accumulation of Na at the interface after electron irradiation of the surface suggests that some of the Na does migrate into the solid due to electron irradiation.

Figure 7 shows the decay of the signal during electron irradiation (without ion bombardment) of a surface produced by sputtering for 16 minutes to reach the glass/steel interface. No significant decay was observed at a current density of 5×10^{-3} A/cm^2. At a current density of 2.5×10^{-2} A/cm^2 the Na peak height becomes progressively smaller. In this case, the Na ions were located at the interface and could not migrate into the solid (none were detected upon sputtering into the solid).

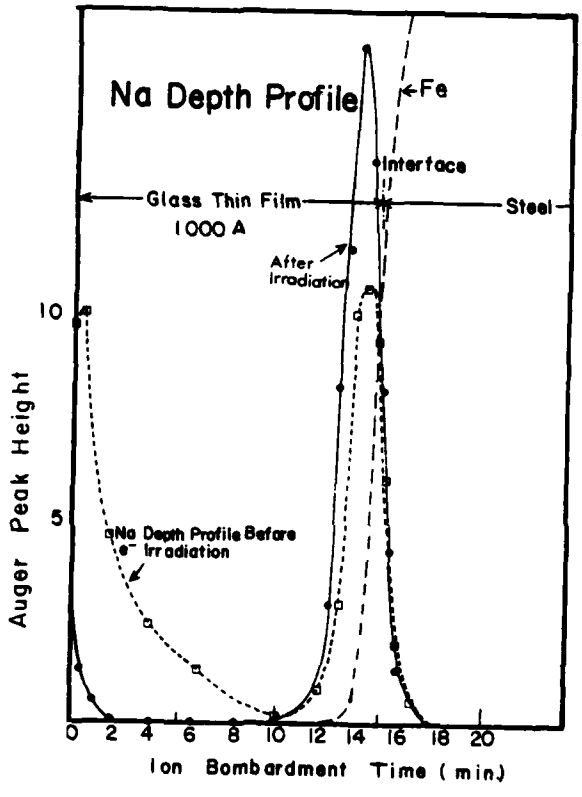

Fig. 6. Na concentration depth profile in the 1000 Å glass film from an unirradiated area (shown by dotted curve) and irradiated area (shown by solid curve).

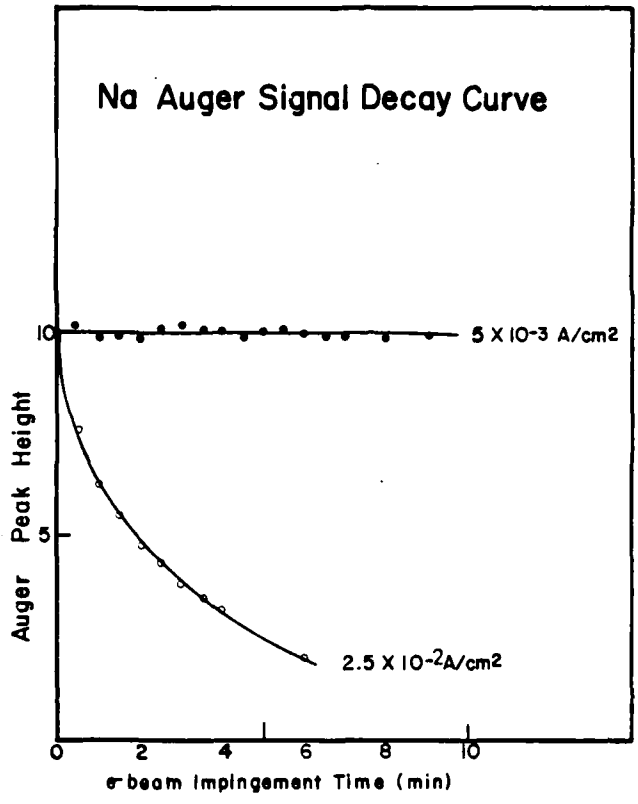

Fig. 7. Auger peak height changes of the sodium located at the tlass-steel interface, using a 3 KeV electron beam.

Therefore, the disappearance of Na at high beam current density can be due to either desorption from the surface or lateral migration. Significant lateral migration can be ruled out in the present case because of the large distances (~300 μm) over which the ions must move to result in measurable signal loss. Therefore, electron stimulated desorption is the most probable loss mechanism.

Discussion

Pantano et al.[2] and Dawson et al.[4] have studied the influence of electron beam upon AES measurement of soda-lime-silica bulk glasses. They found a "resident time period" (on the order of one minute) before observing a significant decay of the sodium signal. However, a significant resident time was not observed from the bulk glass in the present case (Figure 2). This is probably because the ion mobility depends upon composition in a complex manner.

Frischat[14] has compared the activation energies for Na self-diffusion in soda-silica and soda-lime-silica glasses. The values were 20 Kcal/mole and 15 Kcal/mole in the soda-silica glasses containing Na_2O of 15 to 33 mol%, respectively. While the activation energies of more than 20 Kcal/mole was reported in the soda-lime-silica glasses containing the same range of Na_2O the Auger data also indicated that the Na is more mobile in soda-silica than in soda-lime-silica glass.

For thin films, the Na signal decay rates were strongly dependent upon the experimental beam conditions. The decay rate can be controlled by changing either the sodium mobility in the glass or the driving force for diffusion. For thick glass, energetic electrons enter and dissipate

their energy by ionization or other electronic excitation of the atoms. They come to rest at some depth, R, within the glass and produce a net negative charge. Theoretical range expressions can be obtained by integrating the energy loss expression:

$$R = \int_{E=E_o}^{E=0} \frac{1}{dE/dx} \cdot dE$$

A simplified range expression was developed by Cosslett and Thomas[10], where $R = KE_o^n$ with n = 1.2 to 1.7 depending on the definition of range, and K is a constant. For low energy electrons, the range expression of Cosslett and Thomas is not precise because of high inelastic scattering. However, it is certain that as the primary energy is increased, the electrons penetrate further into the solid (a few thousand Å for 1 to 3 keV electrons and more than one micron for 10 keV electrons). When a 3 keV electron beam was used, the decay rate was strongly dependent upon the film thickness as shown in Figure 2. This was not true in bulk glass; the decay rate was independent of energy when the current density was maintained constant. These data can be explained in part by postulating that as the thickness of the film is decreased, the amount of charge trapped also decreased, causing a lower driving force and lower migration rate. Another effect, beam heating, is discussed below.

The electron energy dependent decay rate shown in Figure 3 is interpreted in the same manner. This is shown in Figure 8. Most of the electrons with energy of 1.5 keV are trapped within the 2000 Å film and a space charge builds up leading to field enhanced migration. Higher energy (7.5 and 10 keV) electrons come to rest below the glass thin

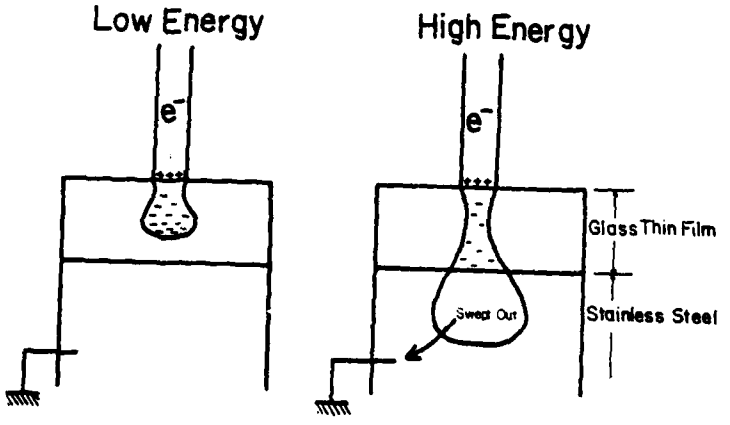

Fig. 8. Schematic illustration of the electron beam penetration area charge accumulation in glass.

film, reducing the space charge build up.

There are other factors varying with the change in experimental parameters. When the beam current density is increased, beam heating causes higher local temperatures and increased Na mobility. In addition, data in Figure 7 show that electron stimulated desorption also occurs. Therefore, these two effects are combined with the electric field effect to provide high decay rates of sodium as shown in Figures 2 through 4. The rate of electron stimulated desorption is given by[11]

$$\frac{d\sigma_d}{dt} = \frac{\sigma_d \phi J^-}{e} \qquad (1)$$

where σ_d is the surface coverage in the binding state which is absorbable by electron impact, ϕ is the total desorption cross section, J^- is the electron current density and e is the electronic charge. Integrating the the equation, the relative coverage Θ is

$$\Theta = \exp(-t/\tau) \qquad (2)$$

where $\tau = e/J^-\phi$.

In Figure 7, an experimental decay rate was observed for a current density of 2.5×10^{-2} A/cm^2 and $\tau \simeq 210$ seconds. We have estimated the total desorption cross section of $\sim 3 \times 10^{-20}$ cm^2 in this case. With such a low cross section, ESD effect is not expected to be significant in the AES analysis except at very high current densities.

The discussion presented above suggests the following model for the Na ion migration during AES analysis. When a space charge results from bombardment with energetic electrons, the negative charge will be concentrated at a depth about equal to the electron range. Not only is

there a negative space charge layer inside the material, but a positively charged layer will exist on the surface since the secondary electron emission yield, δ, is normally greater than unity. The observation that all the Auger peaks are shifted a small equal amount lower in energy is direct evidence for this effect.

A capacitor structure can be used to model the sodium ion migration in thin films. The model consists of the glass thin film sandwiched by two electrodes, as is illustrated in Figure 9. The diffusion equation including the electric field, F (volt/cm), becomes

$$\frac{\partial C(x,t)}{\partial t} = D \frac{\partial^2 C(x,t)}{\partial x^2} - \mu \frac{\partial F(x,t)\, C(x,t)}{\partial x} \qquad (3)$$

where μ is the mobility of the sodium ion and D is the diffusion constant.

For the present problem, it was assumed that F is independent of the time and was taken as an average field strength F_{av} inside the material even though there may exist a non-uniform distribution of sodium ions, electrons and holes. Then the equation (3) becomes

$$\frac{\partial C(x,t)}{\partial t} = D \frac{\partial^2 C(x,t)}{\partial x^2} - F_{av}\, \mu \frac{\partial C(x,t)}{\partial x} \qquad (4)$$

From the Einstein relation[12]

$$\mu = eD/kT \qquad (5)$$

where e, k, and T are the electron charge, Boltzmann constant, and temperature, respectively. Assuming that the sodium concentration, C_o, is uniform before the analysis, leads to the initial condition

$$C(x,t) = C_o \text{ for } t = 0,\ 0 \le x \le \ell \qquad (6)$$

we have assumed that no electron stimulated desorption is occurring at the surface and the sodium ion is physically blocked by the stainless

AD-A089 943 STATE UNIV OF NEW YORK AT BUFFALO DEPT OF BIOLOGY F/G 11/2
STRUCTURE-PROPERTY-ENVIRONMENTAL RELATIONS IN GLASS AND GLASS-C--ETC(U)
MAR 80 L L HENCH AFOSR-77-3210

UNCLASSIFIED AFOSR-TR-80-0778 NL

2 OF 2
AD A089943

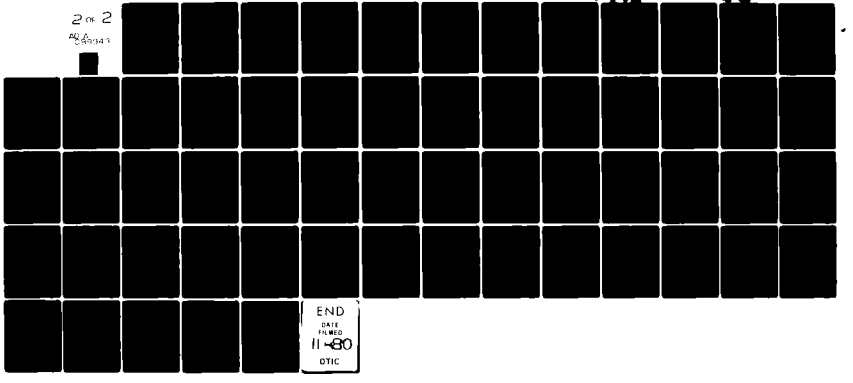

END
DATE FILMED
11-80
DTIC

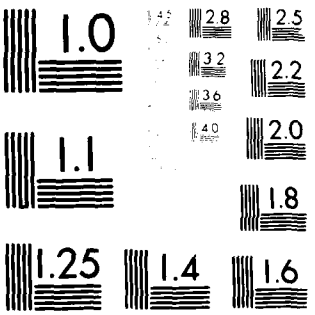

MODEL

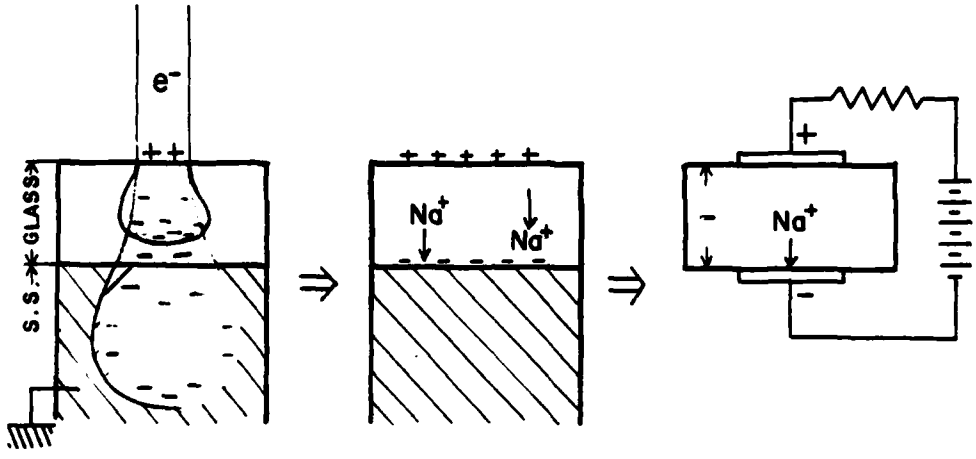

Fig. 9. Schematic illustration of the model used to calculate the sodium ion migration.

steel at the interface. As a result there are no fluxes of sodium ions, J, at the surface and interface, i.e.,

$$J = D \frac{\partial c}{\partial x} - F_{av} \mu c = 0 \text{ for } x = 0 \text{ and } x = \ell \tag{7}$$

Using these boundary conditions, the equation can be analytically solved to yield

$$c(x,t) = \frac{c_o F_{av} \mu \ell \cdot \exp(F_{av} x/D)}{D \cdot (\exp(F \mu \ell/D)-1)} + c_o \cdot 16 \cdot D^2 F_{av} \mu \pi \ell^3 \cdot \exp(F_{av} \mu x/2D) \cdot$$

$$\sum_m^\infty \frac{\exp((4D^2 m^2 \pi^2 + F_{av}^2 \mu^2) \cdot t/4D^2 \ell^2) \cdot m \cdot (1-\exp(-F_{av} \mu \ell/2D))}{(4D^2 m^2 \pi^2 + F_{av}^2 \mu^2 \ell^2)^2} \cdot$$

$$(F_{av} \mu \cdot \sin \frac{m\pi x}{\ell} + \frac{2m\pi D}{\ell} \cdot \cos \frac{m\pi x}{\ell}) \tag{8}$$

The Auger escape depth of sodium is very small compared to the thickness of film, ℓ. Therefore, the sodium surface concentration variation as a function of electron bombardment time can be expressed as x = 0 as

$$\frac{c(o,t)}{c_o} = \frac{F_{av} \mu \ell}{D \cdot (\exp(F_{av} \mu \ell/D)-1)} +$$

$$16 D^2 F_{av} \mu \pi \ell^3 \cdot \sum_m^\infty \frac{2m\pi D}{\ell} \cdot \frac{\exp((4D^2 m^2 \pi^2 + F_{av}^2 \mu^2) \cdot t/4D^2 \ell^2) \cdot m \cdot (1-\exp(F_{av} \mu \ell/2D))}{(4D^2 m^2 \pi^2 + F_{av}^2 \mu^2 \ell^2)^2} \tag{9}$$

Local heating produced by the electron beam causes the temperature of the substrate to increase, thereby increasing the mobility. We have previously estimated this temperature rise to be 100 to 200°C[13]. Therefore, a diffusion constant of 3.5×10^{-15} cm^2/sec is appropriate for

room temperature analysis[14]. The field strength, F_{av}, can then be treated as an adjustable parameter such that calculated curves give a best fit with experimental data. Calculated results for Na migration which give a best fit to the experimental data taken with a 3 keV electron beam are shown in Figure 10. The average field strengths determined from these calculations were 2.2×10^4 V/cm, 3.9×10^4 V/cm, and 1.2×10^5 V/cm for 1000 Å films, 2000 Å films, and bulk glass, respectively.

The surface charging can be determined from the energy of the Na peak. For the 2000 Å film, 1 ± 0.5 eV peak shifts were measured for 3 keV electron beam. Assuming this charge acts over the 2000 Å film, the field strength is estimated to be $\sim 5 \times 10^4$ V/cm. This is approximately the same as the field strength derived from the calculation. The energy of the Na Auger transition from bulk glass shifted from 3 to 6 electron volts. Again, this is reasonably consistent with the value derived by curve fitting the experimental data and assuming an electron range of 3000 Å. However, it is not clear why the surface charge should so accurately reflect the space charge deeper in the sample.

This coincidence does suggest, however, that our assumption of a uniform average field is good for the present case. However, the field in a bulk sample may be significantly different. For example, the electron range in a bulk film is only an average value and the resulting charge will straggle over a large distance about this value. In addition, the sodium diffusion at the electron range ($x=\ell$) is not zero for a bulk glass.

Local heating by the electron beam has been approximated in the present case, based upon our previous experience. This is only a crude estimate. Beam heating was expected to vary when the current density was changed,

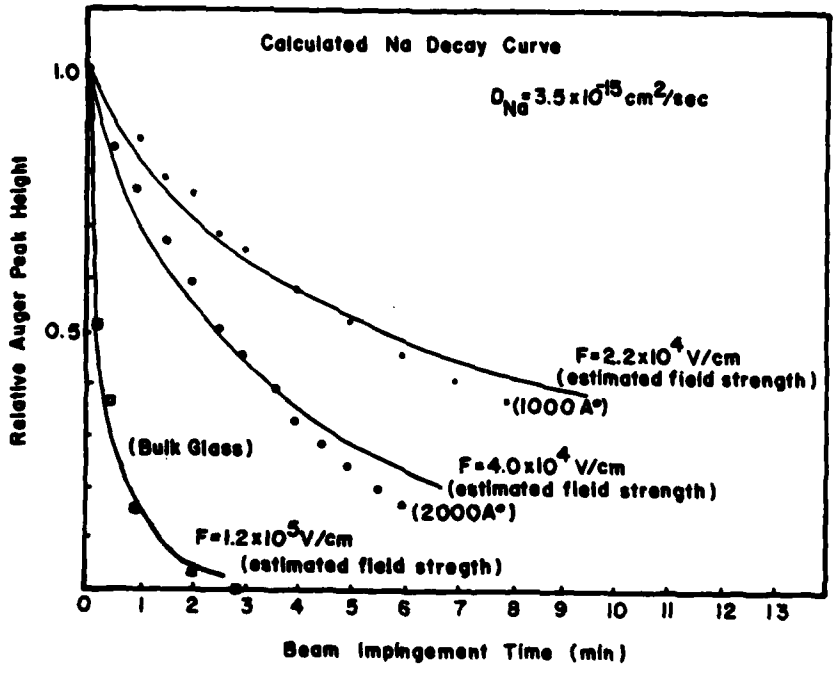

Fig. 10. Calculated Na decay curve that is best fit to the experimental data shown in Figure 2.

as is the case in Figure 4 (a) and (b). However, we could not correlate the rate of sodium decay with the dependence of heating upon current density predicted by theoretical description of the interaction of electron beams with solids[16,17]. This indicates that our understanding of beam heating during AES is very poor and requires further study.

The sodium concentration as a function of depth may be calculated from Equation (7). These calculations show that with electron irradiation, sodium is depleted near the surface and accumulates at the interface region. This is schematically illustrated in Figure 11. This was confirmed experimentally as shown in Figure 6. However, almost complete depletion of Na in the middle of the film cannot be explained by this model. This suggests that the Ar ion beam used for sputtering also causes migration. This is consistent with depth profile shown in Figure 6 for a film not irradiated with electrons prior to sputtering. McCaughnan et al.[15] reported that Ar^+ bombardment caused migration of alkali ions in SiO_2, and a Na depth profile similar to Figure 6 was measured. Therefore, ion beam effects alsc have to be taken into account to precisely determine the Na depth distribution by sputter profiling.

Summary

The decay with time of the Na Auger signal from a soda-silica glass has been studied. By using glass films deposited on steel substrates, the charge trapping and local beam heating of the glass was limited. As a result, the decay rate of the Na Auger signal was very dependent upon the electron energy. For 1.5 keV electrons incident upon a 2000 Å film, the signal decayed to 50% of its initial value in two minutes, while the

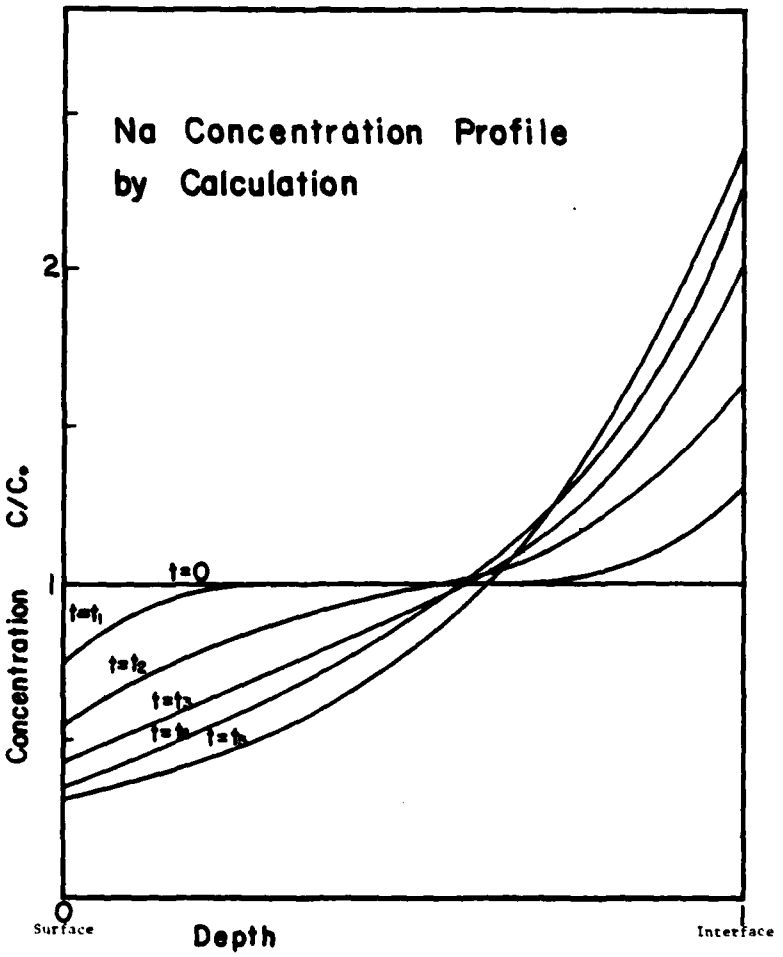

Fig. 11. Calculated sodium distributions in the film after electron beam impingement for time t, where $t_1 = 0 < t_1 < t_2 < t_3 < t_4 < t_5$.

same decay took 40 minutes with 3 keV electrons. For 3 keV electrons, doubling the electron current density onto the sample reduced the 50% decay time by about a factor of three. This indicates that the local temperature is being significantly increased because of the power density of the beam, and we have estimated this local temperature rise to be 100°C to 200°C. These effects were modeled using a configuration similar to a capacitor. Induced electric field strengths were determined by measuring the energy shifts of Auger electrons and dividing by the calculated electron ranges. The model was used to calculate the distribution of Na with depth, but the calculated distribution disagreed with experimental sputter profile data. This probably results from redistributions during ion bombardment for sputtering profiling. The cross section for electron stimulated desorption was measured to be 3×10^{-20} cm^2. With such a low cross section, ESD is not expected to be significant in AES analysis of soda-silica glasses except at very high current densities.

Acknowledgments

This work was partially supported by the Air Force Office of Scientific Research (Grant #77-3210). The authors wish to express their appreciation to N. Yoshida, Nippon Kogaku K.K. Japan, for developing and providing the glass thin film.

References

1. R. A. Chappel and C. T. H. Stoddart, Phys, Chem. Glasses, 15 (5), 130 (1974).
2. A. E. Clark, Jr., C. G. Pantano, Jr., and L. L. Hench, J. Amer. Cer. Soc., 59 (1), 37 (1976).
3. C. G. Pantano, D. B. Dove, and G. Y. Onoda, Jr., J. Vac. Sci. Tech., 13 (1), 414 (1976).
4. P. T. Dawson, O. S. Heavens, and A. M. Pollard, J. Phys. C: Solid State Phys., 11, 2183 (1978).
5. H. L. Hughes, IEEE Trans. Nucl. Sci., NS-16, 195 (1969).
6. L. F. Vassamillet and V. F. Caldwell, J. Appl. Phys., 40 (4), 1637 (1969).
7. J. L. Lineweaver, J. Appl. Phys., 34 (6), 1786 (1963).
8. K. G. Aubouchon, IEEE Trans. Nucl. Sci., NS-18, 117 (1971).
9. P. H. Dawson, Suppl. NUVO. Cimento., Vol. V, No. 2, 612 (1966).
10. J. I. Goldstein, in Practical Scanning Electron Microscopy, edited by J. I. Goldstein and H. Yakowitz (Plenum, New York, 1975).
11. R. A. Redhead, J. P. Hobson, and E. V. Kornelsen, in The Physical Basis of Ultrahigh Vacuum (Chapman and Hall, London, 1968), p. 176.
12. P. G. Shewmon in Diffusion Solids (McGraw-Hill, New York, 1963), p. 137.
13. F. Ohuchi, D. E. Clark, and L. L. Hench, J. Amer. Cer. Soc., 62 (9,10), 500 (1979).
14. G. H. Frischrt, in Ionic Diffusion in Oxide Glasses (Trans. Tech. Publications, Ohio, 1975).
15. D. V. McCaughan, R. A. Kushner, and V. T. Murphy, Phys. Rev. Lett., 30 (13), 614 (1973).

16. S. B. Fisher, Radiation Effects 5, 239 (1970).

17. L. W. Hobbs, 1975 in Surface and Defect Properties of Solids, edited by M. W. Roberts and J. M. Thomas (The Chemical Society, London), Vol. 4, p. 152-250.

SECTION VI

USE OF NEW SURFACE PHYSICS FOR CONTROLLING THE PHYSICAL PROPERTIES OF CERAMICS

By

L. L. Hench

Introduction

During the last 30 years, the control of optical, electrical, and magnetic properties of ceramics has led to the development of a major new industry--Electronic Ceramics. During the next 30 years we must achieve a similar level of control over the high temperature mechanical behavior of ceramics and development of another new industry--Energy Ceramics.

Nearly every aspect of our modern technological society is affected by the use of electronic ceramics. As we examine the history of the development of the electronic ceramics field we find that control over the bulk physical properties of these materials was essential. This control was primarily achieved by understanding the influence of small variations in composition and microstructure on the physical properties of the polycrystalline material. Emphasis on characterization of composition and microstructure and the development of experimental techniques and quality control laboratories for such characterization have been central to the growth of the field.

As was concluded by other introductory lectures in this conference, I too emphasize that achieving further progress in the physical properties of ceramics must follow progress in processing.

Figure 1 illustrates the processing steps involved in the production of high-grade technical ceramic materials. Four primary processing steps are indicated in the top half of the figure. The five major types of

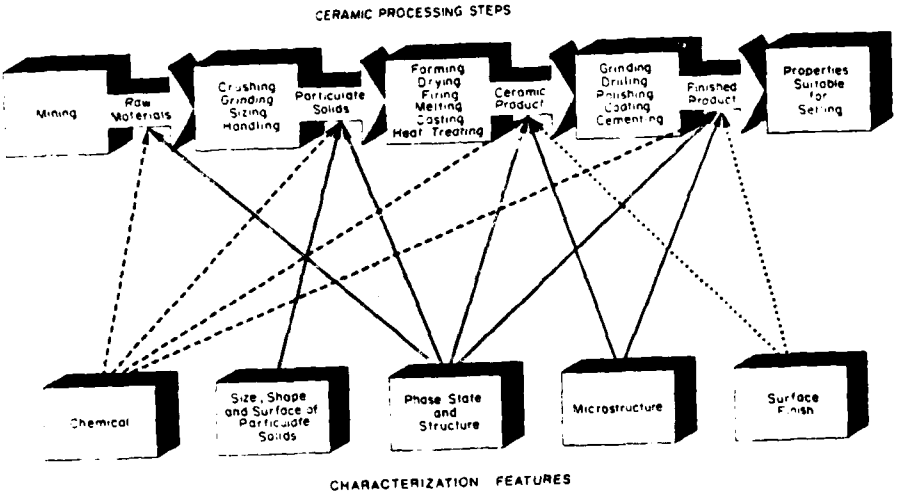

Fig.1. Ceramic characterization features related to ceramic processing steps.

characterization features essential for controlling the final properties of technical ceramics are shown in the bottom half of the fiture. The five characterization features essential for controlling the final properties of technical ceramics are shown in the bottom half of the figure. Of the five characterization featues shown, chemical and compositional analyses are well developed. Likewise, the techniques for analyses and understanding of phase state and structure of materials and the microstructural variability of electronic ceramics are also well established and routinely used.

However, I believe that it is fair to say that our understanding of the characterization of the surfaces of powders and particulate agglomerates that are used to produce polycrystalline ceramics is not well developed. Likewise, characterization of the surfaces of many technical ceramics is often not well understood.

My hypothesis for this paper is that processing innovations and the resulting improvements in the physical properties of electronic and energy ceramics will require new understanding and control of the surfaces and interfaces of powders, compacts, and final products.

Achieving such control, if possible, is defined as "microprocessing of technical ceramics." Table I illustrates the ceramic microprocessing concept. Traditionally the approach of achieving variations in the composition of ceramic powders and changes in the phases of ceramic powders has been to mix oxides, usually in the form of particulate solids. An inherent feature of this is to produce in a green body compact composition and density variations within the compact. Drying and firing

TABLE I

Microprocessing of Ceramics

- Control Powder Surfaces
  - Variable composition-depth profiles
  - Vapor phase coatings
  - Solution Ppt coatings
  - Oxidation-reduction treatments
  - Alter surface electrokinetics
  - Alter reheology and compaction
- Control of Powder Agglomerates
- Control Interfaces
  - Variable glassy phases
- Control Surface-Environment Interactions

of compacts with such gradients of density and composition often do not produce the homogenization of composition and properties desired. This is because it is difficult for compositional homogeniety to be achieved in the vicinity of pore shrinkage and collapse and vice versa. As the particle sizes used in technical ceramics become smaller, the importance of the powder surface becomes greater. Consequently controlling the composition and phase state of the surfaces of powders becomes the direction that must be followed to obtain improvements in both processing and properties. Additives must be introduced in new ways that minimize diffusion paths and prevent formation of undesirable grain boundary phases. Improved control over the microstructures and strength of agglomerates, their performance in compaction, and subsequent drying and firing results from control of powder surfaces and should be of top priority in future ceramics research.

Improving long-term environmental stability of components with large surface and interfacial areas will also be continuing need for research and development in the 1980's. It now appears possible to select specific compositional additives that can serve to passivate ceramic and glass surfaces and control interactions from moisture and damaging gaseous or liquid species. However, in order to make such a selection of environmental passivating additives, it is necessary to understand the fundamental mechanisms of environmental attack.

A purpose of this paper is to show examples from on-going work in our laboratory that illustrates use of new surface physics tools to understand surface and interfacial phenomena in technical ceramics.

In understanding surfaces and interfaces it is important to recognize that analytical techniques sample to different depths within a surface. Secondary ion mass spectroscopy, ion scattering spectroscopy, and Auger electron spectroscopy (AES) obtain data from the near surface of a sample at a depth of 5-50 Å. The middle surface of the sample can be analyzed by using infrared reflection spectroscopy (IRRS) to a depth of ∿0.5 μm. Standard scanning electron microscopy with energy dispersive x-ray analysis and electron microprobe techniques, which are high-energy electron beam methods, penetrate to depths as large as 1.5 μm and such measurements are termed to be from the far surface. It is possible to use argon ion beam milling in conjunction with AES to obtain information from all three regions of surface and what is termed a compositional profile.

A depth compositional profile of the surface of an optical quality commercial soda lime silica glass is shown in Fig. 2. This surface prior to surface compositional analysis had been exposed to distilled water at 37°C for one hour. Several important features are noted from this investigation. The bulk silica concentration of the glass which was nominally 74% before reaction with the water has changed to a nearly 100% SiO_2 near surface layer. The bulk composition is reached at a depth of approximately 800 Å. The silica concentration increase at the surface is a result of the ion exchange of protons from the solution with the mobile alkali ions to the depth of 800 Å. The less mobile calcium ions are also depleted from the surface. However, the depth of loss of calcium within the one hour time period is only to approximately 300 Å.

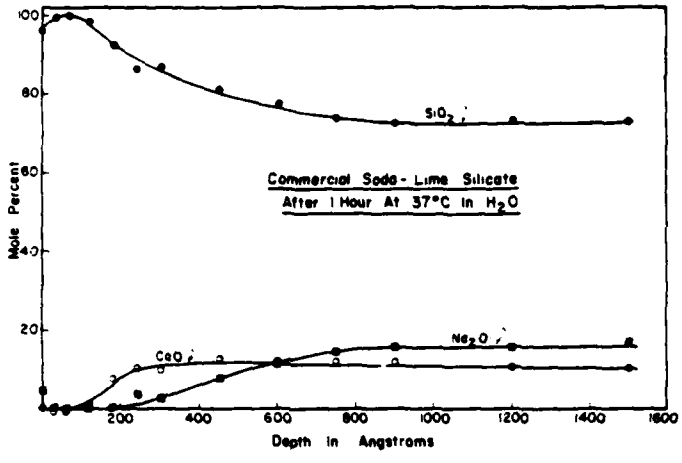

Fig. 2. Surface compositional profile (AES-ion milling) of a soda lime silica glass exposed to distilled water for 1 hr. at 37°C.

Surface analyses such as shown in Fig. 2 make it possible to understand the durability of glasses in a variety of atmospheres and environments. Since many glasses used for specialized optical, electronic, biological, or nuclear purposes are sensitive to environmental changes, the use of AES makes it possible to select specific additives or evaporated films that will protect the glass.

The second surface analysis tool which we now use routinely in our laboratory is infrared reflection spectroscopy. A standard double beam IR spectrometer is the instrument used. The instrument can be operated in two modes. The specimen for analysis can be placed on one aperature and a spectrum obtained in comparison with a highly polished reflective metal mirror. The spectrum that results is termed a single beam spectrum because the purpose of the mirror is simply to eliminate the errors associated with air scattering and instrumental variations. However, for very precise analytical work, or the elimination of certain complex features from spectra, it is possible to compare the surface of the unknown placed on the specimen aperature with a reference standard. The spectrum that results is called a compound difference spectra. The advantage of a compound difference spectrum is that it is possible to compare samples with and without various environmental changes in the surface of the sample. There are several major advantages of the IRRS technique in general. These are listed in Table II.

An example of the type of spectral information that is obtained from a sample glass of optical quality is shown in Fig. 3. A single beam reflection spectrum of pure vitreous silica results in a large IR

TABLE II

Advantages of Infrared Reflection Spectroscopy (IRRS) for Routine Surface Characterization

- Simple (Semi-Skilled Operator)
- Inexpensive ($1.00/Spectrum)
- Rapid (10 Minutes)
- Small Samples (2-3 mm)
- No Sample Preparation or Alteration
- No Vacuum or Electron Beam Artifacts
- Samples an Average of 0.5 μm into the Surface
- Combined with Mechanical Polishing can be Used for Surface Film Profiling to Depth os 1-100 μm

reflection peak at 1120 reciprocal centimeters. This peak is associated with the bridging silicon-oxygen bonds in the surface of the sample. The silica network also gives rise to silicon-oxygen-silicon molecular rocking vibrations which appear in the spectrum at the region of 540 reciprocal centimeters, not shown in this figure. When a glass structure is modified to change its physical properties, oxides other than SiO_2 are added to the glass melt. The silicon-oxygen-silicon stretching vibrations shift to a lower wavenumber as a result of decoupling of the vibrations from each other by addition of the network modifying oxides. A second peak also is observed which is due to the presence of silicon-nonbridging oxygen-modifier-cation vibrations in the glass structure. The spectral changes for the 33 molar percentage lithia-67 mole % silica glass compared to vitreous silica shown in Fig. 3, are typical of the magnitude of spectral changes observed for most silicate glasses.

When the glass surface is exposed to moisture or humidity the mobile cations such as sodium, lithium, or calcium exchange with protons as was shown in the AES compositional depth profiles. As alkali is lost from the glass surface the spectra progressively shifts to that of a surface much like vitreous silica. We can see in Fig. 3 that the stretching vibrations of the corroded lithia silicate glass now look much like that of vitreous silica and this corresponds with the silica rich layer that was observed with AES.

Thus we know from these and many other investigations that the surface of glass is dynamic. It has an electrical and optical character that is dependent upon the starting bulk compostion of the material but

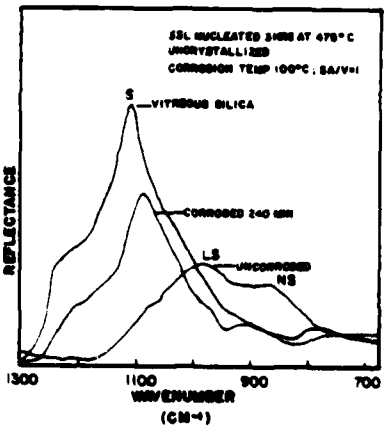

Fig. 3. Infrared reflection spectra of 33L glass uncorroded and corroded for 240 min in 100°C demineralized water.

is also strongly influenced by the processing and environmental history of the material. In order to understand the physical properties of the surface it is necessary to characterize that surface at a particular time in its envrionmental history. It is also essential to recognize that surfaces continue to alter their character with time. Therefore, understanding the time dependence or kinetics of surface alteration is an essential feature to achieve the control the physical properties of glasses.

Only recently has the application of these surface spectroscopy techniques begun to be applied to crystalline technical ceramics. We have recently found a number of new, and we think exciting, results in the use of these techniques in studying single crystal and polycrystalline technical ceramics and the following preliminary results are presented herein for the first time. In most cases our understanding of the surface phenomena is much less than complete. Consequently our main objective is to look at the potential of these tools to understand complicated surface processes including eventually powder surface characterization.

Figure 4 is the infrared reflection spectra of an undoped, pure silicon carbide single crystal. The crystal produces a broad band of silicon-carbon stretching vibrations centered around approximately 900 cm^{-1}, or 11 microns. We know that the physical properties of silicon carbide are strongly dependent upon high temperature exposure to oxygen. The second spectra shown in Fig. 4 arises from analyzing the sample of a 13 minute exposure to air at only 1309°C. The IRRS spectrum shows

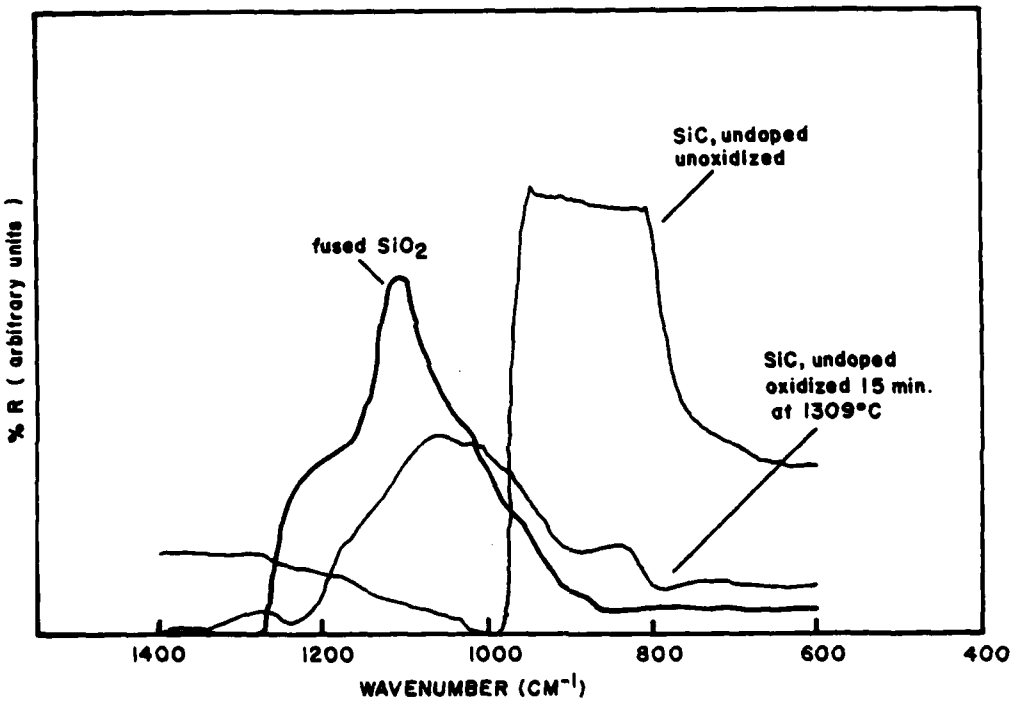

Fig. 4. IRRS before and after oxidation of undoped SiC crystal.

a surface that is now exhibiting a large concentration of silicon-oxygen stretching vibrations at 1050 cm^{-1}. The peak occurs at lower wavenumbers than that of vitreous silica also shown on the figure and corresponds to that of a cation modified silicon dioxide film. We can see that there are still residual silicon-carbon vibrational species in the surface as well. This suggests that a mixed silicon-oxy-carbon layer has formed on the surface.

A fascinating contrast in the surface behavior of impurity doped silicon carbide is seen in Fig. 5. This sample also is a single crystal but this crystal was doped with nitrogen during the growth process. The initial unoxidized spectra is quite similar to the undoped material but more vibrational species are present in the 800-1000 cm^{-1} region which corresponds to the region of silicon-nitrogen vibrational modes as well. The most facinating difference, however, is that 15 minutes of oxidation at 1309°C gives rise to a surface spectra that is not at all like that of the undoped material. There is almost no Si-O stretching vibrations visible in the surface. Si-O and Si-N species are attacked but without the formation of an oxide layer. AES analysis is used to determine if oxygen has diffused into the lattice exchanging with nitrogen rather than forming a film on the surface. Silicon carbide single crystals containing aluminum or various mixtures of cation and anion impurities exhibit spectra after oxidation that is made up of a wide range of vibrations over the range from 1200-600 cm^{-1}.

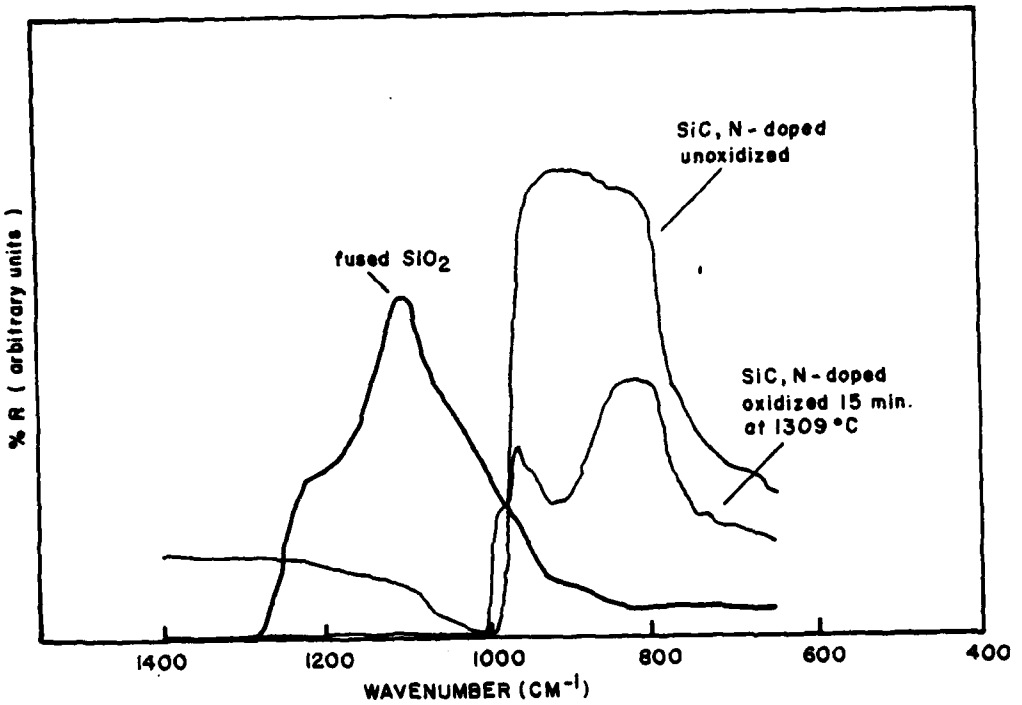

Fig. 5. IRRS before and after oxidation of N doped SiC crystal

Thus we see from these figures that a very minor exposure of silicon carbide crystals to the atmosphere gives rise to surface changes to depths of at least a half a micron, which is the sampling depth of the infrared technique. The spectral characteristics and infrared properties are totally different depending upon small concentrations of dopant ions. It is also quite likely that various species in the atmosphere that the crystals are exposed to will also strongly affect both the surface character and bulk properties due to rapid impurity controlled diffusion. The extreme variation resulting from the nitrogen in the lattice of the silicon carbide suggests that nitrogen in a high temperature atmosphere may be a very important species in surface attack as well.

These large variations in properties with small concentrations of impurities and severe environmental sensitivity may account for the difficulty in producing high quality semiconductor devices from silicon carbide. Also, these experiments suggest that much must be learned about the surface properties of silicon carbide powders, and the interaction of additives with powders, and the effect of processing atmosphere in order to control the processing and eventual properties of polycrystalline silicon carbide.

Figure 6 shows the use of IRRS in evaluating the oxidation of polycrystalline chemically vapor deposited silicon carbide. The peak growing as a function of oxidation time at 1315°C located at 1100 cm^{-1} is identified as silicon-oxygen-silicon stretching vibrations. This peak is associated with the growth of the oxide layer on the material.

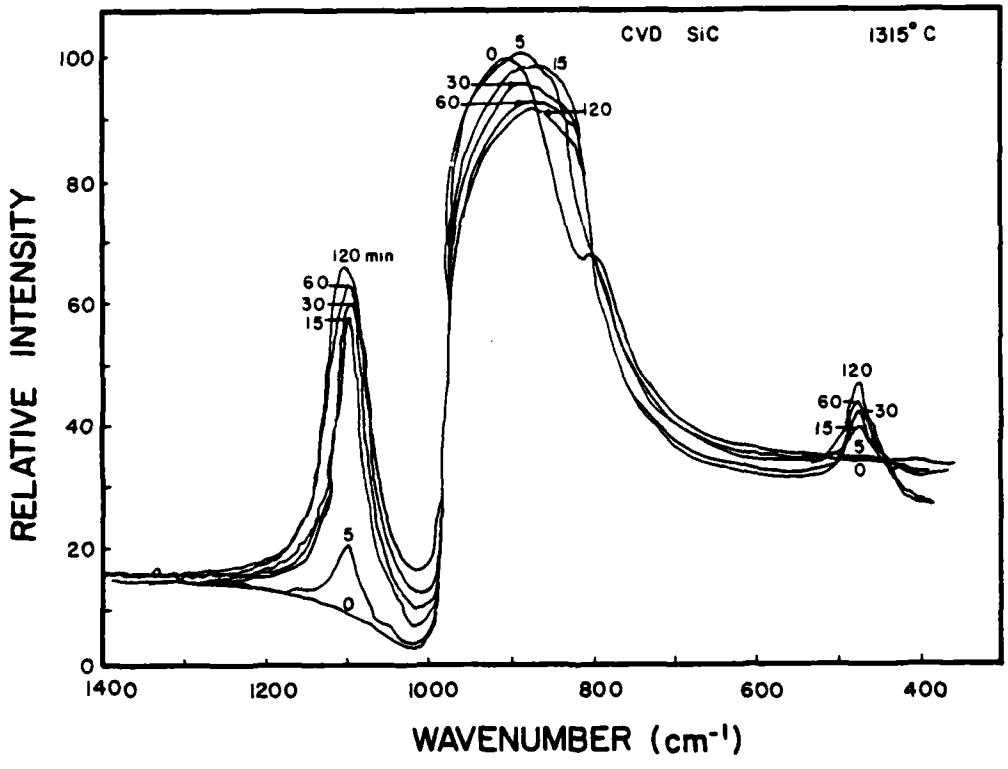

Fig. 6. IRRS of CVD SiC at various stages of oxidation

It is an important finding that the growth of the oxide layer on the polycrystalline material is quite different in its surface spectral features from the growth on the single crystals (Figs. 4 & 5). Figure 6 shows a significant difference in the intensity and distribution of the silicon-carbon vibrational modes in the 800-1000 cm^{-1} region. We see that during oxidation, specific higher frequency vibrational species are eliminated from the spectra as the oxide layer forms. It appears that the formation of the oxide layer is at the expense of specific silicon-carbon bonds. The rapid development of the oxide stretching vibrations from 5-15 minutes suggest that there is a nucleation process occurring on the surface followed by preferred crystallographic attack of the silicon carbide lattice by oxygen atoms. Subsequent growth of the oxide film during the period from 15 minutes to 2 hours appears to be by diffusion through the oxide layer since the spectral changes follow a square root time dependence. At the right hand side of the figure we also see growth of an infrared peak at approximately 480 cm^{-1} which is associated with the rocking vibrations of silicon-oxygen modes in the oxide layer.

Hot pressed silicon carbide containing boron hot pressing additive behaves differently in exposure to oxygen from the CVD material or the carbide single crystals. There is an oxide growth on the surface of the silicon carbide as indicated by the formation of both silicon-oxygen stretching and rocking vibrations. However, this growth follows a square root time, diffusion, behavior from its outset. The oxide growth is at the expense of a much wider range of silicon carbide vibrational species than was observed for the CVD material.

Thus, the comparison of the infrared spectra of the silicon carbide single crystals with the chemical vapor deposited polycrystal material and the hot pressed material shows enormous variation in the optical properties of these materials as a function of their method of manufacture with very small variations in the composition of the material. The comparison of the surface oxidation response of these three types of silicon carbide illustrates the extreme sensitivity of the crystal lattice and the structure of the material to change as a function of impurities and processing method. These comparisons show that it is essential to control the surfaces of starting powders and the distribution of impurities or additives within the grain structure of the dense polycrystalline ceramics in order to produce uniform physical properties of the material.

The change of the IRRS spectra of silicon nitride as a function of oxidation exposure serves as a further example. Other studies have shown that use of zirconia or yittria additives in the hot pressing of silicon nitride prevents the formation of large flaws during oxidation and thereby protects the material from high temperature reduction in strength in oxidizing environments. The mechanisms by which the materials surface is altered to provide a protection of the physical properties is still not fully understood. Figure 7 gives some additional insight of the changes that are taking place on the surface as the material is exposed to oxygen. We see that as the time of exposure to oxygen increases, one of the major silicon-nitrogen stretching vibrations is gradually reduced and eventually eliminated entirely from the spectrum

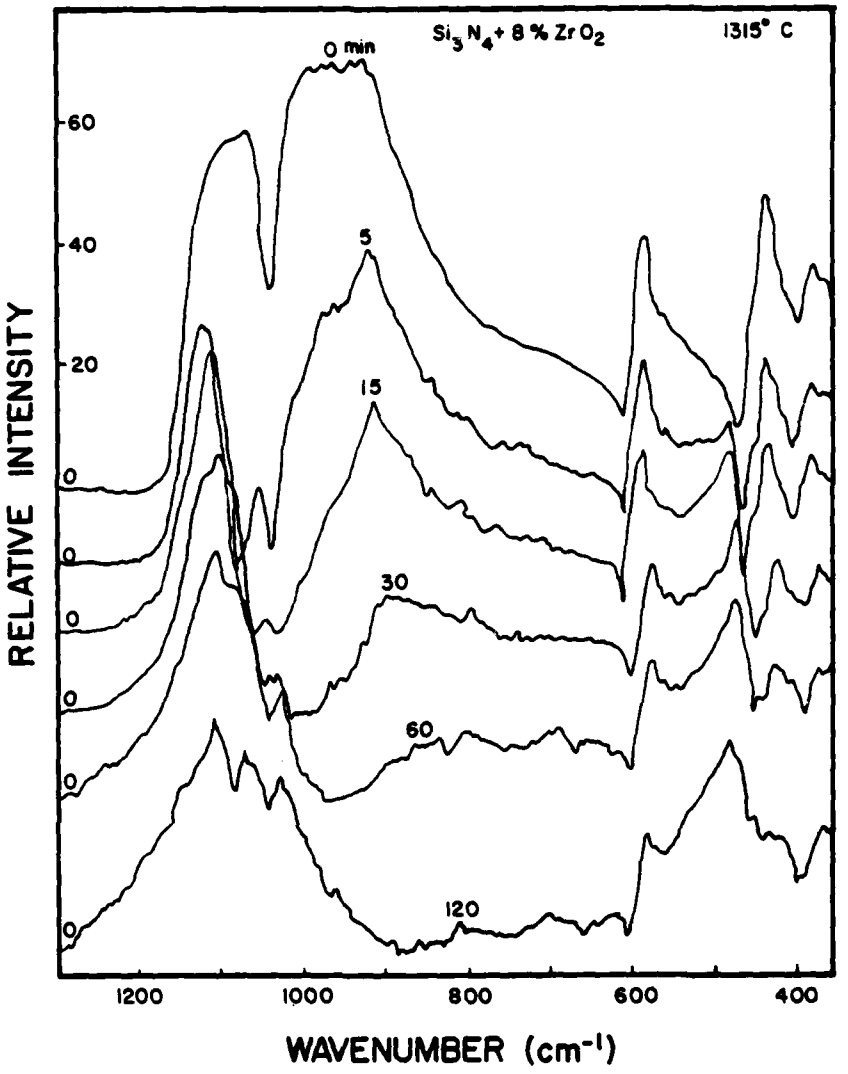

Fig. 7. IRRS spectra for Si_3N_4 + 8% ZrO_2 at various stages of oxidation at 1315°C.

We also see that one of the higher wavenumber modes is shifted as a function of oxidation treatment and eventually changes in its character until it has a broad peak centered around 1100 cm^{-1}. The rocking vibrations have a broad single peak replacing the double silicon-nitrogen peaks which are around 500 cm^{-1}. The spectrum resulting from the 2 hour oxidation at 1315°C is very similar in its features to that of a vitreous or polycrystalline silica-like surface. This layer appears to serve as a diffusion barrier to oxygen to prevent it from migrating into the structure of the material.

Evidence to support the hypothesis that oxygen is forming a mixed silicon-oxy-nitride phase is obtained by the use of Auger electron spectroscopy. Figure 8 is a plot of the oxygen content of the surface versus the nitrogen content of the surface (expressed as peak-to-peak heights of the Auger electron signal) as a function of thickness of layers progressively removed from the surface of a Si_3N_4 sample oxidized for 30 minutes at 1111°C. The depth of the surface profile shown in this figure is approximately 8000 Å. Thus, the left side of the linear curve corresponds to the outer or near surface of the sample which we can see contains a mixture of oxygen and nitrogen. As we move into the surface the oxygen content decreases linearly with depth and nitrogen increases until we reach an interfacial reaction layer which is approximately 200-400 Å wide. The presence of both oxygen and nitrogen at the near surface of the sample indicates that there is a mixed oxynitride phase of ∿0.8 μm thick and most importantly the ratio of oxygen and nitrogen in the phase changes uniformly throughout its thickness until the bulk structure of the material is reached.

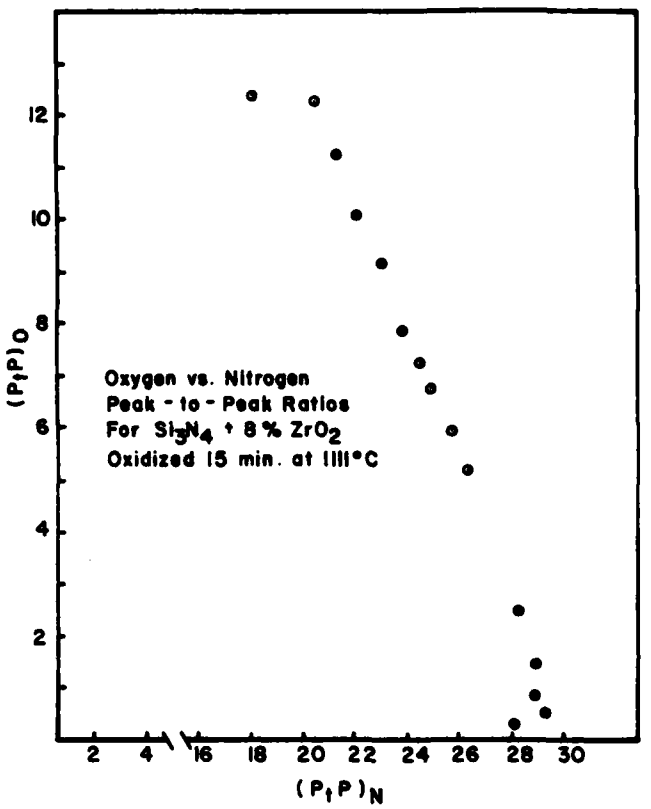

Fig. 8. Oxygen-nitrogen compositional profile within the surface of exidized Si_3N_4 + 8% ZrO_2.

Use of compound difference infrared reflection spectroscopy shows the intriguing find that the mixed oxynitride phase formed on the surface of this material has vibrational modes that are very different from that of vitreous or polycrystalline SiO_2. This is illustrated in Figs. 9A and 9B. The bottom half of each figure is produced as a result of analyzing the silicon nitride sample in comparison to vitreous silica on the experimental beam. The two halves together provide a compound difference spectrum of the vibrational modes of oxygen-silicon-oxygen bonds from those of nitrogen-silicon-nitrogen and nitrogen-silicon-oxygen. Thus, the major peak seen at 930 cm^{-1} is that the nitrogen-silicon-nitrogen stretching vibrations and the peaks at 540 cm^{-1} are nitrogen-silicon-nitrogen rocking vibrations. After oxidation, a new peak appears at 1100 cm^{-1} which is due to the new oxygen-silicon-nitrogen bonds fromed in the surface. The new bonds are characteristic of the new oxynitride phase. An increase in thickness of the surface phase or a change in structure by incorporating additives or crystallization can be followed quantitatively with these techniques. Efforts to relate the character of the surface phase to changes in physical properties of bulk samples and characterization of powders are now in progress. A recent study shows that the isoelectric point of Si_3N_4 powders shifts from pH 4.7 to pH 3.5 when the mixed oxynitride phase forms on the powder surface.

Variation in the surface character of dense polycrystalline alumina electronic substrates potentially affects the adherance, electrical properties, and environmental sensitivity of metallizing interfaces. Characterization of surface roughness and bulk composition does not

(A)

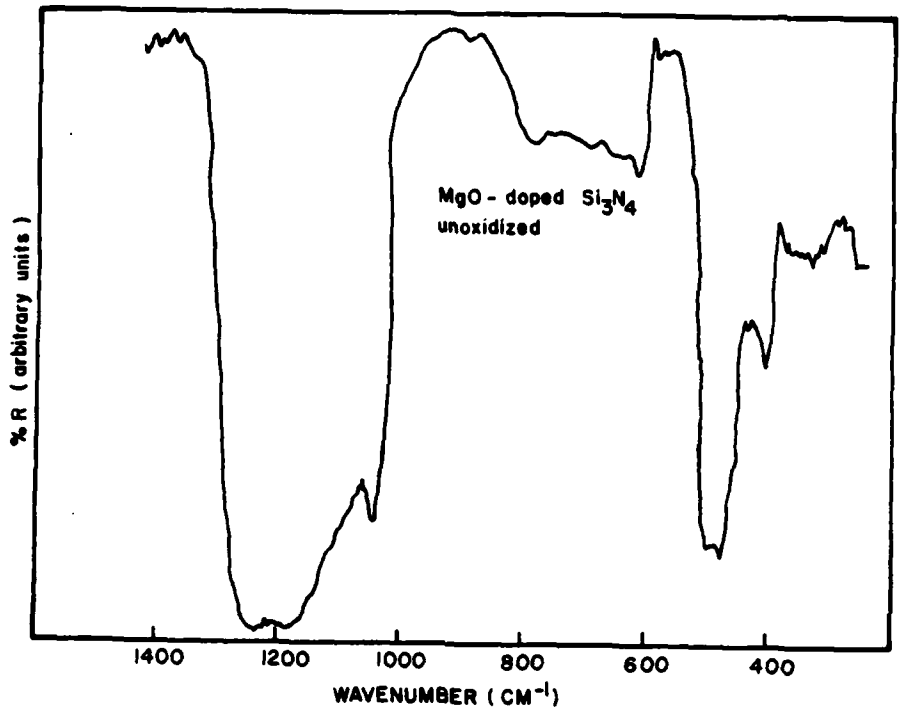

(B)

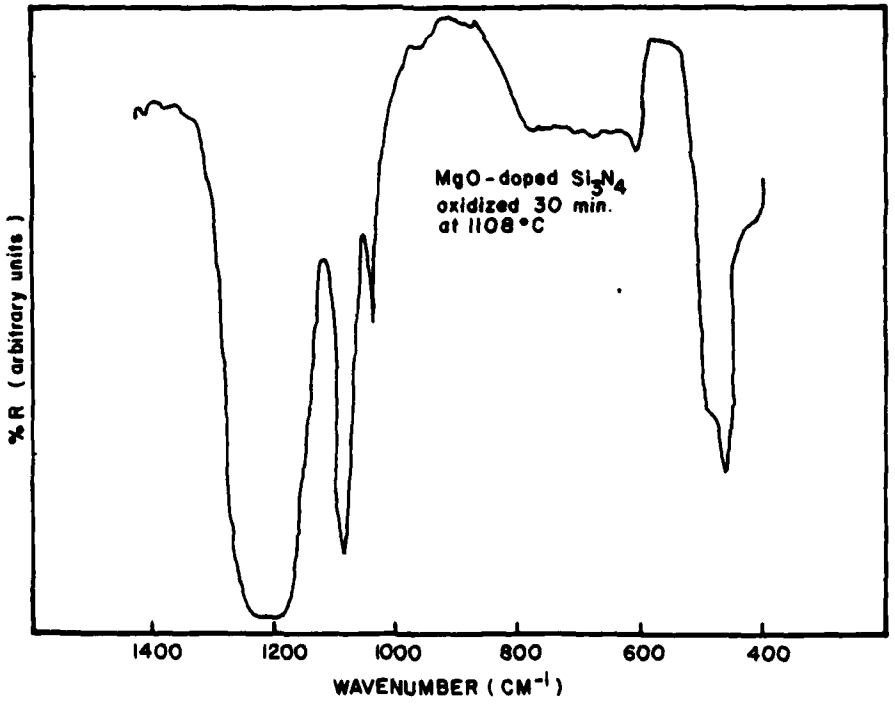

Fig. 9. Compound difference IRRS spectra of (A) unoxidized MgO doped Si_3N_4 and after (B) 1108°C/30 min. oxidation.

appear to be sufficient to understand the variations between different grades of alumina. The following data illustrates use of the new surface analysis methods to try to understand this problem.

Figure 10 shows the single beam IRRS spectra of several grades of commercial alumina compared with the spectrum of single crystal sapphire. All alumina samples were analyzed in their as-received condition without mechanical or chemical treatments after tape casting and sintering. The high purity single crystal sapphire was a flat plate oriented with the c-axis perpendicular to the plate.

A large number of the aluminum-oxygen stretching vibration modes are missing from the surface of the commercial samples over the 850 to 600 cm^{-1} region. The lower the purity of the sample the greater the number of missing molecular vibrations. Although there are only one to five percent of second components in the samples, the infrared method is sensitive to the purity level.

However, the variation in the alumina surface is not simply due to composition differences. There is also a strong effect of orientation of the as-cast and fired surfaces on the IRRS spectra, as illustrated in Fig. 11. The middle curve is a composite of three runs of the 94% alumina sample at 0°, 180°, and 360° orientation to the IR beam. The sample was ground and polished with 6 μm diamond paste which accounts for the greater IR intensity than that of Fig. 10. However, even after grinding and polishing, IR spectra run at orientations of 90° and 270° produce the bottom and top curves respectively. Evidence that this effect is related to a preferred orientation of grains in a surface finish created by the tape cast process is provided by Fig. 12.

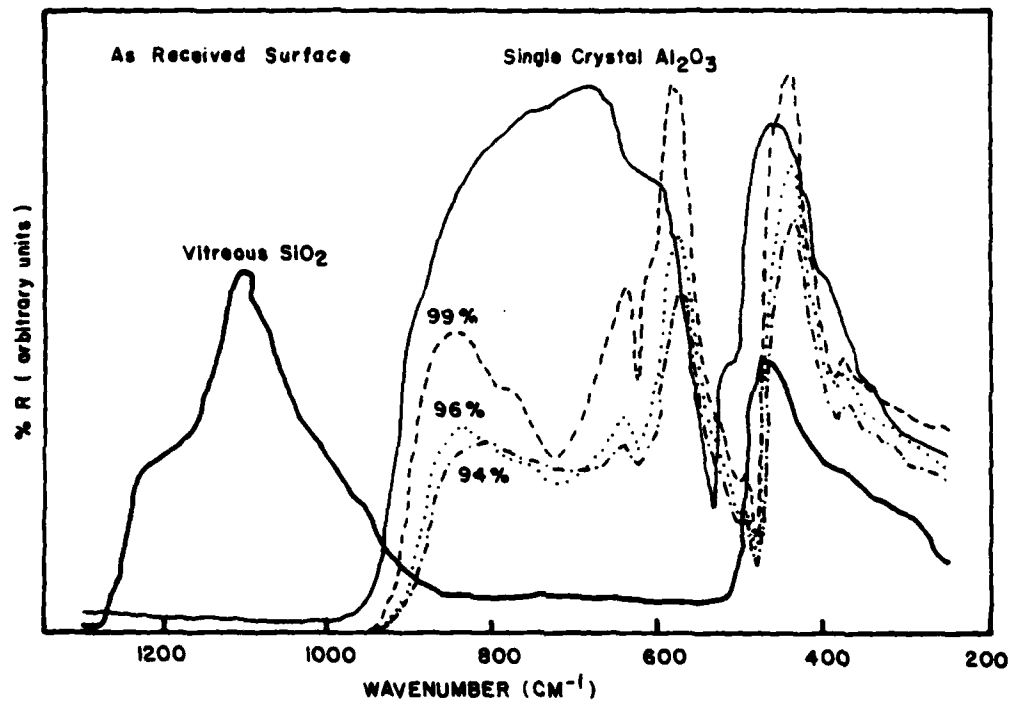

Fig. 10. IRRS of 3 grades of commercial dense alumina compared with single crystal sapphire and vitreous silica.

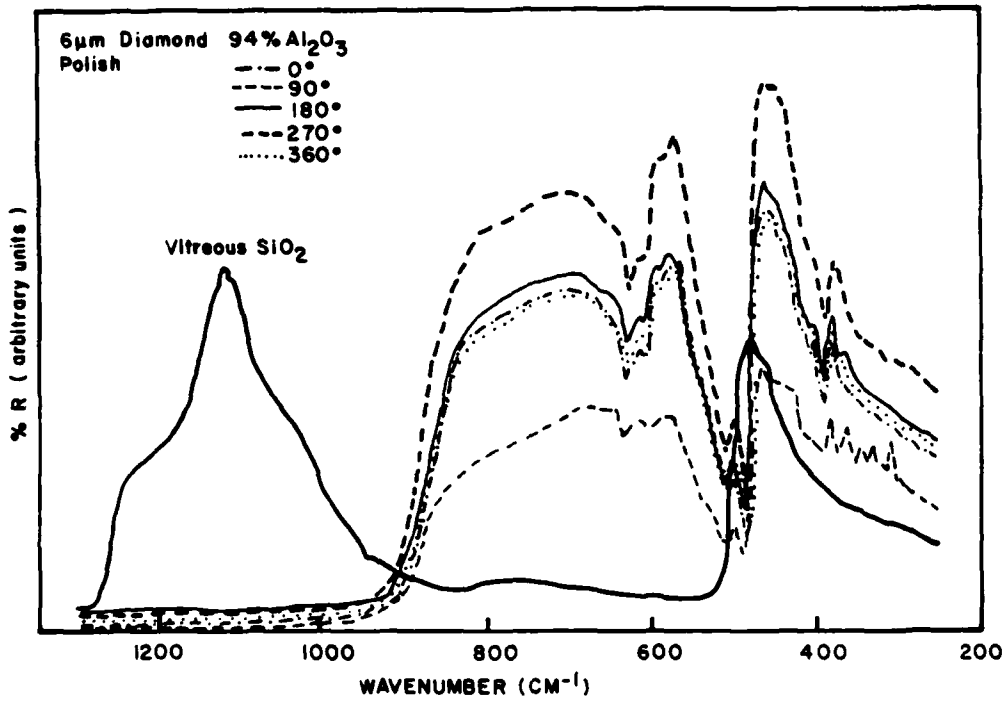

Fig. 11. Tape cast 94% alumina oriented a different rotations with respect to the IRRS beam.

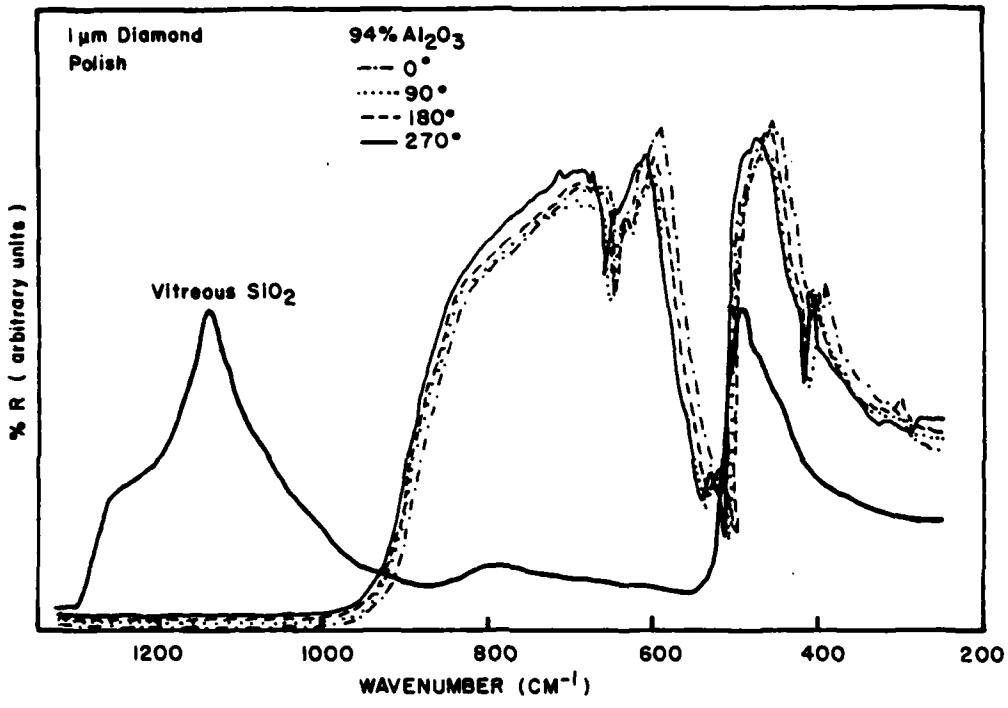

Fig. 12. IRRS spectra of 94% tape cast alumina after removing oriented surface layer with 1 um diamond polish.

The same 94% alumina substrate was polished with a 1 μm diamond paste. The IRRS spectrum of Fig. 12 is now similar to that of the single crystal sapphire and very little preferred orientation of the surface remains. All orientations of the sample in the spectrometer beam nearly superimpose. A similar IRRS analysis of pressed and sintered alumina bodies shows much less surface orientation.

We have also found that exposure of dense alumina to hydrothermal conditions produces irreversible changes in IR spectra which depend on surface layers formed during processing. Thus, a number of variations in properties and stability of fired metallized pastes on alumina may be due to lack of control between surface layers on the alumina with glassy firts in the pastes and humidity in the firing atmosphere. Lack of environmental stability subsequent to firing may be related to the same variables.

Conclusions

Hopefully, the examples selected show that surface physics techniques such as Auger electron spectroscopy and infrared reflection spectroscopy can be used to understand variations in the character of surfaces and interfaces of technical ceramics due to processing methods, additives and environmental exposure. Thus, the sensitivity of surface and interfaces to such variations must be characterized in order to control fully long term performance of high grade technical ceramics.

Acknowledgments

I greatfully acknowledge the assistance of D. E. Clark, T. M. Barrett, S. Bernstein, M. Blare and L. Ogbuji in obtaining data shown

herein and the UF COEE and AFOSR Grant #77-3210 for partial financial assistance for the SiC and Al_2O_3 studies and NASA Grant #NSG 3254 for the Si_3N_4 work.

SECTION VII

SUMMARY REPORT (3/1/77-2/28/80)

Application of surface sensitive techniques for characterizing surfaces of ceramic materials has been evaluated in this study. Emphasis has been placed on glass and glass-ceramics, but analysis of Si, SiC, Si_3N_4, and Al_2O_3 indicates that the techniques can be used for surface characterization of these important ceramic materials as well. The major thrust has been the correlation of structure with mechanical and chemical properties, and the development of models for predicting long-term behavior of ceramics in a variety of environments. Glass-ceramics have provided a good model system due to the wide range of possible microstructures attainable with these materials. Preliminary results suggest that glass-ceramics may be used as analogs for understanding the chemical and physical properties of more complicated polyphase, polycrystalline ceramic materials. Additionally, concepts developed in this three year probram may be utilized in achieving better correlations between ceramic processing, surface structure, and properties. A summary of our most significant results are presented in the following paragraphs.

Due to their excellent mechanical properties, glass-ceramics present an extremely important class of ceramics. These materials are typically prepared from preformed cast glass articles via a specific nucleation-crystallization treatment. This ceraming process produces local

compositional and structural alterations in the material that are often difficult to evaluate with conventional X-ray and optical techniques. It has been shown in this investigation that infrared reflection spectra (IRRS) are sensitive to changes associated with nucleation-crystallization of glass. This technique can be used quantitatively to monitor crystallization in the glass-ceramic systems.

In general, the environmental sensitivity of glass and glass-ceramics are not well understood. The mechanisms of corrosion for uncrystallized $Li_2O \cdot 2SiO_2$ glass (33L) have been previously investigated in detail by Sanders, Person and Hench in a series of papers and the corrosion kinetics of 33L glass have been established by Ethridge. Furthermore, the nucleation and crystallization kinetics of 33L glass have been extensively studied by Hench, Freiman and Kinser. Therefore, both the corrosion and crystallization behavior of this glass system are well characterized, albeit separately. The corrosion behavior of stoichiometric $Li_2O \cdot 2SiO_2$ (33L) glass and glass-ceramics in acidic, neutral and basic solutions has been studied using infrared reflection spectroscopy, scanning electron microscopy and solution analyses. Glass-ceramics containing volume fractions of crystallization ranging from 0-90% were investigated. The composition of the glassy phase is the same as the crystalline phase. Selective Li^+ leaching from the glassy phase and glass network dissolution are the major mechanisms of corrosion in 33L glass and glass-ceramics. In addition, phase boundary attack contributes significantly to surface deterioration of the glass-ceramics. The relative importance of network dissolution, Li^+ leaching

and phase boundary attack is dependent on both the extent of crystallization and solution pH. In general, the materials containing high volume fractions of crystals (90%) corrode via a network dissolution mechanism in all media, materials containing no crystals (0%) corrode by ion exchange in low pH media and network dissolution in high pH media and materials containing 20-60% crystals corroded via all three mechanisms.

The procedure of ceraming to produce a glass-ceramic usually improves the mechanical strength of the final product, but its effects on chemical durability are not always predictable. For instance, when a non-stoichiometric glass is crystallized the composition of the glass may be significantly different from the crystalline phase producing a different major mode of corrosion than observed for stoichiometric materials.

In the present investigation, a Li_2O-Al_2O_3-CaO-SiO_2 glass was heat-treated to provide various stages of crystallization. The glassy phase was much richer in alkaline and alkaline earth species than the crystalline phase. The corrosion behavior of the resulting glass-ceramics was studied using infrared reflection spectroscopy (IRRS), scanning electron microscopy (SEM), and solution analyses. The mechanisms controlling the extent of corrosion vary depending on the degree of crystallization (V_v). The higher V_v glass-ceramics exhibited poorer resistance to aqueous attack than did the low V_v glass-ceramics, even though the crystalline phase itself was more durable.

The effects of alumina additions on the durability of lithia-alumnia-silicate glasses have also been investigated. Progressive improvement in durability continues to 11 mol % Al_2O_3, the limit of this study. In order

to explain the role of alumina in improving durability, Auger electron spectroscopy, infrared reflection spectroscopy and scanning electron microscopy, infrared reflection spectroscopy and scanning electron microscopy were utilized to show that both stable and unstable surface films can form on alumina glasses during aqueous attack. Solution analysis was used to determine isochronal corrosion diagrams and compositional corrosion paths. These data also provide additional evidence that passivating film formation assumes an important role in the corrosion behavior on Li_2O-Al_2O_3-SiO_2 glasses.

Further understanding of the role of high valence cations on glass corrosion was obtained by studying the effects of soluble Al compounds on the corrosion behavior of 33 mol % Li_2O-67 mol % SiO_2 glass (33L). A maximum in glass corrosion occurs at 25 ppm Al^{+3} in solution. The presence of >50 ppm Al^{+3} in solution decreases the network dissolution but has little effect on the selective leaching of Li^+ from the glass. When Al_2O_3 was added directly to the glass melt, a reduction in both selective leaching of Li^+ and network dissolution is observed. The 33L glass exhibited similar corrosion behavior and surface film formation for all soluble Al compounds investigated, suggesting that Al is the effective corrosion inhibiting specie. The primary mechanism of corrosion retardation is due to Al^{+3} passivation of the surface active sites in the silica-rich layer that develop during corrosion.

Another important composition variable which affects the durability of glasses is the mixture of different types of alkali ions. It is well known that the presence of certain ratios of alkali oxide species can

improve the chemical durability of glasses. Several theories have been proposed for this mixed alkali effect (MAE). We have discovered that the magnitude of the MAE is dependent on both the dominant mechanism of corrosion and the corrosion kinetics. When ion exchange is rate controlling, the MAE may be large. When network dissolution is rate controlling, the MAE may become insignificant. Studies of the interaction of alkali and alkaline earth cations suggest that the major role of Ca^{+2} in the MAE is to prolong the time during which the ion exchange reaction is rate controlling. This effectively increases the time during which the MAE may be operative and thus reduces the environmental reactivity of the glass.

During this 3 year contract a number of environmental parameters important to understanding long term lifetime performance of glasses, glass-ceramics, and ceramics were investigated. One of the most important of these parameters is the ratio of the surface area of glass (SA) to volume of solution (V); i.e., (SA/V). For polished bulk glass surfaces, plots of the concentration of corrosion products in solution (after a given time of corrosion) vs. the SA/V ratio and plots of the time to reach a given concentration of corrosion product in solution vs. the SA/V ratio yield results in agreement with derived equations. The corrosion of glass grains, however, is complicated by the change in effective surface area with time which requires a modification of the simple corrosion kinetic equations. A new technique was developed for predicting glass corrosion in closed systems based on a logarithmic plot of the time to reach a critical corrosion event vs. the SA/V ratio.

One of the primary objectives of this contract was the investigation of environment sensitive physical properties of glasses and glass-ceramics with well characterized chemical responses to water. The Li_2O-SiO_2 glass and glass-ceramic system was generally used.

The mechanical strength of $Li_2O \cdot 2SiO_2$ glass was measured as a function of stressing rate both in air and in distilled water. The fatigue parameters, B and N, can be determined from the following equation.

$$S^{N+1} = B(N + 1)\ S_i^{N-2}\ \dot{\sigma} \qquad (1)$$

where

S = strength at a given stressing rate, $\dot{\sigma}$

S_i = strength of the glass as measured in liquid nitrogen (inert strength)

It was found that the glass was more susceptible to stress corrosion (i.e., lower value of N) when tested in water. Using the above parameters, design diagrams were constructed for the glass in each environment. These diagrams permit the design of a proof test to guarantee a desired lifetime at a given applied stress. The following equation was used to construct these diagrams:

$$t_{min} = B\sigma_p^{N-2}\ \sigma_a^{-N} \qquad (2)$$

where

t_{min} = minimum lifetime (in seconds) expected at a given applied stress, σ_a, after some proof test σ_p

Using the same proof test, it was found that the glass is less susceptible to failure in air than in an aqueous environment.

The fatigue properties of lithia disilicate glass and glass-ceramics exposed to several environmental conditions have also been studied. The objective was to understand the behavior of the materials in both reactive (humid air and triply distilled water) and nonreactive (liquid nitrogen) environments under dynamic loading conditions. The proof test stress required to guarantee a lifetime of 10 years at 10,000 psi varies greatly with the amount of water present. Similar effects were also observed with the crystalline materials.

A major objective of the program was to continue developing quantitative means of characterizing surface behavior of glasses, glass-ceramics and ceramics. Because Auger electron spectroscopy is routinely used for this purpose in our lab we felt it was necessary to understand this techniques. Problems associated with Auger analysis of glasses are well recognized. When an electron beam impinges on the surface of a glass specimen, the Auger signal produced by the alkali species decreases with exposure time. The rate at which the signal decays depends on the glass composition, beam current density, accelerating potential of the primary beam and substrate temperatures, all of which must be carefully controlled in order to obtain a reliable analysis. A similar decay of the alkali Auger signal is observed for glass-ceramic systems. The rate of decay for the crystalline phase is different from that for the glass and is dependent on the extent of crystallization. This behavior may provide a basis for using Auger electron spectroscopy for microstructural as well as compositional analysis.

Migration of sodium in thin films of soda-silica glass deposited on a stainless steel substrate were also studied. The amounts of charge trapping and local heating were a strong function of beam parameters for thin films. For example, the time required for the sodium Auger signal to decay to 50% of its initial value increased as the beam energy was increased or as the current density was decreased. The rearrangement of sodium due to charge trapping was calculated and compared to experimental data. The calculated and experimental data agree well and indicate fields of $\sim 10^5$ V/cm exist during analysis. The depth distribution of sodium indicates that either electrons or ion bombardment can cause sodium migration during analysis. The cross-section for electron induced desorption was measured to be 3×10^{-20} cm^2 for sodium in this glass, therefore it is only important at very high current densities.

Our decade long efforts in this subject area led to requests during the 3 years of the contract for review paper contributions. Thus, several extensive review of the physical chemistry of glass surfaces were written and are listed in the publication list for the contract. These provide an understanding of the long-range objectives of this project. Six typical problem areas requiring improved understanding of glass surfaces are identified. Results obtained from several surface analysis instruments show that five types of surfaces are characteristic of a silicate glass at any time in its history. The type of surface is dependent on the environmental history of the glass and may be defined in terms of surface compositional profiles. Several

important glass surface topics of current interest are discussed. These include: glass corrosion mechanisms; the mixed alkali effect; surface passivation with solution ions; protective film formation on glasses; the role of CaO, R_2O/SiO_2, and Al_2O_3 in glass corrosion; glass surface area to solution volume ratio; and the relevance of autoclave procedures in testing glass durability.

During the last year of the 3 year program we made an effort to apply the techniques of surface characterization used in our glass studies to the study of single crystal and polycrystalline ceramic materials. An initial study to characterize the surface condition of Si_3N_4 materials used infrared reflection analysis (IRRS) to analyze the surface structural changes that occur upon prolonged heating (100 h at 1430°C) of various Si_3N_4 materials. It was discovered that hot pressing with additions of 2 to 12% ZrO_2 produced a glassy silicate surface film that restricts formation of an oxidation layer to 20-30 μm deep. In contrast, standard 3% MgO hot pressing additions do not produce a protective glassy surface film and an oxidation layer develops to a depth of 7-90 μm. The mechanical strength of the Si_3N_4 materials before and after heating correlates with the integrated area under the IRRS spectra over the spectral range of 1300-300 cm^{-1}. The correlation may be related to the concentration of surface flaws and thus the IRRS technique may be an effective means for nondestructive evaluation of mechanical properties of Si_3N_4.

Infrared reflection spectroscopy (IRRS) has been applied as a very sensitive quantitative method to follow the first stages of oxidation of Si, SiC, and Si_3N_4 materials. Simple diffusion controlled kinetics

describe the early oxidation of Si. Oxidation of SiC varies significantly depending on the purity and method of processing. In some SiC samples nucleation of the oxide is a critical step in the kinetics whereas other samples exhibit only growth kinetics. Evidence of heterogeneous surface attack is present. In contrast, Si_3N_4 + 8% ZrO_2 oxidizes by forming a homogeneous glassy silicate film on the surface.

Flaw sizes in hot pressed Si_3N_4 were determined by fractography and fracture mechanics calculations and related to changes observed in infrared reflection spectra of samples oxidized for various times. A correlation between flaw size and IRRS spectra of oxidized Si_3N_4 samples would allow use of infrared reflection spectroscopy in predicting the stability of this high-temperature structural material. Infrared reflection spectroscopy was found to be useful in characterizing phase changes which occur in the surface oxide layer. These phase changes are influenced by the depth to which the oxidized layer extends into the material, which in turn affects the strength of Si_3N_4.

It is proposed that progress in improving the properties of technical ceramics will require improved understanding of ceramic processing, especially the surfaces, interfaces and agglomeration of powders, and the interaction of surfaces with the environment. New surface analysis instruments such as infrared reflection spectroscopy (IRRS) and Auger electron spectroscopy are used to describe surface compositional changes of SiC, Si_3N_4, and Al_2O_3. Preferred crystallographic pathways of surface attack are observed for both SiC and Si_3N_4 single and polycrystalline samples. Formation of an oxynitride surface phase on Si_3N_4 powders significantly alters the surface charge distribution and decreases the

the isoelectric point of the powders. Variations in processing of dense Al_2O_3 result in a deep surface layer of preferred orientation which can be detected non-destructively with IRRS methods.

SECTION VIII

LIST OF PUBLICATIONS AND PRESENTATIONS

EITHER PARTIALLY OR FULLY SUPPORTED BY THIS GRANT

1. "Surface Characterization of Ceramed Composites and Environmental Sensitivity," presented at the Conference on Composites and Advanced Materials, Cocoa Beach, Florida, January 1978.

2. "Aqueous Corrosion of Lithia-Alumina-Silicate Glasses," Am. Ceram. Soc. Bull. 57[11], 1040-1044 (1978).

3. "Effects of Glass Surface Area to Solution Volume Ratio on Glass Corrosion," J. Phys. & Chem. Glasses, 20[2], 35-40 (1979).

4. "Ceramic Surface Degradation," presented at 70th Annual Meeting of American Institute of Chemical Engineers, New York City, November 1977.

5. "Role of Ca^{+2} in the Mixed Alkali Effect," submitted to the J. Am. Ceram. Soc.

6. "Mechanical Properties of $Li_2O \cdot 2SiO_2$ Glass," submitted to J. Am. Ceram. Soc.

7. "Infrared Reflection Analysis of Thermal Changes in Si_3N_4 Surfaces," submitted to the J. Am. Ceram. Soc.

8. "Physical Chemistry of Glass Surfaces," J. Non-Crystalline Solids 28, 83-105 (1978).

9. "Physical Chemistry of Glass Surfaces," Survey Lecture for the XIth International Congress of Glass Conference, Prague, Czechoslovakia, July 4, 1977.

10. "Physical Chemistry of Glass Surfaces," Glass '77, A Survey of Contemporary Glass Science and Technology, Jeri Gotz, ed., published by CVTS-DUm Techniky, Praha, 343-370, July 1977.

11. "Surface Analysis of Si_3N_4 Oxidation," paper presented at the Conference on Composites and Advanced Materials, Cocoa Beach, Florida, January 24, 1978.

12. "Effects of Heat Treatment Time on the Oxidation of Pressed Si_3N_4 as Determined by Infrared Reflection Analysis," presented at the Conference on Composites and Advanced Materials, Merritt Island, Florida, January 21-24, 1979.

13. "Corrosion Behavior of Lithia Disilicate Glass in Aqueous Solutions of Aluminum Compounds," Am. Ceram. Soc. Bull., 58[11], 1111 (1979).

14. "Aqueous Corrosion of $Li_2O \cdot 2SiO_2$ Glass-Ceramics," submitted to the J. Am. Ceram. Soc.

15. "Determination of Fatigue Parameter for $Li_2O \cdot 2SiO_2$ Glass and Partially Crystallized $Li_2O \cdot 2SiO_2$," presented at the 80th Annual Meeting of the American Ceramic Society, Detroit, Michigan, May 6-11, 1978.

16. "Effect of Crystallization on the Auger Electron Signal Decay in a $Li_2O \cdot 2SiO_2$ Glass and Glass-Ceramic," J. Am. Ceram. Soc., 62[9-10], 500-503 (1979).

17. "Durability of $Li_2O \cdot 2SiO_2$ Glass-Ceramics," presented at the 80th Annual Meeting of the American Ceramic Society, Detroit, Michigan, May 6-11, 1978.

18. "Compositional Analysis of Alkali Glasses Using Auger Electron Spectroscopy," presented at the 80th Annual Meeting of the American Ceramic Society, Detroit, Michigan, May 6-11, 1978.

19. "Fatigue Properties of $Li_2O \cdot 2SiO_2$ Glass and Glass-Ceramics," J. Am. Ceram. Soc., 62[5-6], 319-320 (1979).

20. "Corrosion of Glass Surfaces," accepted by Surface Science.

21. "Aqueous Corrosion of Li_2O-Al_2O_3-CaO-SiO_2 Glass-Ceramics," submitted to J. Am. Ceram. Soc.

22. "Use of New Surface Physics for Controlling the Physical Properties of Ceramics," presented at the Science of Ceramics 10, Munich, Germany, September 2-4, 1979.

23. "Use of New Surface Physics for Controlling the Physical Properties of Ceramics," to be published in the Proceedings Science of Ceramics 10 (1980).

24. "Surface Characterization of Ceramed Composites and Environmental Sensitivity," to be published in Ceramic Engineering and Science Proceedings, No. 7-8, July-Aug. (1980).

25. "Surface Analysis of Si_3N_4 Oxidation," to be published in Ceramic Engineering and Science Proceedings, No. 7-8, July-Aug. (1980).

26. "Effects of Heat Treatment Time on the Oxidation of Pressed Si_3N_4 as Determined by Infrared Reflection Analyis," to be published in Ceramic Engineering and Science Proceedings, No. 7-8, July-Aug. (1980).

27. "Durability and Strength of Li_2O-Al_2O_3-CaO-SiO_2 Glass-Ceramics." presented at 81st Annual Meeting of the American Ceramic Society, Cincinnati, Ohio, April 29-May 2, 1979.

28. "Effects of Solution pH on Corrosion Behavior of $Li_2O \cdot 2SiO_2$ Glass-Ceramics," presented at 81st Annual Meeting of the American Ceramic Society, Cincinnati, Ohio, April 29-May 2, 1979.

29. "Nondestructive Evaluation of Surface Flaws Using Infrared Reflection Spectroscopy," presented at 81st Annual Meeting of the American Ceramic Society, Cincinnati, Ohio, April 29-May 2, 1979.

30. "Corrosion of Glass Surfaces," an invited paper presented at the Seventh Canadian Seminar on Surfaces, Pinawa, Canada, July 1979.

31. "Electron Beam Effects During Analysis of Glass Thin Film with Auger Electron Spectroscopy," to be published in J. of Surface and Interface Analysis, Aug./Sept. (1980).

32. "Electron Beam Effects During Analysis of Glass Thin Film with Auger Electron Spectroscopy," to be presented at the 8th International Conference on Surface Science, Cannes, France, September 1980.

DISTRIBUTION LIST

Dr. Donald R. Ulrich Program Manager Director of Chemical Science Department of the Air Force Air Force Office of Scientific Research/NC Bolling Air Force Base, NC 20332	6
Lt. Col. Richard W. Haffner Air Force Office of Scientific Research/NC Bolling Air Force Base, NC 20332	1
Dr. Stephen W. Freiman U.S. Department of Commerce National Bureau of Standards Washington, DC 20234	1
Dr. Arthur M. Diness Director of Metallurgy and Ceramics Program Department of the Navy, Code 471 Office of Naval Research Arlington, VA 22217	1
Dr. Sunil Dutta NASA Lewis Laboratories Mail Stop 49-3 21000 Brookpark Road Cleveland, OH 44135	1
Dr. R. Nathan Katz Ceramic Research Laboratory U.S. Army Materials Research Agency Watertown, MA 02172	1
Dr. Pedro B. Macedo Catholic University of America Vitreous State Laboratory Physics Department Washington, DC 20017	1
Dr. Robert Leachman Energy Subcommittee U.S. House of Representatives Rayburn Office Building Washington, DC	1

DISTRIBUTION LIST (Continued)

Dr. S. Wiederhorn National Bureau of Standards Materials Building 223 Washington, DC 20234	1
Professor A. R. Cooper Division of Metallurgy & Materials Science Case Western Reserve University Cleveland, OH 44106	1
Professor L. David Pye College of Ceramics Alfred University Alfred, NY 14802	1
Dr. Douglas Mackenzie Materials Division School of Engineering University of California Los Angeles, CA 90024	1
Dr. Robert J. Eagan Sandia Laboratories Box 5800 Albuquerque, NM 87185	1
Lawrence Livermore Laboratory Livermore, CA 94550	1
Professor Rustum Roy Materials Research Laboratory Pennsylvania State University University Park, PA 16801	1
Dr. Carlo G. Pantano Department of Materials Science & Engineering 218 Steidle Building Pennsylvania State University University Park, PA 16802	1
Dr. Harold Posen RADC/ESM Hanscom Air Force Base, MA 01731	1
Dr. Joseph H. Simmons Physics Department Catholic University of America Washington, DC 20064	1

DISTRIBUTION LIST (Continued)

Dr. Wayne A. Ross 1
Battelle Pacific Northwest Laboratories
P. O. Box 999
Richland, WA 99352

Dr. J. E. Mendel 1
Battelle Pacific Northwest Laboratories
P. O. Box 999
Richland, WA 99352

Dr. Kyo Kim 1
Nuclear Regulatory Commission
Washington, DC 20555

Dr. P. A. Parrish 1
Metallurgy and Materials Science Division
U. S. Army Research Office
Research Triangle Park, NC 27709

Dr. D. L. Kinser 1
Materials Science and Metallurgical
Engineering
Vanderbilt University
Nashville, TN 37203

Dr. David M. Sanders 1
National Bureau of Standards
Washington, DC 20234

Solar Energy Research Institute 1
1536 Cole Boulevard
Golden, CO 80401

Dr. J. L. Crandall 1
Advanced Planning Section
D.I. DuPont de Nemours & Co.
Atomic Energy Division
Savannah River Laboratory
Aiken, SC 29801

Dr. George Wicks 1
E. I. DuPont de Nemours & Co.
Atomic Energy Division
Savannah River Laboratory
Aiken, SC 29801

DISTRIBUTION LIST (Continued)

Dr. John Wiley 1
E. I. DuPont de Nemours & Co.
Atomic Energy Division
Savannah River Laboratory
Aiken, SC 29801

Dr. Donald H. DeClerck 1
Pfaudler Co.
1000 West Avenue
Rochester, NY 14603

Dr. Gary McVay 1
Battelle Pacific Northwest Laboratories
P. O. Box 999
Richland, WA 99352

Dr. Ronald Palmer 1
Rockwell, Hanford Operations
200W/2225
Richland, WA 99352

Dr. Alexis G. Pincus 1
Department of Ceramics
College of Engineering
Rutgers University
University Heights Campus
New Brunswick, NJ 08903

Dr. James W. McCauley 1
U.S. Army Materials & Mechanics
Research Center
Watertown, MA 02172

Dr. Paul Johnson 1
N.Y.S. College of Ceramics
Alfred University
Alfred, NY 14802

Ms. Joy Barrett 1
Solar Energy Research Institute
1535 Cole Boulevard
Golden, CO 80401

Dr. Ronald T. Flynn 1
Owens-Corning Fiberglas Corp.
Box 415, Building 20
Granville, OH 43023

DISTRIBUTION LIST (Continued)

Prof. J. Zarzycki
Laboratoire des verres du CNRS
Université de Montpellier 2
Place Eugène Bataillon
34060 MONTPELLIER-CEDEX
FRANCE
1

Mr. Makoto Ogino
Glass Division
Sagamihara Factory
Nippon Kogaku K.K.
Asamizodai 1773
Sagamihara-Shi
Kanagawar-ken
228 JAPAN
1

Dr. John R. Hutchins, III
Corning Glass Works
104 Corning Blvd.
Sullivan Park
Corning, NY 14803
1

Dr. Daniel R. Stewart
Owens-Illinois Technical Center
1700 N. Westwood Avenue
Toledo, OH 43666
1

Prof. R. G. Newton
5, Hardwick Crescent
Sheffield S11 8WB
ENGLAND
1

Dr. Peter Tayler
Atomic Energy of Canada Research Company
Whitesheel Nuclear Research Establishment
Pinawa, Manitoba ROE 1LO
Canada
1